Norwegian University of Life Sciences

Master's Thesis 2020 30 ECTS

Faculty of Science and Technology

Supervisors:

Prof. Roberto Tomasi (NMBU) & Prof. Roberto Crocetti (KTH)

Beam-Column Connections in Glulam Structures, with Gusset Plates of Birch Plywood and Self-Tapping Screws

Bjelke-søyleforbindelser med innslisset kryssfinér av bjørk og selvborende skruer i limtrekonstruksjoner

Eystein Fredrik Furuheim
Pål Marius Nesse

Structural Engineering and Architecture

Faculty of Science and Technology (REALTEK)

Abstract

Multi-storey timber buildings are often built around a post and beam system made of glulam. Typically adopted connections for such structures are those which make use of slotted-in steel plates and dowels. Even though such connections are able to transfer large loads, they have a number of deficiencies. Besides being relatively costly in terms of both materials and manufacturing, connections with slotted-in steel plates and dowels require a very high level of accuracy both in manufacture and assembly. By replacing steel plates and dowels with plates of birch plywood and self-tapping screws, there are possible benefits; The connection would be lighter, cheaper, and easier on the environment by avoiding the great carbon dioxide emissions from steel production. One could also benefit from the superior fire properties of wood compared to steel, as well as the possibility of adding external plywood plates to the outside of the connection. This thesis presents an experimental investigation of the mechanical characteristics of such plywood connections, ended with an assessment of its use in real design.

The experimental work of this research was introduced with preliminary tests to identify weaknesses in the test setup. Changes were made and main tests with eight different test groups were conducted. Six of these portrayed a situation where continuous plates of birch plywood connect a column to a beam on both sides. Two configurations represented connections between lateral columns with beams attached on one side. The effects of using both one and two slotted-in plates were investigated, along with the effect of variation of grain angle in the plywood. Configurations were also made to represent the case where a glulam column is prefabricated, with glued continuous plywood plates throughout the column.

Test results and hand calculations have confirmed that beam-column connections with gusset plates of birch plywood, may reach sufficient capacities for realistic design in the Ultimate Limit State (ULS). By utilizing both external and slotted-in gusset plates of plywood, one could reach the same capacity and stiffness as a slotted-in steel plate connection. To further reduce the amount of steel in the connections, results showed that prefabricated glued columns with plywood can be an opportunity.

Keywords: Timber Construction, Beam-Column Connection, Screw Connection, Birch Plywood, Gusset Plates

Sammendrag

Trekonstruksjoner som strekker seg over flere etasjer er ofte bygd rundt et bjelke-søyle-system bestående av limtre. Typiske forbindelser i slike systemer, benytter seg av innslissede stålplater og ståldybler. Selv om forbindelser som disse er i stand til å overføre store laster, har de en rekke svakheter. I tillegg til at de er relativt kostbare både når det gjelder innkjøp og produksjon, krever stålplateforbindelser med dybler en veldig høy grad av nøyaktighet, både ved fabrikasjon og montering. Ved å erstatte stålplater og dybler med kryssfinér av bjørk og selvborende treskruer, er det flere mulige fordeler; Forbindelsen vil være lettere, billigere, og mindre belastende på miljøet ved å unngå de store CO_2-utslippene fra stålproduksjon. Man kan også dra nytte av de utmerkede brannegenskapene til tre sammenlignet med stål, i tillegg til muligheten til å feste eksterne kryssfinérplater til utsiden av forbindelsen. Denne oppgaven presenterer en eksperimentell undersøkelse av de mekaniske egenskapene til slike kryssfinér-forbindelser. Avslutningsvis legges det frem en vurdering av mulighetene for bruk av slike forbindelser i reelle konstruksjoner.

Det eksperimentelle arbeidet i laboratoriet ble innledet med prøvetester for å avdekke svakheter i testoppsettet. Forbedringer ble gjort, og en hovedtest med åtte ulike testgrupper ble gjennomført. Seks av disse forestilte situasjonen der kontinuerlige plater av kryssfinér kobler en søyle med en bjelke på to motstående sider. To testgrupper representerte en forbindelse i sidesøyler, der en bjelke monteres kun på den ene siden. Effektene av å bruke både en og to innslissede plater ble undersøkt, samt virkningen av ulike fiberretninger i platene. Testgrupper ble også laget for å gi en modell av en situasjon der søylen er prefabrikkert med innlimte, gjennomgående kryssfinérplater.

Testresultater og beregninger kan bekrefte at bjelke-søyleforbindelser med slisseplater av bjørke-kryssfinér, kan oppnå tilstrekkelige kapasiteter for realistisk dimensjonering i bruddgrensetilstanden (ULS). Ved å benytte seg av både innslissede og eksterne kryssfinérplater på utsiden av forbindelsen, kan forbindelsen nå den samme kapasiteten og stivheten som en innslisset stålplateforbindelse. For å ytterligere redusere mengden stål i slike forbindelser, har testresultater vist at innlimte plater i søylen er et godt alternativ.

Preface

This research finalizes our five years of education at the master's study Structural Engineering and Architecture at the Norwegian University of Life Sciences (NMBU). The planning started in October 2019 when the topic was introduced by Roberto Crocetti, professor at KTH, Stockholm. The main work and dialogues with collaborators started in January, and steady progress was maintained until finalization.

We wish to express our deepest appreciation to professors Roberto Tomasi and Roberto Crocetti, our supervisors, for their professional support and guidance throughout our master's project. Their knowledge and expertise have contributed remarkably to the outcome of the project. We would also like to thank Dag Pasquale Pasca for his advice and help during the planning phase and lessons in testing procedure and software. Our gratitude is also directed towards Roar Økseter for his time assisting us in the laboratory, and Øyvind Hansen among his coworkers at the faculty workshop for their creative solutions and positivity.

We would like to thank Harald Liven and the team at Moelven Limtre AS, for donating glulam for the testing. We are also grateful for the initial support and discussion around the project, as well as the informing and intriguing tour of their production facility. We are also thankful towards Jostein Halvorsen and the people at Metsä Wood for the generous donation and unproblematic delivery of the plywood. Appreciation is directed towards Eugenio Facchini and Rothoblaas for providing the screws, and Dynea and Ronny Bredesen for generously donating the glue. This project would not be feasible without their participation.

Finally, we wish to thank our family and closest friends for the support and encouragement throughout our years of studying at NMBU.

Ås, June 2020

Eystein Fredrik Furuheim & Pål Marius Nesse

Table of Contents

List of Tables

List of Figures

Abbreviations and Acronyms

A	Area	$f_{t,k}$	Characteristic tensile stress capacity
CEN	European Commitee for Standardization	$f_{v,k}$	Characteristic planar shear strength
CLT	Cross Laminated Timber	$f_{v,mean}$	Mean planar shear strength
d	Diameter of fastener	Glulam	Glued laminated timber
D_u	Ductility ratio	I_p	Polar moment of inertia
δ	Deformation	K	Stiffness/Slip modulus
δ_{max}	Maximum deformation	K_{el}	Elastic/Initial stiffness
δ_u	Ultimate deformation	K_{global}	Global stiffness of test specimen
δ_y	Yield deformation	K_{pl}	Plastic stiffness
ε	Strain	K_{ser}	Estimated slip modulus for connection
EC3	Eurocode 3	k_φ	Rotational stiffness
EC5	Eurocode 5	kN	Kilonewton
F	Force	L	Length
$F_{ax,Rk}$	Withdrawal resistance	LVL	Laminated Veneer Lumber
F_u	Ultimate load	L_0	Initial length
F_y	Yield load	MUF	Melamine Urea Formaldehyde
FE	Finite Element	$M_{y,k}$	Characteristic yield moment
F_{est}	Estimated maximum load	m	Mass
F_{max}	Maximum load	m_0	Dry mass
$F_{max,ply}$	Maximum load per plywood plate	m_w	Mass before drying
$f_{ax,k}$	Withdrawal stress capacity	N	Newton
$f_{c,k}$	Characteristic compressive stress	PU	Polyurethane
f_h	Embedment strength	P_y	Yield point
$f_{m,k}$	Characteristic bending stress capacity	S355	Structural steel grade

SD	Standard Deviation
SLS	Serviceability Limit State
STA	Dowel model from Rothoblaas
φ	Rotation
φ_{max}	Maximum rotation
ρ	Density
ρ_m	Mean density
σ	Normal stress
σ_c	Compressive stress due to bending
σ_t	Tensile stress due to bending
σ_u	Ultimate stress
τ	Shear stress
ULS	Ultimate limit state
V	Volume
VGZ	Wood screw from Rothoblaas
w	Moisture content
Y&K	Yasumura & Kawai
Ø	Hole diameter

1 Introduction

1.1 Background

Nowadays, renewable and environmentally friendly materials are highlighted as the future of the construction industry. The interest in timber constructions has increased throughout the past decades, due to both the increased environmental awareness, and architectural reasons.

For long span construction, timber is one of the best materials due to its high strength to weight ratio. Timber products, such as glued laminated timber (glulam), Laminated Veneer Lumber (LVL), plywood, and Cross-Laminated Timber (CLT), have become more frequently used in buildings. Although it is naive to believe that inorganic and less environmentally friendly building materials such as steel and concrete, can entirely be replaced by timber, society should strive to limit their usage where it is possible. In a construction made of frames with glulam columns and beams, the amount of steel used in connections alone can add up to a surprisingly large amount. By being able to utilize plywood in some of these connections, it may reduce the climate impact, save weight, time, and money.

1.2 State of the Art

In a multi-storey timber building, many connections have to be considered in the design. In this work, the focus is directed at so-called beam-column connections. There are many different kinds of beam-column connections used in structures. In the case of timber buildings with several floors, continuous columns extending over several floors are not uncommon. In these situations, the beams are connected directly onto the sides of the column by using different types of fasteners, some are illustrated in Figure 1-1.

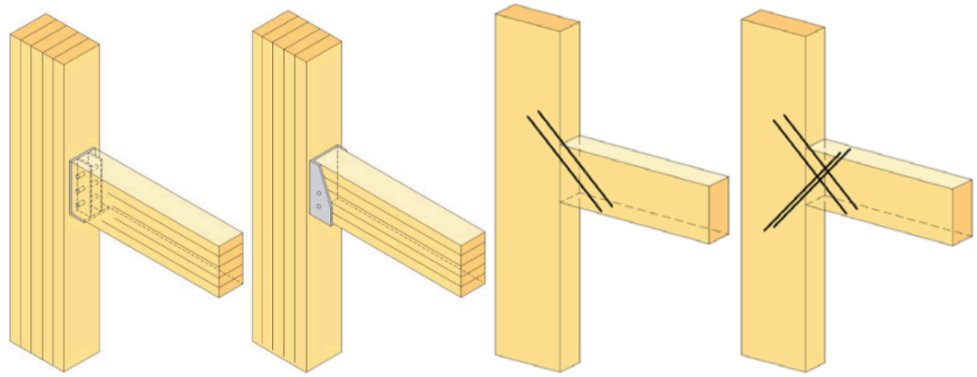

Figure 1-1 – Common beam-column connection variations (Norske Limtreprodusenters Forening, 2015).

In most cases of big-scale construction, slotted-in steel plates installed with steel dowels are used to connect beams to a continuous column. An example is presented in Figure 1-2, where steel plates are fitted into pre-cut slots in the glulam, and then fixed into place with steel dowels.

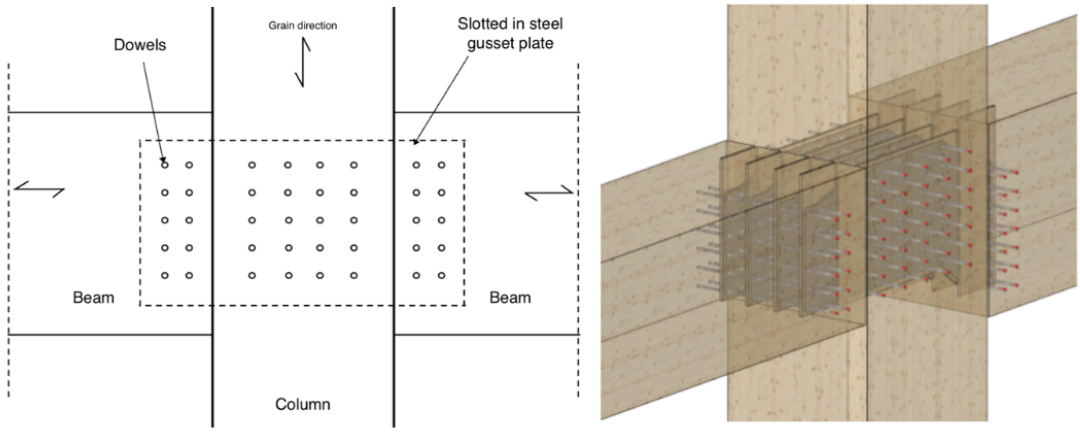

a) b)

Figure 1-2 – A steel gusset plate connection with beams attached on both sides of the column (a). Actual connection in Mjøstårnet, Norway, designed by Moelven Limtre (b).

There are several disadvantages of using steel plates in connections, one of them being the need for a very high degree of accuracy for the holes. In case of erroneous placement of the holes, which is not a very uncommon event, the connection needs to be adjusted at the building site, typically by re-drilling several holes or by enlarging their size, thus affecting the load-carrying capacity of the connection. Hole accuracy would not be a problem in a plywood gusset plate connection, as pre-drilling would not be required. Steel also has far weaker fire resistance properties than wood. When reaching high temperatures, steel lose a significant portion of its strength, while wood keeps most of its load-bearing capacity due to

its good heat isolative properties. These problems tied to using steel could be solved by using plates of wood-based materials instead.

1.3 Earlier Work

There has not been performed much research on using birch plywood as gusset plates in beam-column connections but using plywood in timber truss joints is studied. The effects of secondary stresses due to truss deflection and joint slip in semi-rigid joints in timber trusses (Massé & Salinas, 1988) has been analyzed. Douglas Fir plywood and not birch plywood was used in said research. There has been done experiments on timber truss connections with gusset plates of LVL where tension was investigated (Lappalainen & Backman, 2019; Åström, 2019).

The variation of plywood strength and stiffness properties with the grain angle has been determined (Bier, 1984). The stiffness and strength properties of Pinus Radiata wood for different grain angles was calculated, by assuming values for shear and axial strength, and then compared with test results (Bier, 1984).

The capacities of different bamboo-steel slotted-in connections has also been investigated. The capacity increase when using two slotted-in plates versus one slotted-in plated was 90 %, not doubled, but this needs to be confirmed by a larger number of tests (Debije, 2017).

1.4 Aim and Objectives

This thesis aims to investigate how birch plywood behaves as gusset plates in timber-to-timber connections while being subjected to shear stress and bending moment. By overdesigning the screw connections, the objective is to find modes of failure from bending and shear stress in plywood for different grain angles. The variation in capacity for the different grain angles in relation to stress will be analyzed. The stiffness of the connections will also be investigated, along with an assessment of the ductility and brittleness of the failure. To visualize the usability of plywood in real connections, capacities will be compared with a realistic steel plate connections and feasible design loads. An assessment will thereby be made to introduce the advantages.

2 Wood as Material in Connections

Some basic theory of wood, glulam, plywood, and engineering mechanics of timber is introduced as a background for understanding timber connections and their properties. A load distribution example of a beam-column connection is presented.

2.1 Properties of Wood

Timber is different from other widely used materials like steel or concrete when it comes to their properties as an engineering material. It has an excellent strength-and-stiffness to weight ratio, which allows for long-spanned beams and trusses. However, timber has some unusual properties which has to be accounted for when designing structures, such as its orthotropy.

Unlike steel and other homogeneous materials, the mechanical properties of wood vary with the direction of the load. Timber is therefore an anisotropic material, because the mechanical properties are not the same for every direction. The different directions are illustrated in Figure 2-1. The direction parallel to the length of the tree is referred to as the fiber or grain direction, and it has the highest mechanical capacities, both for tension and compression (United States Forest Service, 1999). The radial and tangential directions however (often referred to as directions perpendicular to the grain), have significantly weaker capacities (Kollmann & Cöté, 1968).

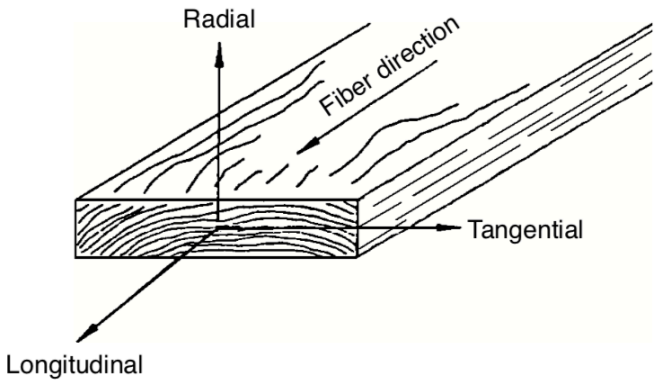

Figure 2-1 – The three anisotropic directions of timber as a material (United States Forest Service, 1999).

The strength of a material is often characterized by the ultimate stress σ_u at time of failure. However, ultimate stress is not always achieved by doing mechanical tests, for instance when

testing compression capacity perpendicular to grain. Failure does not only imply fracture, but can also mean that the deformation has reached an excessively large value (Bodig & Jayne, 1993).

The stress-strain relationship of materials is understood in order to establish failure criteria. A stress-strain diagram explains several of a material's mechanical properties, with stress and strain as fundamental parameters. The diagram can be used to analyze the failure modes and the ductility or stiffness of materials or connections, as done in this project.

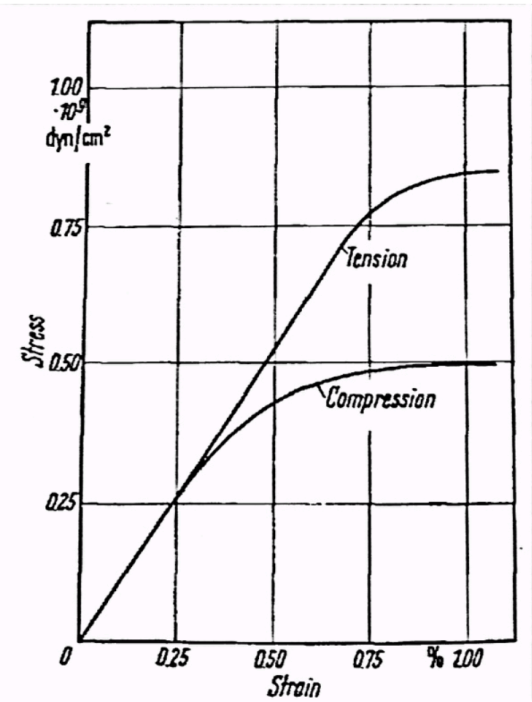

Figure 2-2 – Stress-strain diagram for softwood for tensile and compressive stresses (Kollmann & Côté, 1968).

The y-axis on the diagram represents the stress (σ), which is defined by Formula 2.1. The x-axis of the diagram represents the strain (ε), which is defined by Formula 2.2.

$$\sigma = \frac{F}{A} \tag{2.1}$$

$$\varepsilon = \frac{\delta}{L_0} = \frac{L - L_0}{L_0} \tag{2.2}$$

Where:

F The applied force

A The element's cross section area

δ Elongation/compression of the element

L_0 Original length of the element

L New length of the element

Figure 2-2 shows how the tension and compression stress-strain relation typically looks like for softwood timber. The linear part of the lines in the graph represents the elastic area of the stress and strain. When the stress exceeds this interval, the strain occurs in a plastic nature with a permanent deformation when the stress is relieved. The stress level approaches values that lead to failure; the stress-strain relationship is no longer linear, and a small increase in stress causes a big increase in strain. When the limit for strain is reached, the failure occurs.

For most homogeneous engineering materials, the ultimate compression capacity is greater than the tensile capacity. For wood parallel to the grain it is opposite; the tensile capacity is always greater than the compressive capacity. This is a consequence of the porous and fibrous nature of wood compared to homogeneous materials like steel (Bodig & Jayne, 1993). Common failure modes for wood subjected to bending is displayed in Figure 2-3.

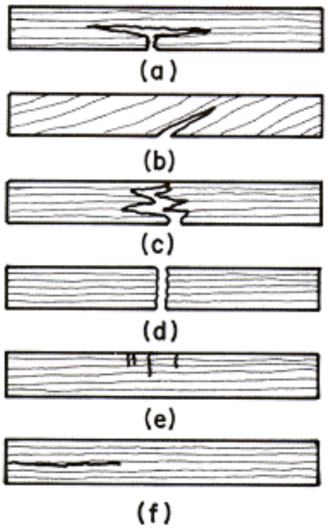

Figure 2-3 – Failure types of clear wood in bending with span parallel to grain: (a) simple tension, (b) cross-grain tension, (c) splintering tension, (d) brash tension, (e) compression, (f) horizontal shear (Bodig & Jayne, 1993).

When a beam is subjected to bending, both compressive and tensile stresses act on the cross-section. When the compressive stress σ_c reaches its limit, compressive failure like in Figure

2-3 e) happens and the neutral axis moves downwards due to the loss of capacity in the top part. This development of bending stresses is illustrated in Figure 2-4. The tensile stress σ_t will continue to increase rapidly due to the lowered neutral axis and the beam will eventually suffer a tensile failure in the bottom part of the cross-section.

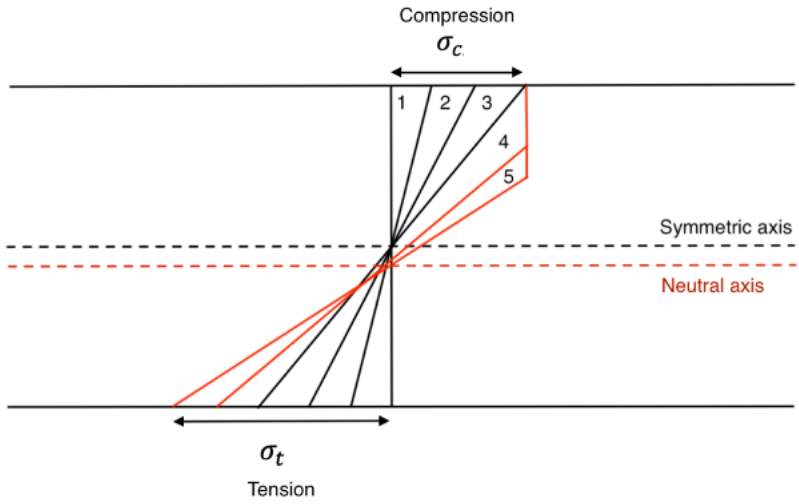

Figure 2-4 – Stress development of a beam during bending. The numbers 1-5 represent the different development stages of stress over time. σ_c represents the compressive stress from bending. σ_t represents the tensile stress from bending.

2.2 Glulam

Glulam has become a widely used structural materials together with steel and concrete. For great span construction, it is one of the better materials to use due to its high strength to weight ratio. Because of its esthetic value, it is a popular material for visible load-carrying elements as well as furniture (Swedish Wood, 2013). Glulam is an engineered product containing lamellas of timber which is glued together by thin adhesive layers. This gives the opportunity to make one single structural member out of several smaller pieces, and the element can therefore be produced in almost any size and shape (Norske Limtreprodusenters Forening, 2015).

The glulam can be sorted into two types; homogeneous and combined. This refers to the composition of different strength gradings of timber in the cross-section, as illustrated in Figure 2-5. The two types of glulam are identified by the abbreviations GLXXh and GLXXc, where XX refers to the characteristic bending capacity and *h* and *c* refers to either homogeneous or combined cross section (Bell, 2017).

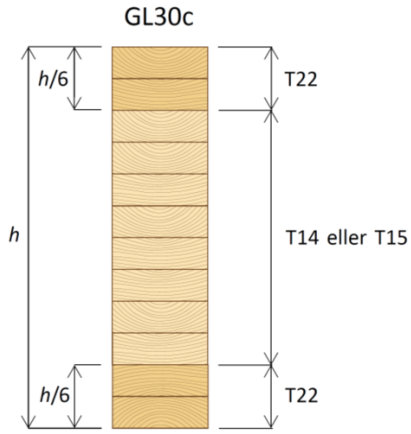

Figure 2-5 – Cross section of a combined glulam beam (Norske Limtreprodusenters Forening, 2015). T22 and T14/15 represents the tensile strength grading of the lamellas, and h is the height of the beam.

Glulam has the same mechanical properties as timber, but in addition the measured strengths are higher with a lower deviation. The industrial process makes glulam very versatile, by varying the cross-section and the possibility to produce long and continuous beams which give geometrical opportunities. The width is limited by the availability of wide laminations, which varies with the geographic area. The maximum width of a glulam member is typically 215-240 mm.

The fracture of glulam beams can be characterized by brittleness. They are often caused by imperfections in the timber or the finger joints of the tensioned lamellas of the cross-section (Norske Limtreprodusenters Forening, 2015).

2.3 Plywood

Plywood is a processed wood product made with layers of thin plies laid cross-banded, glued together. The nominal thickness of the veneers for birch is 1,4 millimeters and for softwoods it varies between 1,4 – 3,2 millimeters. Birch is a type of hardwood with a higher density than softwood species like spruce. This positively affects the strength values. The mean and characteristic values for density are 680 and 630 kg/m^3. The main use for plywood in general is formwork for concrete, and furniture production. The high planar shear strength and impact resistance of birch plywood also makes it suited for heavy-duty floor and wall structures, and other building elements subjected to heavy wear (Koskisen Group, 2002).

Relations between the modulus of elasticity with grain angle, and the bending strength of plywood with grain angle is presented in Figure 2-6 (Bier, 1984).

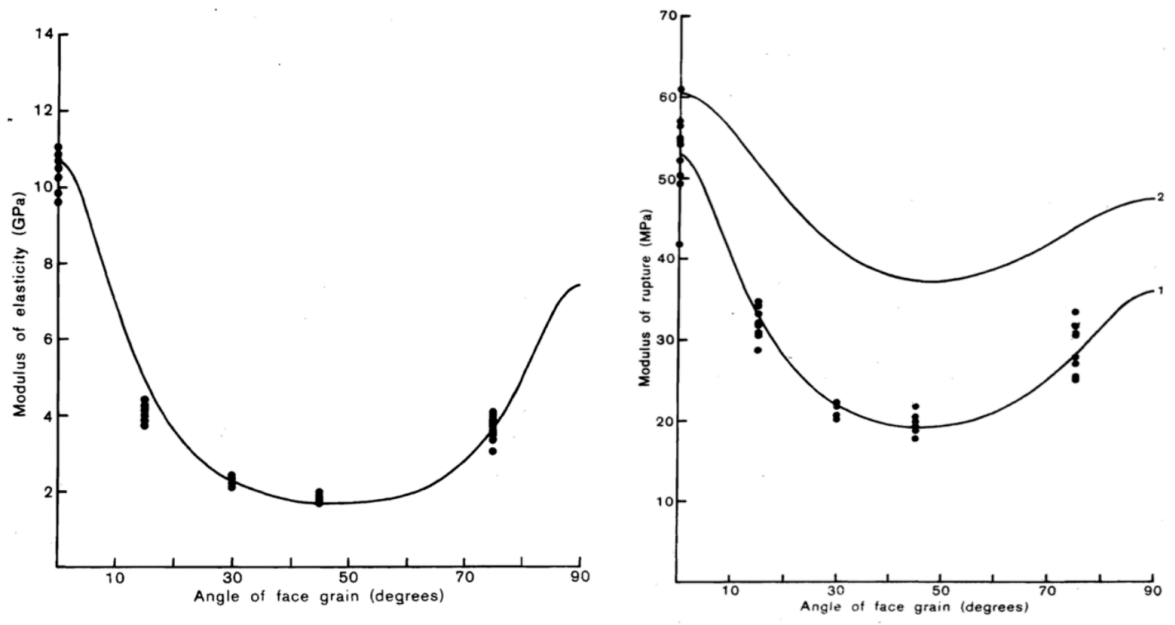

a) b)

Figure 2-6 – The relationship between the modulus of elasticity and face grain angle (a) and curves representing tension and compression, forming an outline for the strength envelope of bending (b) (Bier, 1984).

The curve in Figure 2-6 b) shows two curves representing the tension and compression ratios, forming an outline for the strength envelope for bending, in which all bending failures should occur within (Bier, 1984). The figures presented gives a clear understanding of how Pinus Radiata plywood behaves for various grain angles. It appears that the strength properties are significantly lowest when the grain angle is 45-degrees. It is assumed that the curves for birch plywood have similar behavior.

In a real structure with plywood gusset plate connections between columns and beams, the plates would be subjected to both shear and bending stress. It is therefore reasonable to assume that this relation will have some impact on how the tests with a grain inclination perform.

2.4 Mechanical Characteristics of Connections

To describe the test results and compare different test groups, different mechanical parameters has to be established. The stress-strain diagram in Figure 2-7, illustrates the different interesting characteristics to gather from a mechanical test. The parameters described in the following paragraphs are; ultimate and maximum load, yield point, elastic and plastic stiffness and ductility ratio.

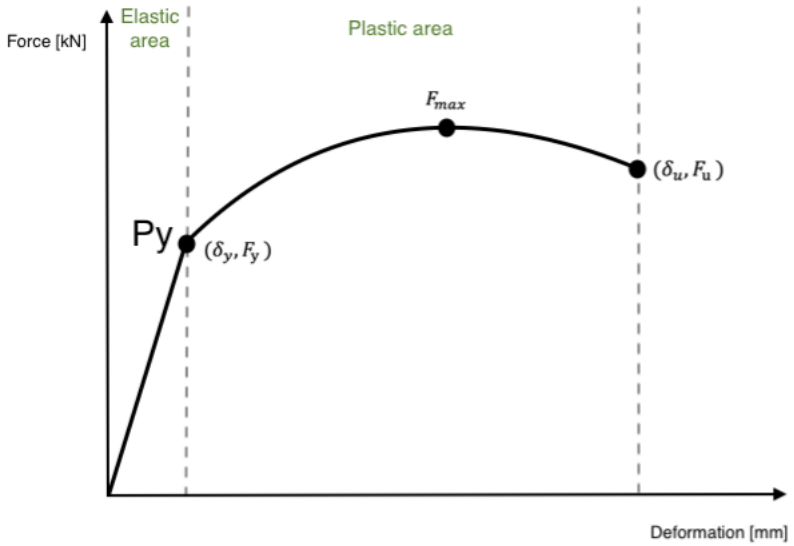

Figure 2-7 – Force-deformation diagram illustrating the relevant mechanical characteristics that can be found by doing mechanical tests.

2.4.1 Ultimate and maximum load

The ultimate load F_u is the load in effect at the exact time of failure. This value is often lower than F_{max} for ductile materials like steel, but it is not uncommon that F_{max} and F_u are equal for more brittle materials like plywood or high carbon steel. The ultimate deformation δ_u (referred to as δ_{max} in this work) is the corresponding deformation of the specimen at the time of F_{max}.

The maximum load F_{max} is defined as the peak value of the load during the whole testing procedure. As seen in Figure 2-7, this value can be higher than the ultimate load.

The ultimate load (F_u) and maximum load (F_{max}) are in this work regarded as the same value, because the failure occurred at the maximum load across all test groups.

2.4.2 Yield point

The yield point P_y of the specimen is defined as the point on the stress-strain curve where the deformation goes from linear to non-linear, in other words elastic to plastic. P_y has the associated yield force F_y and yield deformation δ_y. The yielding of timber connections often happens as a result of a both the wood and connectors deforming, eventually leading to the failure of the connection. Several methods have been developed to find the yield point of timber structures and connections. In North America, three methods are commonly used; The equivalent energy elastic-plastic (EEEP) curve is made for analysis of shear walls. The 5%

method relies on the diameter of the dowels used in the connection to find the yield point (Muñoz et al., 2008). The third method from (Karacabeyli & Ceccotti, 1996) utilizes the point on the curve at 50 % of the maximum load F_{max}, see Figure 2-8. Formula 2.3 can thus be used to find the yield force:

$$F_y = F_{max} * 0{,}50 \tag{2.3}$$

Where:

F_{max} The maximum load on the connection

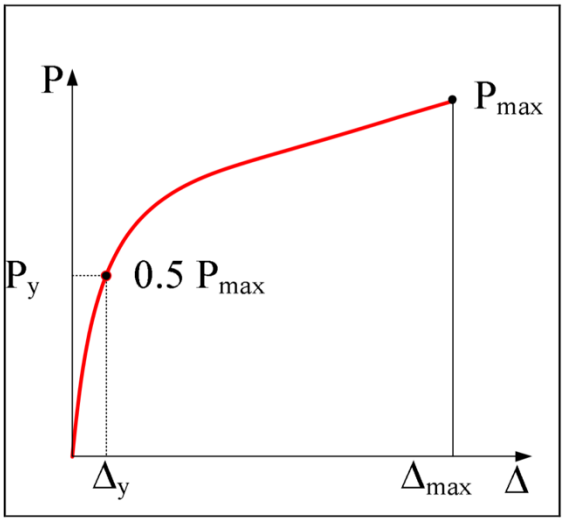

Figure 2-8 – The (Karacabeyli & Ceccotti, 1996) method of finding the yield point (Muñoz et al., 2008). Δ refers to the displacement and P refers to the applied load. P_y is the yield load, referred to as F_y in this research.

2.4.3 Stiffness

The stiffness of a material or connection is defined as its ability to withstand deformation while being subjected to a load. The European Standard has a method for estimating the slip modulus K_{ser} per shear plane per fastener for mechanical connectors. K_{ser} describes the stiffness of a connection between two connected materials, while loaded elastically (NS-EN 1995-1-1:2004, 2004). For screws and dowels in a timber-to-timber connection, Formula 2.4 is used:

$$K_{ser} = \rho_m^{1,5} \frac{d}{23} \tag{2.4}$$

Where:

ρ_m The geometric mean density of the two connected wood materials

d The diameter of the fastener

The geometric mean density is found with Formula 2.5:

$$\rho_m = \sqrt{\rho_{m,1}\rho_{m,2}} \tag{2.5}$$

Where:

$\rho_{m,1}$ The mean density of timber material 1

$\rho_{m,2}$ The mean density of timber material 2

To describe the failure behavior of a connection; elastic stiffness (K_{el}) and plastic stiffness (K_{pl}) can be used. The elastic stiffness (K_{el}) is the elastic region of the material prior to the yield point of the force-deformation diagram. This is also often referred to as the initial stiffness and is found according to the guidelines in the Eurocode (NS-EN 26891:1991, 1991). The elastic stiffness is the slope of the curve in the elastic part of the stress-strain diagram. More accurately the curve between point 21 and 24 in Figure 3-22, if the loading procedure described in the Eurocode is used. Formula 2.6 is thus applicable:

$$K_{el} = \frac{0{,}4F_{est} - 0{,}1F_{est}}{\delta_{0,4} - \delta_{0,1}} \tag{2.6}$$

Where:

F_{est} The estimated load capacity of the specimen, which is put into the software of the test machine

$\delta_{0,4}$ The deformation of the specimen at $0{,}4F_{est}$

$\delta_{0,1}$ The deformation of the specimen at $0{,}1F_{est}$

The plastic stiffness (K_{pl}) represents the slope of the plastic part of the curve after passing the yield point. The plastic stiffness is always lower than the elastic stiffness. Several different methods, specifically made for different materials and failure types, have been devised to find this value. The Y&K method is used in this work, since the slope found is quite consistent

with the curves found in the tests (Yasumura & Kawai, 1998). The method described in the Eurocode could also be used (NS-EN 12512:2002, 2002).

The Y&K method illustrated in Figure 2-9 was originally used to evaluate the behavior of wood frame shear walls but has been adopted by others to find the yield point and stiffness values of different timber test configurations. The Y&K method is also referred to as the modified CEN procedure or the 10-40-90 procedure (Fragiacomo et al., 2011). The method of finding the plastic stiffness, is finding the slope between the $0{,}40F_{max}$ and $0{,}90F_{max}$ points on the load-deformation curve in the same manner as the Eurocode recommends for the elastic stiffness, as expressed in equation 2.6 (NS-EN 12512:2002, 2002).

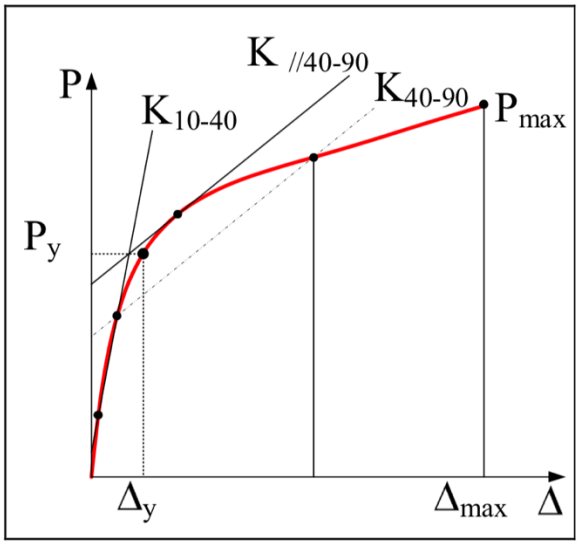

Figure 2-9 – The Yasumura & Kawai procedure to find the yield point and plastic stiffness (Muñoz et al., 2008). Δ refers to the displacement and P refers to the applied load. P_y is the yield load, referred to as F_y in this research. K_{10-40} is the elastic slope and K_{40-90} is the plastic slope of the curve.

Formula 2.7 can thus be used to find K_{pl}:

$$K_{pl} = \frac{0{,}9F_{max} - 0{,}4F_{max}}{\delta_{0,9} - \delta_{0,4}} \tag{2.7}$$

Where:

F_{max}	The tested maximum load capacity of the connection
$\delta_{0,9}$	The deformation of the specimen at $0{,}9F_{max}$
$\delta_{0,1}$	The deformation of the specimen at $0{,}4F_{max}$

2.4.4 Ductility ratio

The ductility is a parameter which describes a material or connections ability to deform plastically. A material such as steel which has a relatively high ability to deform beyond the elastic zone, is considered ductile. Cast iron is a brittle material and has almost no plastic deformation before failure and thus a low ductility. Normally, structures are designed to only have elastic behavior when subjected to loads. Ductility of structures is an important factor to consider when designing for seismic loads, as these must have the ability to deform and absorb the seismic forces to avoid collapse.

The ductility ratio D_u, describes the ductility of a connection or test specimen. It relies on a correct estimate of the yield load and the selection of the ultimate or maximum load. As discussed in 2.4.2, there are different methods for finding the yield point, and each one produces different estimates (Muñoz et al., 2008). A common way to find D_u is calculating the ratio of the ultimate and yield deformation, as seen in Formula 2.8:

$$D_u = \frac{\delta_u}{\delta_y} \tag{2.8}$$

Where:

δ_u The deformation at failure

δ_y The deformation at the yield point

2.5 Timber Joint Design

When calculating the strength of a mechanical timber connection, section 8 in EC5 is often used. This chapter enlightens the Johansen approach in EC5 for a timber-timber connection (NS-EN 1995-1-1:2004, 2004). This method is based on three important parameters; embedding strength of the wood, the fastener's withdrawal resistance, and the fastener's yielding moment.

2.5.1 Embedding strength

The timber or wood-based material's embedding strength (f_h) is related to the largest stress which can be transferred between a fastener and the wood without compressive failure in the

wood. The embedding strength of wood depends on the density, the fastener diameter, the angle between the force and grain direction and the area of the wood in contact with the fastener (Bell, 2017). EC5 gives an approach, based on experience, for calculating a material's embedding strength for different angles between the grain and load direction.

For plywood materials, the embedding strength is defined as a value independent of the grain direction due to its structure. The grain angle has neglectable influence on the embedding strength, seen in experiments (Bouchair et al., 2007).

2.5.2 Withdrawal resistance

In a loaded connection where a screw forms a plastic hinge, the screw is subjected to a tensile force due to its threads creating a withdrawal resistance ($F_{ax,k}$). The withdrawal resistance from the threads could increase the capacity of the connection by a phenomenon called the rope effect (Blaß & Sandhaas, 2017). A threaded screw can contribute with 100% of its withdrawal resistance to the capacity of the connection, compared to a dowel, which has no rope effect contribution to the capacity due to its smooth surface. EC5 restricts the capacity increase of the connection to a maximum of 25% of the withdrawal resistance (Bell, 2017).

2.5.3 Yielding moment

When a fastener is exposed to a uniform load, as it often is in a shear plane connection, yielding of the fastener may occur. When and how much the fastener yields, depends on the characteristic yielding moment capacity ($M_{y,k}$) of the fastener. When the force gets large enough, the steel starts to yield, and a plastic hinge occurs in the fastener. The yielding moment is an essential parameter in Johansen's equations used in EC5, and is dependent of the steel quality and the fasteners effective diameter (NS-EN 1995-1-1:2004, 2004).

2.5.4 Minimum distances

Spacings between the fasteners play an essential role in the design of any connection. The minimum distances between fasteners and from fasteners to edges of the timber are defined in EC5 and are based on investigations and experiences. The spacings depend on the diameter of the fastener, whether holes are pre-drilled, the grain direction, and whether the edge of the timber is loaded or not (Bell, 2017).

2.5.5 Failure modes

A method for calculating dowel-type joint capacities was first presented by K. W. Johansen. The theory was based on different failure modes and the characteristic capacity of the joint. The failure modes that occur are dependent on the geometry of the connection and the mentioned material properties. When designing a connection, all failure modes have to be considered. The mode with the lowest resistance is the critical one, and the design capacity is based on the resistance of this failure mode (Blaß & Sandhaas, 2017).

Failure in timber connections should be ductile due to yielding of the fasteners, but brittle failure can sometimes occur before the load bearing capacity is reached, from unexpected splitting. The member thickness, spacings between fasteners, angle between the load and the grain direction, and the edge distances are all affecting the likelihood of splitting. There are several methods to help avoid splitting of the wood in connections. Increasing the spacing between fasteners and arranging the fasteners offset from the center line (common in nailed connections) is effective. Other well-known methods described by (Blaß & Sandhaas, 2017), are reinforcing externally by gluing plywood to the outside of the wood, or reinforcing internally by inserting fully threaded screws in the critical splitting areas.

2.5.6 Multiple shear planes

EC5 includes an approach used to calculate the resistance of a double shear joint based on Johansen's theory, where four different failure modes can be considered. When designing a connection with more than two shear planes, EC5 recommends seeing each shear plane as a part of a joint in a double shear connection (NS-EN 1995-1-1:2004, 2004). The book Timber Engineering (Blaß & Sandhaas, 2017) gives an example of a connection consisting of four shear planes. The possible failure modes for this type of connection are presented in Figure 2-10.

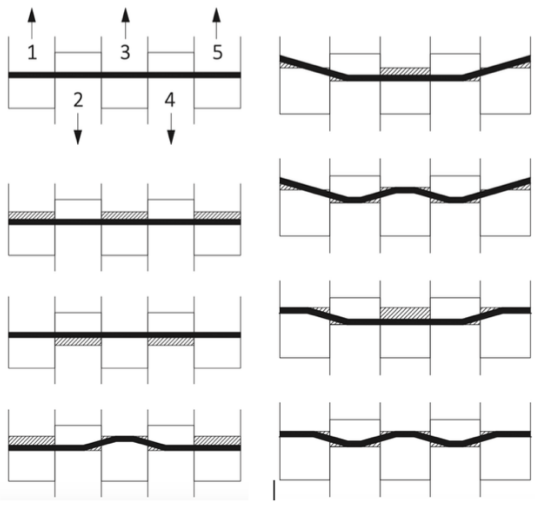

Figure 2-10 – Possible failure modes of a connection with four shear planes (Blaß & Sandhaas, 2017).

The approach for calculating the capacity of a multiple shear plane connection follows the failure modes described in EC5 with the corresponding formulas. The total load-bearing capacity of the multiple shear plane connection is the sum of the capacities of each shear plane. The method for connections with four shear planes is illustrated in Figure 2-11, where symmetry of shear planes 1 and 5, and 2 and 4 is assumed.

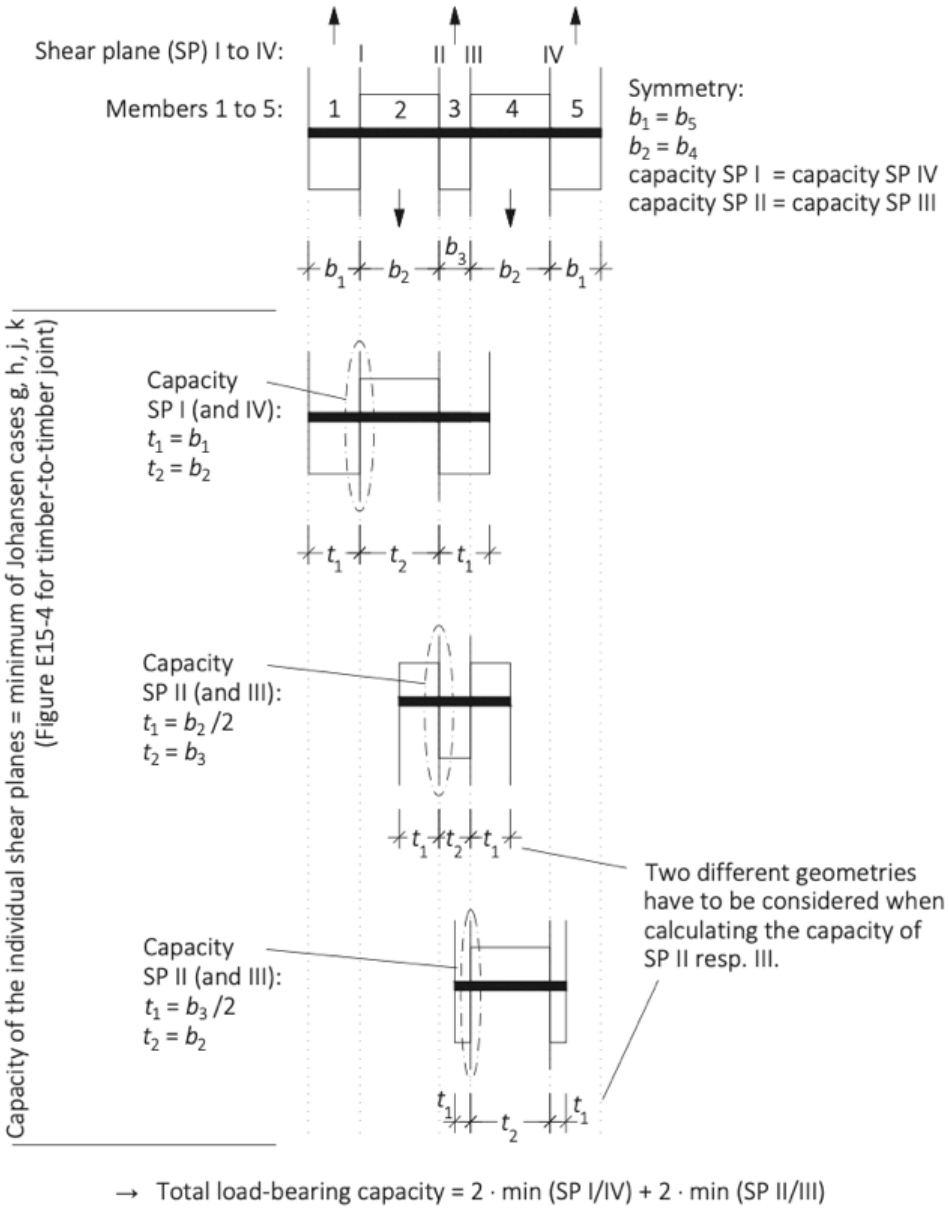

Figure 2-11 – Step-by-step approach for calculating the load bearing capacity of a four shear plane timber to timber connection (Blaß & Sandhaas, 2017).

2.6 Load Distribution example of Beam-Column Connection

An Ultimate Limit State (ULS) design example is made to get an approximation of the forces acting on a realistic beam-column connection. It is based on a multi-storey glulam office building with a 300 mm thick combi slab (200 mm CLT and 100 mm reinforced concrete) as floor. The slab is supported by glulam beams (165 mm x 630 mm) which are 8 meters long and are attached to continuous columns. The beams have a 3,6-meter center to center distance. The column in this example is a regarded as a central column.

The load calculation is based on the self-weight of the materials and generic imposed loads. The self-weights are calculated and transformed into line loads on the beams. The national annex in EN-1991-1-1 recommends an imposed load of 3,0 kN/m^2 in office buildings (NS-EN 1991-1-1:2002, 1991). The design line load on the beam is then calculated to be 31,8 kN/m, which leads to a lateral force of 127,2 kN on the connection from each beam, resulting in a reaction design load of 254,4 kN on the column screw group. An illustration of the calculated design loads on the connection is showed in Figure 2-12, and the entire calculation is attached in Appendix A – Connection Example.

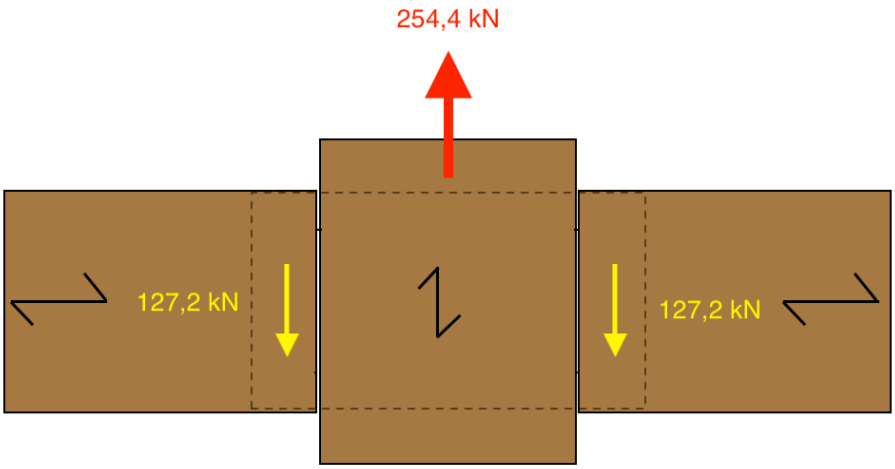

Figure 2-12 – An example of realistic lateral loads acting on a beam-column connection with beams of 8 m length and a center to cecnter beam distance of 3,6 m. The connection components are not displayed at scale.

3 Experimental Investigations: Materials and Methods

This chapter presents the specifications of the various materials, test groups, equipment and methods used in this research. Finally, the use of a FE (Finite Element) model of the plywood plates is presented. For the experiment, specimens were constructed by hand with materials provided by the various collaborators. The samples consisted of glulam made of Norwegian spruce, plywood made of Finnish birch, wood screws, and construction grade glue. A custom-made steel construction was designed, and then produced by the faculty workshop, to fix the specimens into place while tested in the hydraulic press machine.

3.1 Glulam

The glulam elements used in this project were produced and cut at Moelven Limtre AS. The glulam was generously donated and delivered in two batches, one for the preliminary tests and one for the main tests. The quality of the glulam was GL30c with a lamella thickness of 45 mm, which is the standard quality and lamella thickness for straight beams. The use of GL30c gave a characteristic density of 390 kg/m^3 and a mean value of 430 kg/m^3, which was the most relevant parameter in the calculations. The elements were cut into desirable sizes from a 115 mm x 270 mm beam. The elements were had dimensions 270 mm x 270 mm, and a thickness of respectively 35 mm and 55 mm depending on the configuration, illustrated in Figure 3-1. The squared design gave the opportunity to use the same elements for different grain directions in the experiments.

Figure 3-1 – Glulam elements picked up at Moelven Limtre AS, ready for specimen production.

3.2 Plywood

The plywood used in this research is made from birch grown in Finland. It is made up of 15 plies; eight plies in the longitudinal direction and seven plies in the transversal direction, with a total thickness of 21 mm. The plywood for the main tests was generously donated from Metsä Wood, and the small amount used in the preliminary tests were bought at a local distributor. The mechanical properties of the plywood were the same for both the preliminary and main tests.

The difference in characteristic and mean density for the plywood equals a percentage increase of around 8 % from characteristic to mean value. When plywood capacities are considered in this work, mean values are often used. The mean capacities are not listed in the declaration of performance for the plywood. Therefore, the mean values are assumed to be 1,10 times the characteristic capacities in this research (Metsä Wood, 2019).

The plywood plates were delivered in sizes of 3000 x 1500 mm. The most relevant plywood characteristics of this research are given in Table 3-1.

Table 3-1 – Sample of the essential mechanical characteristics of birch plywood (Metsä Wood, 2019). ρ_m refers to the mean density. $f_{m,k}$, $f_{t,k}$, $f_{c,k}$ and $f_{v,k}$ are the characteristic bending, tension, compression and shear stress capacities respectively.

Parameter	ρ_m [kg/m^3]	$f_{m,k}$ [MPa]	$f_{t,k}$ [MPa]	$f_{c,k}$ [MPa]	$f_{v,k}$ [MPa]
Value	680	39,4	39,0	27,0	9,5

3.3 Screws

Fully threaded, self-tapping screws (VGZ) delivered from Rothoblaas, were used. The screws are made of carbon steel, with high strength properties. They are usable in different wood products, in connections, as splitting reinforcement in wood, and as timber coupling. The screw diameters used were 7 mm of lengths 160 and 180 mm, and 5 mm with length of 120 mm. The mechanical characteristics in Table 3-2 were used and taken from the manufacturer's data sheet (Rothoblaas, 2019).

Table 3-2 – Mechanical properties of the VGZ screws from Rothoblaas (Rothoblaas, 2019) $M_{y,k}$, and $f_{ax,k}$ refers to the characteristic yielding moment capacity and withdrawal stress capacity.

Screw type	**VGZ 7 mm**	**VGZ 5 mm**
$M_{y,k}$ [Nmm]	14174	6876
$f_{ax,k}$ [N/mm^2]	11,7	11,7

3.4 Glue

Two kinds of glue have been used in this project. A polyurethane (PU) glue from Essve was used for the unsymmetrical configurations in both the preliminary and main tests, to reinforce the dowel hole from embedding failure (ESSVE Norway, 2019).

Ronny Bredesen from Dynea assisted with helpful consulting of what glue should replace the screws in some glued test groups. A MUF-system (Melamine-Urea-Formaldehyde) Prefere 4546 with the hardener Prefere 5022 was chosen for this purpose. It is approved for gluing hardwood to softwood like birch to spruce, whereas the PU glue is not. The adhesive Prefere 4546 is also well suited for use in load-bearing timber structures and is used by Moelven, among others, in their glulam products. The adhesive is weather- and waterproof and is classified for Norway spruce, Scots pine, and birch, among others. It has good creep properties and requires a low curing pressure, which made the production of the specimens in this experiment easier (Dynea, 2019).

3.5 Preliminary Tests

Before starting with the main tests for this project, preliminary tests were conducted to unveil problems or detect errors in calculations. The preliminary tests were also helpful for determining that the equipment was working properly. Training in the use of equipment was implemented to prevent user errors during the main testing.

The preliminary test groups were two types of unsymmetrical configurations and one symmetrical configuration. The unsymmetrical ones were illustrating a beam with slotted-in plates. These plates were respectively long and short (long and short eccentricity from the load). The symmetrical configuration was portraying a column-beam-column situation, where the beam element was connected to the column elements with two slotted-in plywood plates.

3.5.1 Experiences and measures

Several problems surfaced during the preliminary tests, interfering with the results. Some of these are presented in Figure 3-2:

- the specimens with two plywood plates slotted in had glulam elements with a thickness of only 35 mm. It became clear that this thickness, in reality, could be too narrow for screws of diameter 7 mm with the screw distance used. Glulam splitting occurred before plywood failure in all tests;
- the rotation was so severe in the unsymmetrical samples that the plywood plates collided with the steel plate on top of the specimens, increasing the stiffness before failure;
- the symmetrical column-beam-column setup turned out to be unfavorable, as the forces from the screws acted perpendicular to the glulam grain direction of the middle glulam element, leading to splitting;
- in the symmetrical specimens, there was a gap of 10 mm between the plywood plates in the middle. Due to the rotation of the plates, they collided at the top before failure was reached.

Figure 3-2 – Complications experienced in the preliminary testing. The top row presents issues from the symmetrical tests (splitting and collision of plywood plates) and the bottom row from the unsymmetrical tests (splitting and collision between plywood and steel plate).

Several measures were implemented ahead of the main tests to enhance the test configuration:

- the middle 35 mm glulam elements of each 2-plate specimen were reinforced against splitting by inserting Rothoblaas VGZ 5 mm wood screws into the glulam to increase splitting resistance;
- reinforcing strips of plywood were glued to the outside of each outwards-facing glulam element, to prevent splitting;
- the symmetrical configuration was changed from column-beam-column to beam-column-beam to reduce the risk of splitting in the middle element, as well as it is more comparable to a real situation;
- the plywood plates in the symmetrical configuration are changed to be continuous throughout the whole specimen, instead of two separate ones. This made it possible to increase the distances between the screws in the column element;

- the screw rows in the middle glulam element in the symmetrical configurations were adjusted so that the screws were placed some distance offset from the screw row line to prevent splitting between the screws;
- holes in the glulam were predrilled in order to reduce the risk of splitting between the holes, due to short distance between the screws.

3.6 Specimen Production

The process of producing the specimens started by cutting the plywood into desired sizes. The glulam was delivered pre-cut. 4 mm holes, recommended by Rothoblaas, were pre-dilled in all of the glulam elements. The reinforcement plywood was glued onto the glulam with the MUF adhesive delivered by Dynea. The glulam parts were then stacked on each other with a heavy object on top to create sufficient pressure for the curing process. The reinforcement for the dowel connection to the unsymmetrical specimens was glued with PU glue. The specimens were assembled by measuring and placing all the parts in the right place, followed by clamping to avoid gaps between the parts while inserting the screws, see Figure 3-3. An 18-volt hand drill was used for both pre-drilling and inserting screws. The screws were longer than the width of the specimens to make sure the screws were led entirely through the sample.

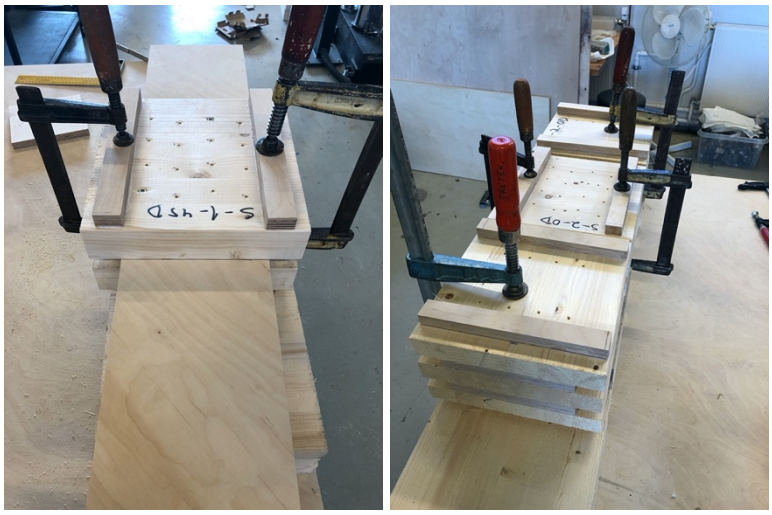

Figure 3-3 – Clamping of specimen components before inserting the screws, to avoid gaps between plywood and glulam.

The glued specimens were glued together with the MUF-system and then pressurized while curing. It was important to get a thin glue-line, to fully utilize the capacity of the glue. Figure 3-4 shows how pressure was applied. The screwed connections were assembled some days later when the glue had cured.

Figure 3-4 – Loading of glued parts for the curing process. Heavy steel objects were used to gain sufficient curing pressure.

Figure 3-5 – Collection of all the 24 finished specimens.

3.7 Test Specimen Geometry and Design

3.7.1 Test groups

There were done some changes from the preliminary test configurations due to the unexpected degree of rotation and splitting. Some new test groups were added to avoid splitting of the glulam. In total, eight test groups were designed, with three identical specimens produced for each test group, resulting in a total of 24 specimens. All test groups are explained in detail in this chapter. 3D models of all test groups are presented in Figure 3-12, Figure 3-13, and Figure 3-14. An identification code was made for each configuration. The first letter referred to the configuration: Symmetrical or unsymmetrical. The following number referred to the number of slotted-in plywood plates, and then a number which referred to the angle of the face grain of the plywood: respectively 0D and 45D. To the identification code for the glued configurations a "G" was added. The test group overview for the main experiments is as presented in Table 3-3:

Table 3-3 – Overview of all eight test groups, with a brief description.

Test group	Brief description
S-1-0D	Symmetrical setup. Three glulam elements connected to each other through one continuous birch plywood plate with 0-degree fiber orientation.
S-2-0D	Symmetrical setup. Three glulam elements connected to each other through one continuous birch plywood plate with 0-degree fiber orientation.
S-1-45D	Symmetrical setup. Three glulam elements connected to each other through one continuous birch plywood plate with 45-degree fiber orientation.
S-2-45D	Symmetrical setup. Three glulam elements connected to each other through two continuous birch plywood plate with 45-degree fiber orientation.
S-1-0D-G	Symmetrical setup. Three glulam elements connected to each other through one continuous birch plywood plate with 45-degree fiber orientation. The middle glulam element is fastened to the plates with glue instead of screws.
S-2-0D-G	Symmetrical setup. Three glulam elements connected to each other through two continuous birch plywood plate placed with 0-degree fiber orientation. The middle glulam element is fastened to the plates with glue instead of screws.
U-1-0D	Unsymmetrical setup. One birch plywood plate with 0-degree fiber orientation.
U-2-0D	Unsymmetrical setup. Two birch plywood plates with 0-degree fiber orientation.

Test groups S-1-0D and S-2-0D

Glulam elements of dimensions 270 mm x 270 mm were screwed together with 7 mm Rothoblaas VGZ screws, to fasten continuous birch plywood plates with dimensions 830 mm x 190 mm throughout the specimen. The specimens of test group S-1-0D had one plywood plate, while group S-2-0D had two. The lateral glulam on the sides represented beams, and the middle glulam represented a column with vertical grain direction. Each outer glulam element was reinforced against splitting with two vertical 260 mm x 30 mm glued-on plywood strips, placed 20 mm from the nearest screw. The sandwiched glulam elements of test group S-2-0D were reinforced against splitting with four 5 mm Rothoblaas VGZ screws, inserted as shown in Figure 3-7.

Test groups S-1-45D and S-2-45D

Test groups S-1-45D and S-2-45D were identical to S-1-0D and S-2-0D, with the exception of the plywood plates. The plywood had a face grain direction of 45 degrees to the horizontal axis instead of 0. The geometries of the test groups are presented in Figure 3-6 and Figure 3-7.

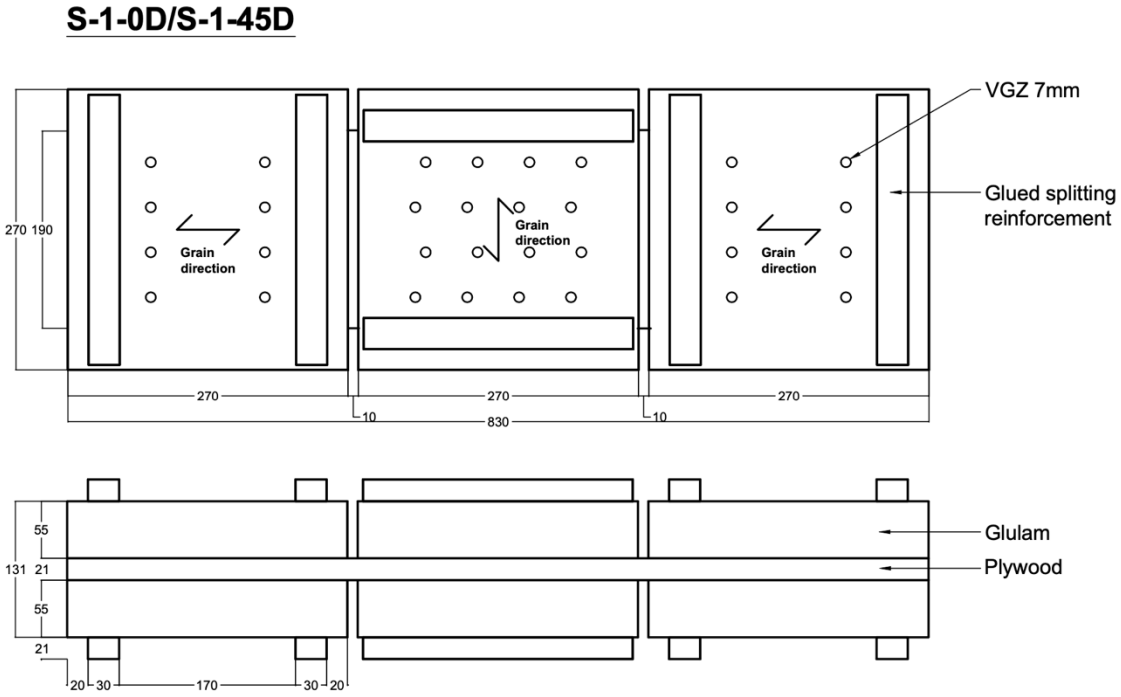

Figure 3-6 – Test specimen S-1-0D/S-1-45D. All dimensions are measured in millimeters. The grain directions symbolize the fiber orientation of the glulam.

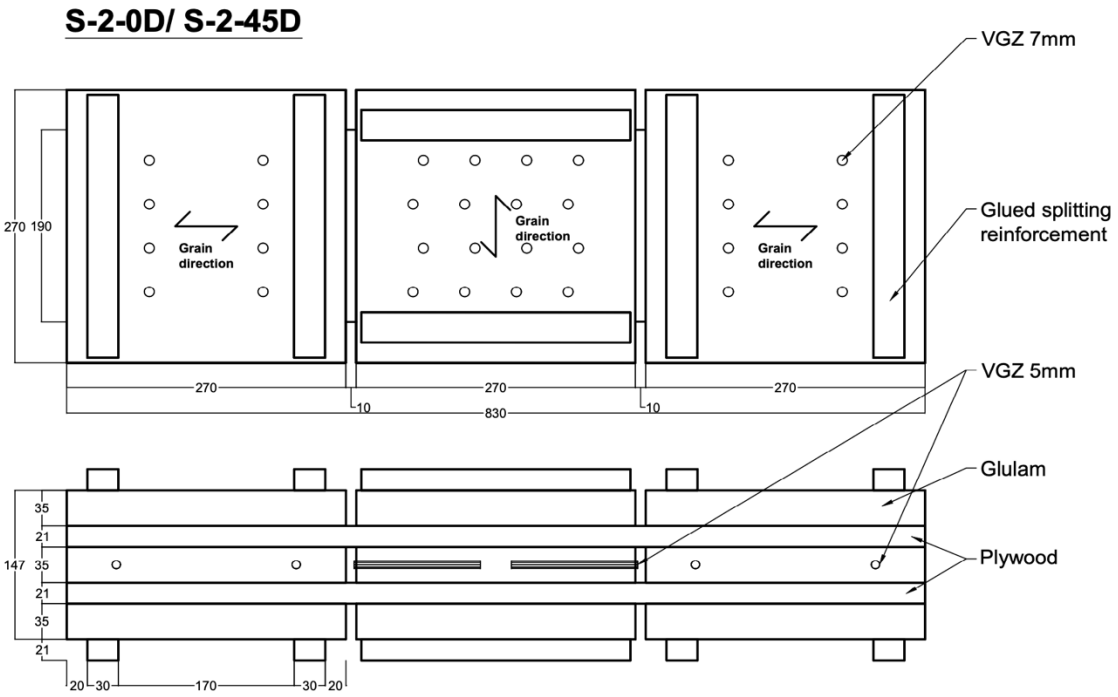

Figure 3-7 – Test specimen S-2-0D/S-2-45D. All dimensions are measured in millimeters. The grain directions symbolize the fiber orientation of the glulam.

Test groups S-1-0D-G and S-2-0D-G

Test groups S-1-0D-G and S-2-0D-G were identical to S-1-0D and S-2-0D, except for the column part of the specimen. Instead of having a connection of 16 screws, the column part was assembled with the MUF glue described in Chapter 3.4. Figure 3-8 and Figure 3-9 shows the glued configurations.

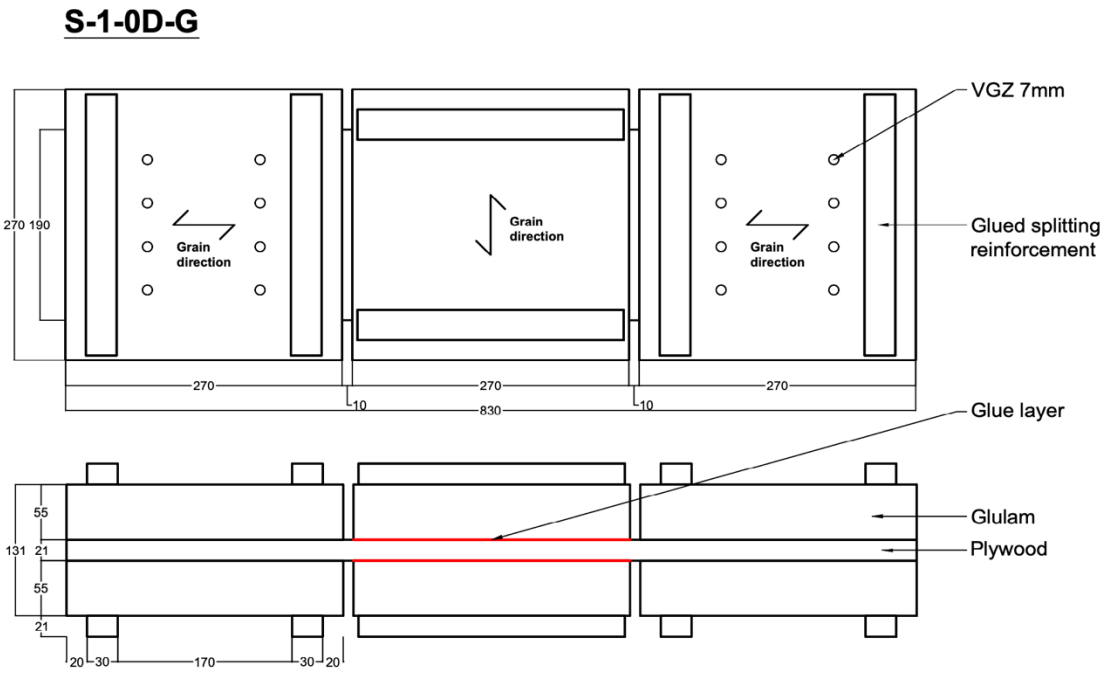

Figure 3-8 – Test specimen S-1-0D-G. All dimensions are measured in millimeters. The grain directions symbolize the fiber orientation of the glulam.

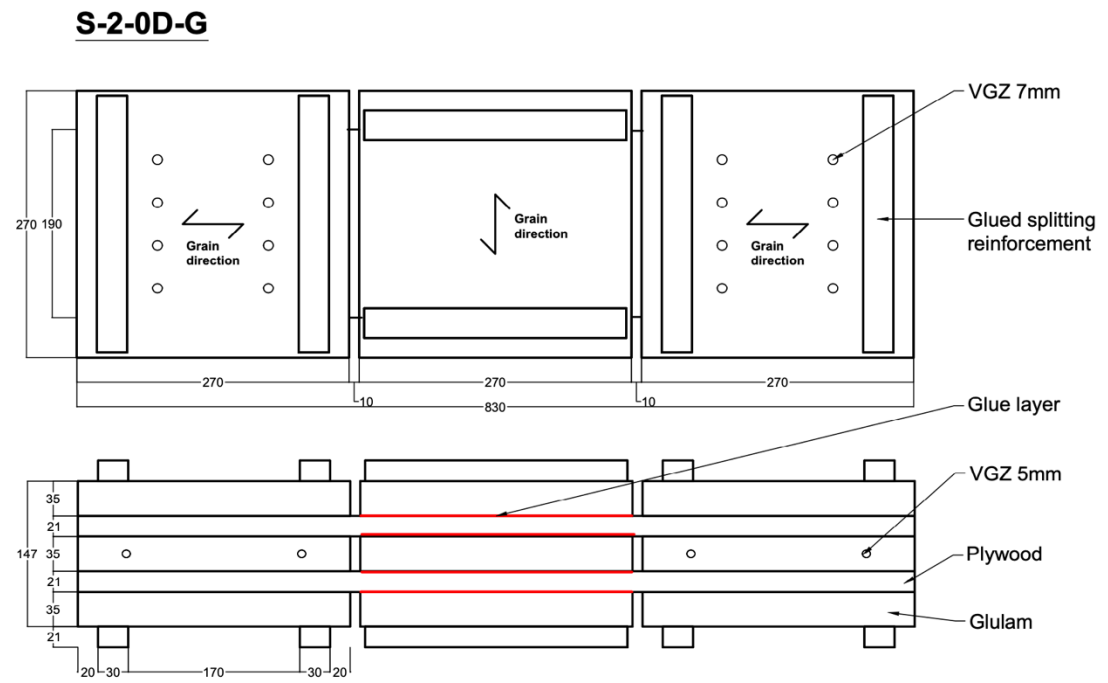

Figure 3-9 – Test specimen S-2-0D-G. All dimensions are measured in millimeters. The grain directions symbolize the fiber orientation of the glulam.

Test groups U-1-0D and U-2-0D

Glulam elements of dimensions 270 mm x 270 mm were screwed together with 7 mm Rothoblaas VGZ screws to fix the birch plywood plates with dimensions 495 mm x 190 mm. The grain direction of the glulam was horizontal, to represent a beam. The thickness of the glulam elements were 55 mm for U-1-0D and 35 mm for U-2-0D. Two vertical plywood strips with dimensions 260 mm x 30 mm were glued to the outside of each outer glulam element in both U-1-0D and U-2-0D. The sandwiched glulam element in U-2-0D was reinforced with four 5 mm Rothoblaas VGZ screws. A 32 mm hole was drilled in the plywood for the 30 mm dowel which was fixed to the testing machine. The hole was reinforced for embedding failure with two 170 mm x 190 mm plywood plates glued onto each side with PU glue. Illustrations with measurements are presented in Figure 3-10 and Figure 3-11.

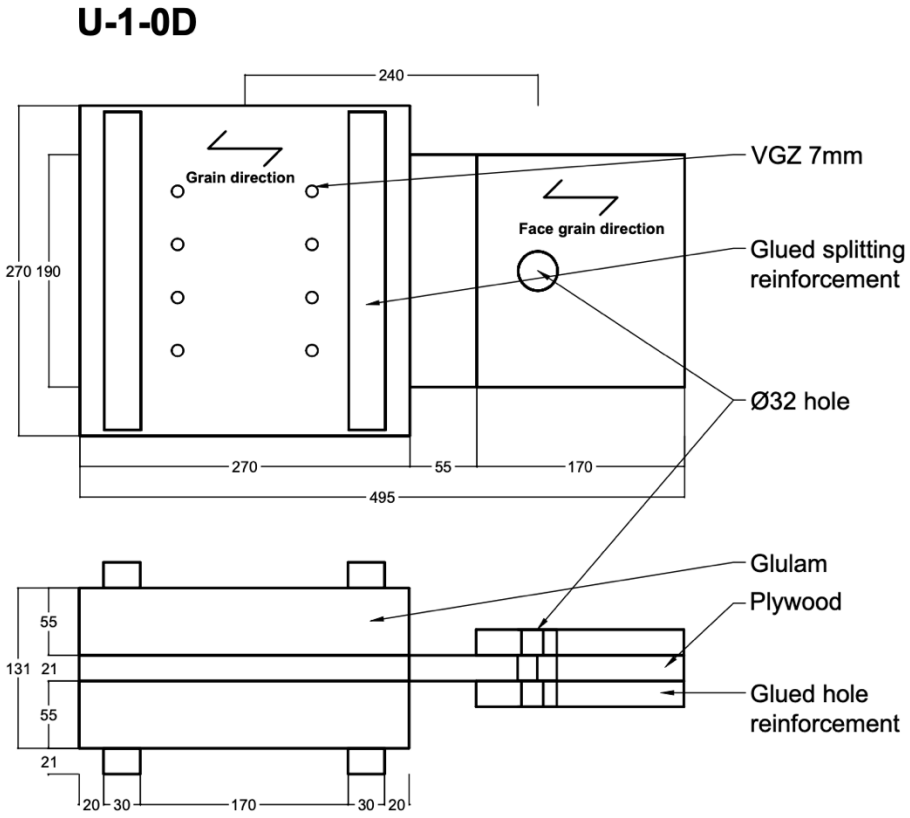

Figure 3-10 – Test specimen U-1-0D. All dimensions are measured in millimeters.

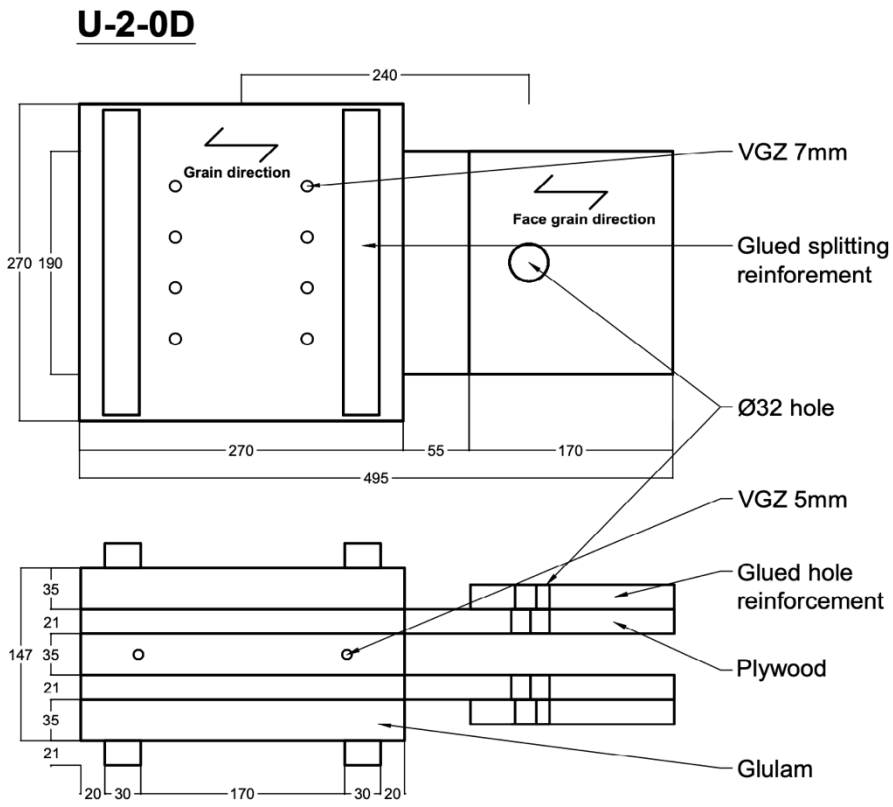

Figure 3-11 – Test specimen U-2-0D. All dimensions are measured in millimeters.

3.7.2 3D models of test group configurations

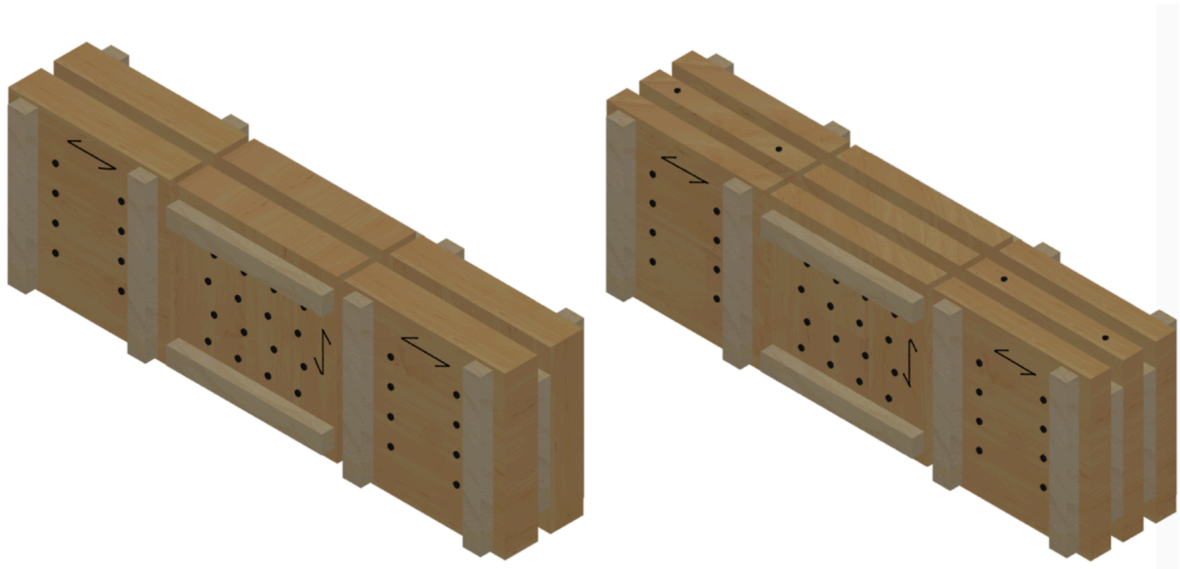

a) b)

Figure 3-12 – 3D models of test groups S-1-0D/S-1-45D (a), and S-2-0D/S-2-45D (b).

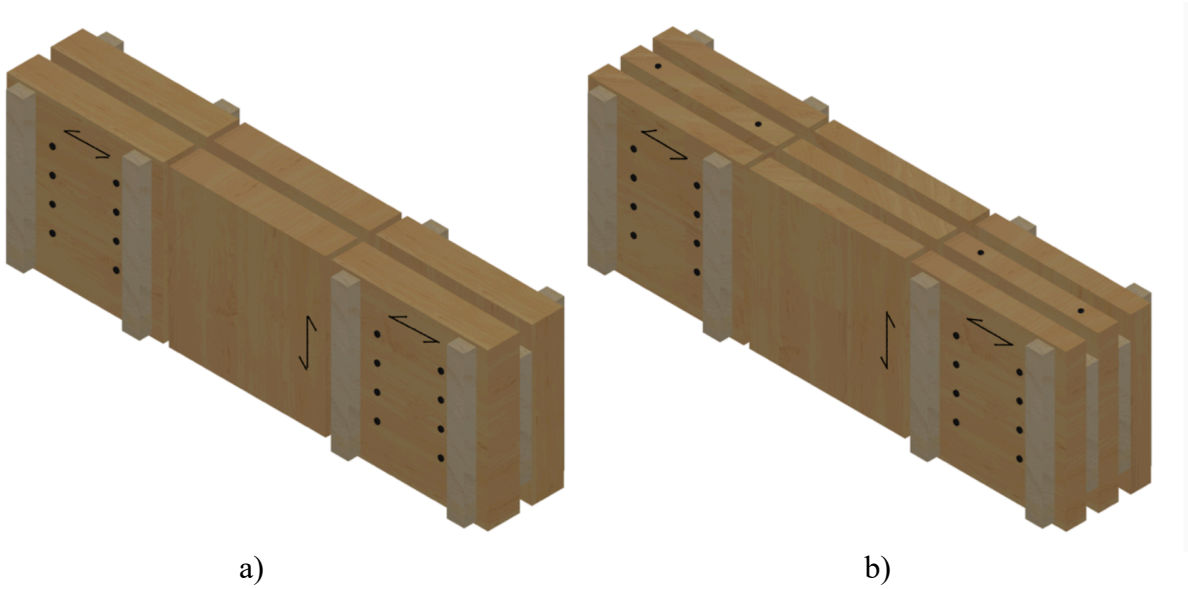

a) b)

Figure 3-13 – 3D models of test groups S-1-0D-G (a) and S-2-0D-G (b).

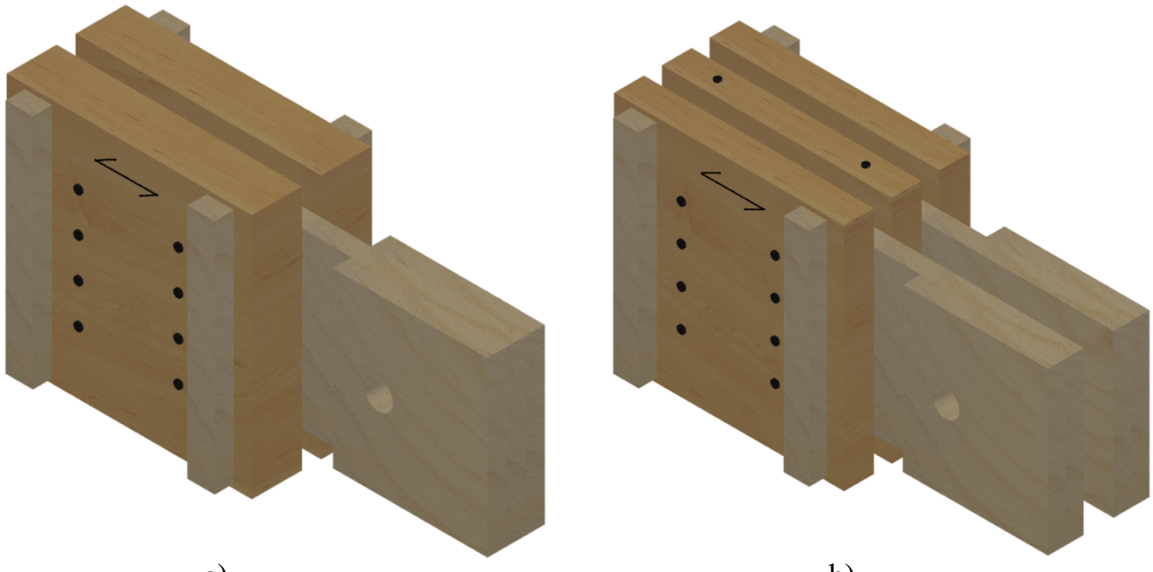

a) b)

Figure 3-14 – 3D models of test groups U-1-0D (a) and U-2-0D (b).

3.7.3 Screw geometry

The screw arrangement was checked against EC5 and is illustrated in Figure 3-15 (NS-EN 1995-1-1:2004, 2004). The screw arrangement for the unsymmetrical specimens was identical to the lateral screw groups of the symmetrical specimens.

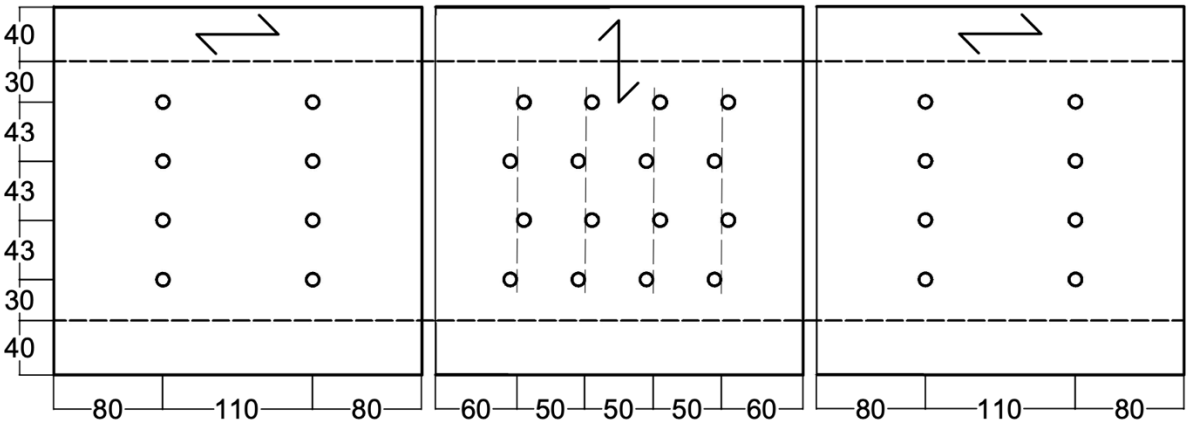

Figure 3-15 – Screw geometry of the symmetrical test configurations. All dimensions are measured in millimeters. The grain directions symbolize the fiber orientation of the glulam.

3.8 Hydraulic Press Machine

Both the preliminary and main experiments were conducted with the Instron SATEC series 8800 model 300 kN static hydraulic press machine pictured in Figure 3-16. The machine has a maximum load capacity of 300 kN and can measure global displacement data with a precision of 10^{-3} mm. The loads applied to the specimens were measured with the load cell included with the machine.

Figure 3-16 – INSTRON hydraulic press machine used in the experimental testing.

3.9 Steel Holding System

A steel holding system was used to fix the glulam part of the specimens in place and to transfer the load applied. Two steel systems were designed to fit three different configurations in the preliminary testing and two configurations in the main testing. The steel was designed and checked according to EC3, to avoid deformation or failure (NS-EN 1993-1-1:2005, 1993).

The symmetrical configuration was a downwards push test which required enough room for the mid element to deform downwards, see Figure 3-17. H-beam with steel plates welded on

both sides were used as supports for the specimens. The glulam was fixed to the supports with four threaded rods and a steel plate on top. A steel plate was designed and attached to the load cell to apply a uniform load on the mid element.

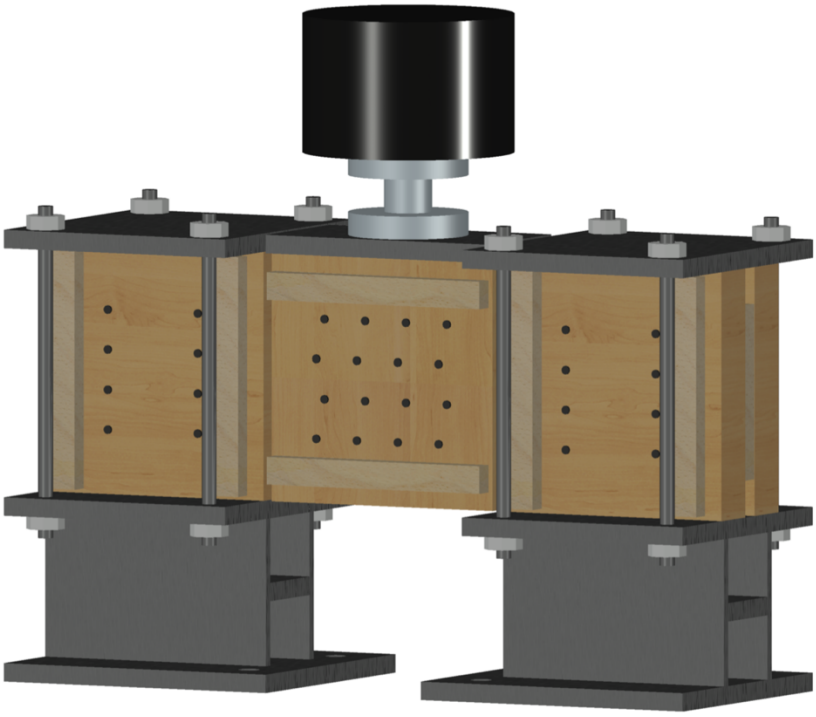

Figure 3-17 – 3D model of the steel system used in the symmetric configurations. The load is applied vertically downwards from the press machine.

The steel system for the unsymmetrical configuration was composed of a thick steel plate that was connected to the base of the testing machine. This plate was produced with threaded holes, which allowed screwing threaded steel rods into the plate. The glulam part of the specimens was fixed to the plate with four threaded rods and a steel plate on top. The load was applied upwards through a steel dowel connected to two steel bars, which were connected to a steel plate attached to the load cell. See Figure 3-18 for a 3D model of the steel setup for the unsymmetrical configuration.

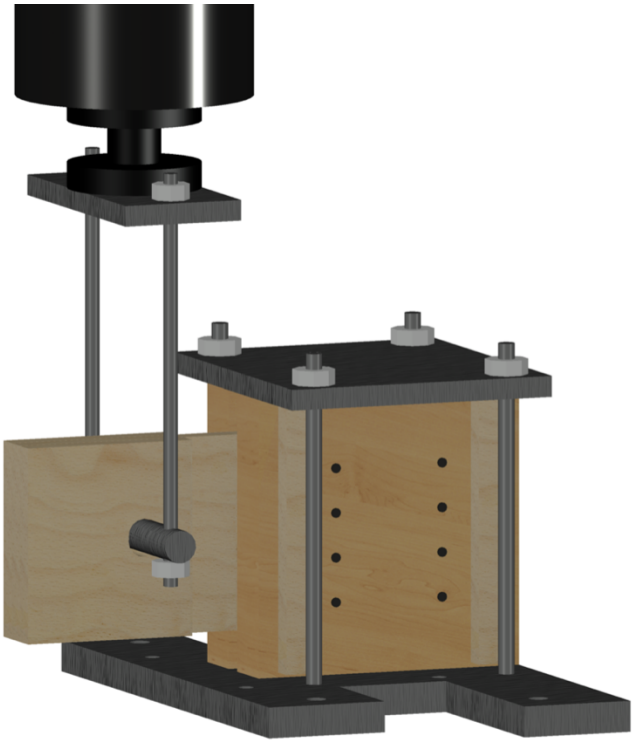

Figure 3-18 – 3D model of the steel system used in the unsymmetric configurations. The load is applied to the plywood vertically upwards from the dowel.

3.10 Displacement Measurements

To measure the vertical displacement of the specimens of the main testing, multiple LDT 50 mm displacement transducers made by Italian company AEP, were used. The transducers measure linear displacements with a high resolution of measure, below 1 μm. The 50 mm model used in this work had a maximum measurement span of 50 mm, and the instrument had a total length of 233 mm, not including the cable attachment. (AEP Transducers, 2020) The displacement data was transmitted to the computer through voltage signals of 2 millivolt/volt, later transformed to millimeters through a Python script. The transducer model used (with measures) is illustrated in Figure 3-19.

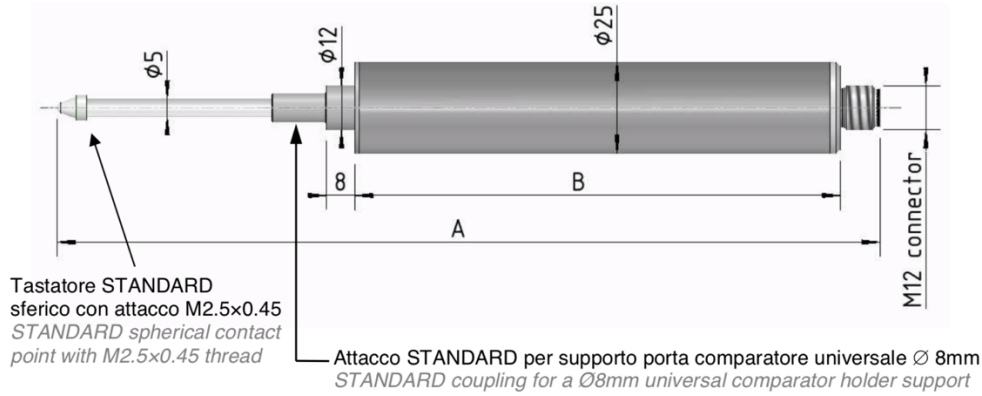

Figure 3-19 – Illustration showing the measurements of the AEP LDT 50 mm transducer (AEP Transducers, 2020). Dimensions are measured in millimeters.

To measure the local displacement, two displacement transducers were used to gather the vertical displacement for all the test groups, and one additional one was used for the unsymmetrical test groups, U-1-0D and U-2-0D, to measure the rotation of the plywood plate around the screw group center. To make sure that the transducers were fixed in place with no chance of vibrations or movements affecting the measurements, they were attached to two standing steel frames, screwed in place to the bottom of the hydraulic press and was used for the six symmetrical test groups, see Figure 3-20 a). For the two unsymmetrical test groups, these steel frames were replaced with smaller steel angles that fit the unsymmetrical configuration better, pictured in Figure 3-20 b). The vertical movement in all test groups was transmitted by a stiff plywood rod connected to the specimen.

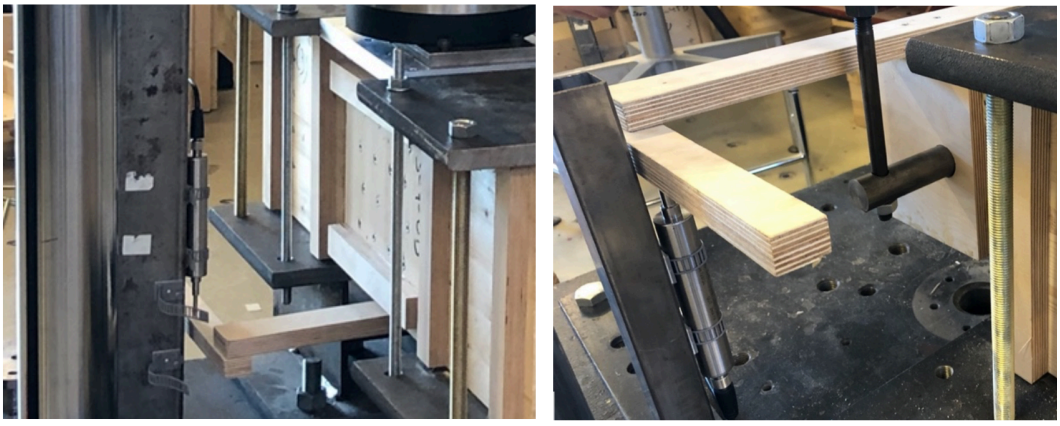

a) b)

Figure 3-20 – Demonstration of how the symmetrical (a) and unsymmetrical (b) test groups were connected to the vertical displacement transducers on each side.

The rotation of the plywood plate in the unsymmetrical test groups was also measured using an AEP LDT 50 mm linear transducer. The instrument measured the inwards movement of the bottom corner of the plate as it rotated upwards, see Figure 3-21. The exact rotation was calculated by measuring the distance from the plate and screw center to the transducer and then plotted as a graph through a Python script.

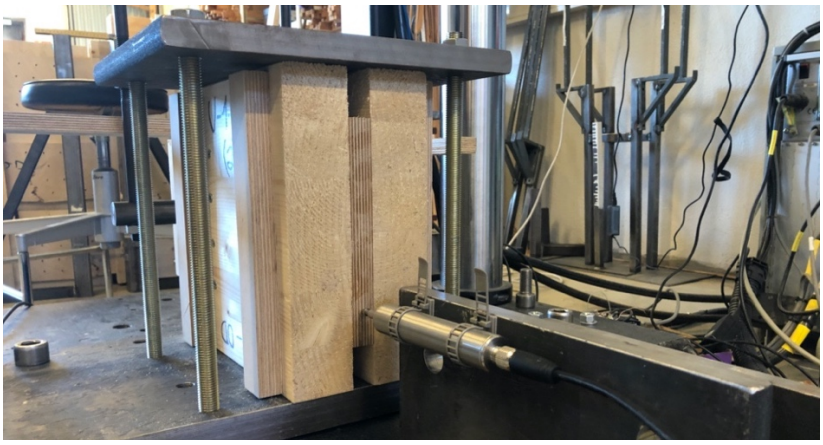

Figure 3-21 – Rotation measurement setup. The rotation about the screw group was calculated from the displacement data from the shown transducer.

3.11 Testing Protocol according to EN26891:1991

All tests were conducted while following the European Standard (NS-EN 26891:1991, 1991). This standard presents principles that should be followed in order to achieve test results that are comparable to related tests performed in different laboratories. The standard is mainly applicable to joints for statically loaded timber structures made with mechanical fasteners but can also be used for other joints.

When performing tests, a specific loading procedure had to be followed and programmed into the software controlling the press machine. The variable F_{est} was calculates as the estimated maximum load of the joint. The standard allows this variable to be lowered or adjusted if experience or preliminary tests show a different F_{max} than what was calculated. The procedure is shown visually in Figure 3-22. The load was initially increased from zero up to $0{,}4F_{est}$ and maintained for 30 seconds before it was lowered to $0{,}1F_{est}$. Then again, the load was maintained 30 seconds before increasing until failure. The constant loading speed was set to $0{,}2F_{est}$ per minute(NS-EN 26891:1991, 1991). This cycle was used to let the fasteners "set" in the connection before the load was increased from $0{,}1F_{est}$ to failure.

Based on the experiences from the preliminary testing, F_{est} was chosen to be lower than what was estimated. This was because the preliminary results showed early plastic behavior of the joints. Ideally, the cycle mentioned in the previous paragraph should be within the elastic region of the stress-strain diagram. F_{est} was set to 35 kN for the one-plate symmetrical test groups, 70 kN for the two-plate symmetrical test groups, and respectively 30 kN and 40 kN for the unsymmetrical test groups.

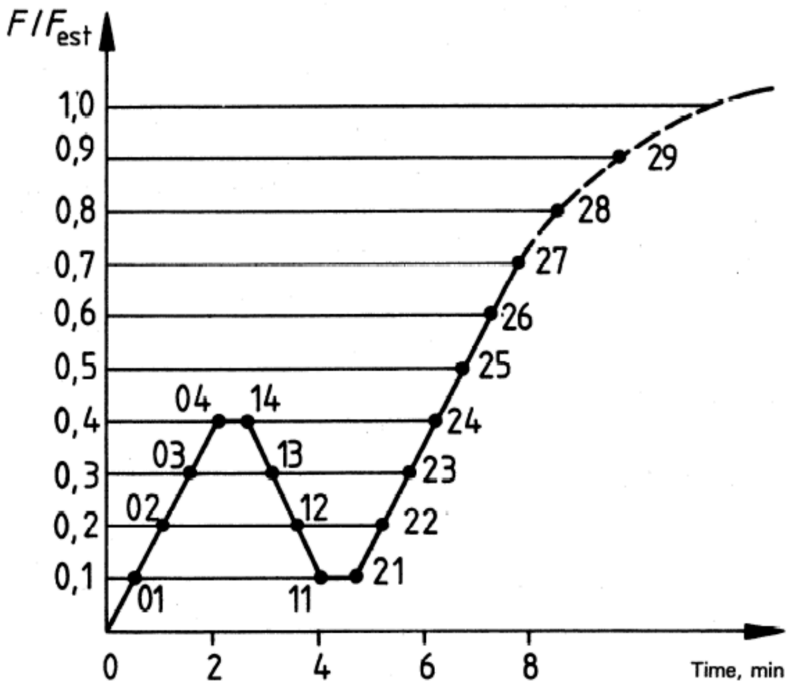

Figure 3-22 – Loading procedure. Point 01 – 11 shows the preloading stage. Load increases until failure from point 21 (NS-EN 26891:1991, 1991).

The standard also requires attention to the condition of the timber before manufacturing of the joint, to portray a realistic joint in a structure. This is to account for moisture content affecting the strength properties of the timber, as well as gaps occurring as a consequence of shrinkage. Conveniently, the lab used in this project has an air humidifier which controls the humidity in the lab to stay at 60%, maintaining a moisture content of approx. 12% in the timber.

3.12 Data Processing

3.12.1 Testing software

The software which controlled the hydraulic press machine was programmed to follow the loading pattern presented in the former chapter. The pattern is visible on the panel to the right in Figure 3-23. The panel to the left in the figure shows the load-deformation curve for each test, with position data gathered from the vertical movement of the load cell. Before starting the load cycle, an estimated force F_{est} had to be determined for each test group. In this work, F_{est} were set to the calculated values for the preliminary tests and then lowered for the main tests to make sure $0{,}4F_{est}$ was within the elastic area of the curve.

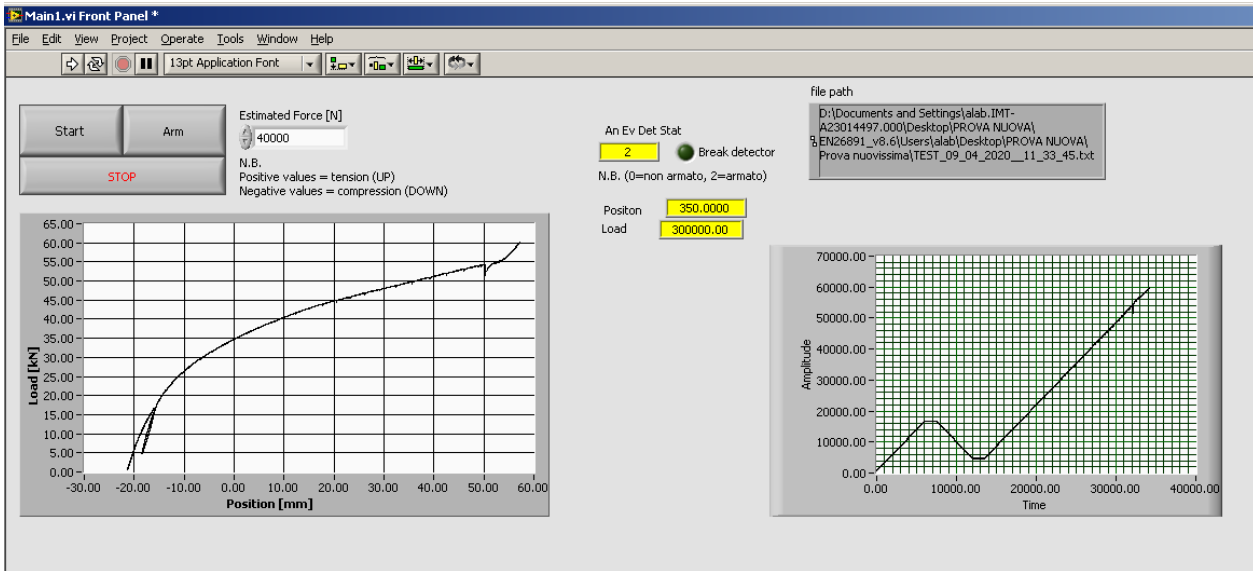

Figure 3-23 – Hydraulic press operating software used in the tests. The load-deformation curve is shown to the left and the loading pattern from Chapter 3.11 to the right.

The press operating software and the LabView software connected to the local displacement transducers generated .txt files contained the force applied and the corresponding displacement values, and through a Python program, the data files were transformed into relevant graph plots and mechanical parameters were calculated.

3.12.2 Data processing in Python

To process data and plot the results, Spyder was used. Spyder is a powerful scientific program written in the Python language. The script was carefully designed to get the desired plots of the test results. Excerpts from the programs are attached in Appendix E – Python Scripts.

3.13 Mechanical Parameter Explanations

The data files acquired from the testing were ran through a Python script to gather various mechanical parameters for each test group. Most of these parameters are illustrated in Figure 3-24, which is the force-deformation diagram for test specimen S-1-45D (3).

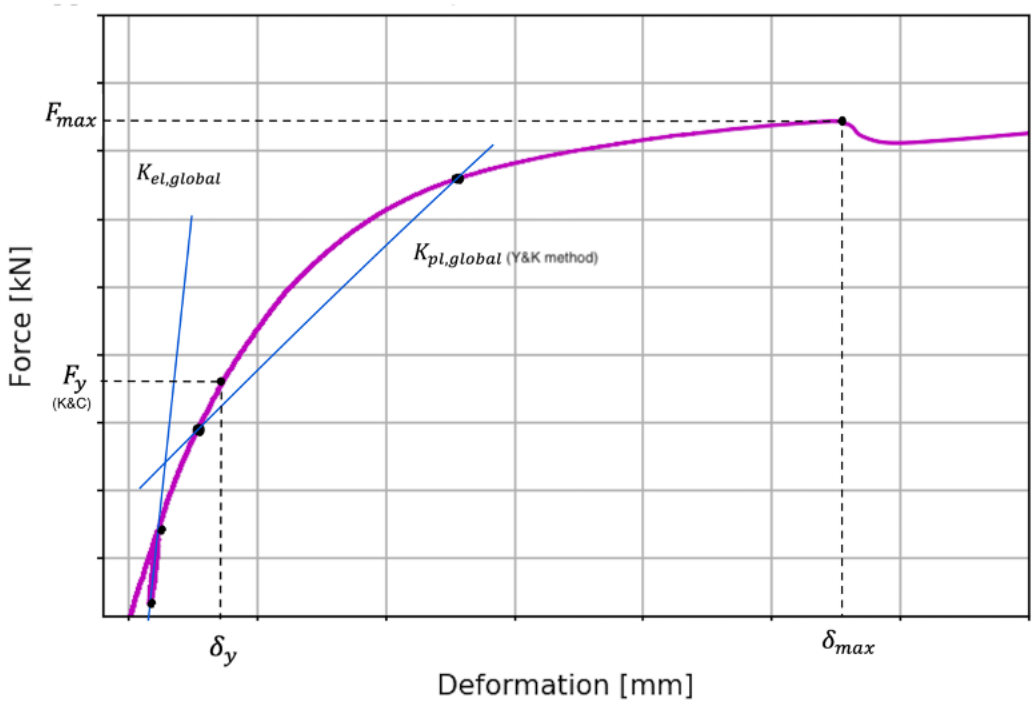

Figure 3-24 – Force-Deformation diagram illustrating mechanical parameters calculated for each test group.

F_{max} is the maximum load achieved before failure of the test specimen. δ_{max} is the corresponding maximum deformation. F_y is the yield point load of the connection. This value was found by using the method of (Karacabeyli & Ceccotti, 1996), due to the simplicity and the fact that the yield point matched relatively well with the load-deformation curves in this experiment, compared to other methods. δ_y is the corresponding deformation present at the yield point. The ductility ratio D_u was calculated to describe and compare the ductility of the different test groups.

It needs to be clarified that the stiffness values calculated for each specimen in this work, were not the same as the stiffness, or slip modulus, usually found with the methods explained in Chapter 2.4.3. In this work, K_{global} was found, which described a global stiffness for the whole system and not only the slip between the glulam and the plywood. $K_{el,global}$ was the global elastic stiffness, and $K_{pl,global}$ was the global plastic stiffness of the connection.

$K_{pl,global}$ was calculated using the method from (Yasumura & Kawai, 1998) described in 2.4.3. Normally, both $K_{pl,global}$ and F_y is found with this method. Since the goal was solely to compare the different test groups, this was regarded as unnecessary. $K_{el,global}$ was found with the Eurocode method also presented in Chapter 2.4.3 (NS-EN 26891:1991, 1991). For the unsymmetrical test, also the maximum rotation (φ_{max}) was included.

It also has to be pointed out that since the local displacement transducers turned out to be useless for test groups U-1-0D and U-2-0D due to excessive deformation, displacement data were gathered from the hydraulic press for these samples. This lowered the accuracy since this deformation was global and did not only include the connection deformation, but also included tiny deformations in the steel holding system.

3.14 Density and Moisture Measurements

Both density and moisture content have a significant effect on the wood based material's mechanical properties (Kollmann & Cöté, 1968). Measurements on the moisture content and density of the glulam were conducted to compared to normal and recommended values to see if they deviated enough to make an impact on the results of the tests.

Six cubes of equal dimensions were cut out from random leftover glulam, both the 35 mm and 55 mm thick elements. The chosen cubes were made sure to have been from elements with the opportunity to absorb and emit moisture from the air. Six cubes were cut from six glulam elements and was chosen to be measured. The amount of imperfections such as knots that could affect the weight was considered. Since the glulam used was combined, the cubes were cut from the middle part of the glulam cross-section where the screws were inserted in the specimens. This part of the cross-section should, in theory, have a lower density than the outer parts.

3.14.1 Density of glulam

The density of the glulam cubes was measured by calculating the volume of each cube and then weighing the exact weight. The density was calculated by Formula 3.1:

$$\rho = \frac{m}{V} \tag{3.1}$$

Where:

m The mass in kg

V The volume in m^3

A Heidenhain dimension measurer with an accuracy of 0,001 mm and a Sartorius digital scale with an accuracy of 0,01 grams, were used to do the density calculations.

The overview of the different densities calculated is illustrated in

Appendix B – Density and Moisture Values . The mean density was calculated to be 474,25 kg/m^3. This deviates quite a bit from what is stated for GL30c in Limtreboka, which is 430 kg/m^3 (Norske Limtreprodusenters Forening, 2015).

3.14.2 Moisture content of glulam

The moisture content of the glulam was measured by the weighing and drying method. This method compares the weight of the cubes before and after drying to a moisture content of zero and divide by the dry weight to obtain the moisture content in percent (%) of the cube's mass in absolute dry condition. The cubes were weighed at normal conditions, put in a drying cabinet at 103 degrees Celsius for 24 hours, and then weighed again. After removing the dry cubes from the cabinet, they were instantly placed in a desiccator (airtight glass container with silica gel crystals in the bottom). This was to prevent the air from affecting the moisture content of the cubes while they cooled down, as the temperature may have an influence on the weight. The cubes were then weighed directly after removal from the glass container and the moisture content was calculated by following Formula 3.2:

$$w = \frac{m_w - m_0}{m_0} * 100 \qquad 3.2$$

Where:

m_w The mass of the wood before drying

m_0 The mass of the wood after drying

The table with each cube's measurements can be found in

Appendix B – Density and Moisture Values . The average moisture content calculated was 11,04 % and therefore in accordance with the recommended value for construction timber, which is between 10 – 12 % (Kollmann & Côté, 1968).

3.15 SAP2000 Modeling

A finite element model of the plywood plate was made to investigate the estimated distribution and magnitude of stresses. SAP2000 (a structural FE software for analysis and design) was used in this investigation. Models were made to estimate and locate the maximum theoretical stresses, and then compare these to the material capacities and failure locations. The method was simplified by modelling the plates as beams. SAP2000 allows determines the deflection, but this was not done due to the complexity of plywood and the simplicity of the model. Different support compositions imitating the screws were modeled to find the most realistic one. For the symmetrical test groups, one pinned support with a rotational spring was decided to be the best imitation of each lateral screw group. The supports were located in the middle of the screw groups. The stiffness values for the rotational springs were calculated by Formula 3.3 (Swedish Wood, 2013):

$$k_{\varphi} = K_{ser} I_p \qquad 3.3$$

Where:

k_{φ} Rotational stiffness of the screw group [Nmm]

K_{ser} Estimated stiffness per fastener per shear plane [N/mm]

I_p Polar moment of inertia of the screw group [mm^2]

In the SAP2000 model for the unsymmetrical test groups, each screw row was represented by one pinned support, as this configuration gave a more correct moment and stress distribution to describe the failure.

An important aspect of the modelling was the load application. The models for the screwed symmetrical configurations had a 150 mm distributed load applied in the area between the screw columns on the mid-element, showed in Figure 3-25. For the glued symmetrical tests, a 270 mm uniform load was applied on the middle of the plywood plate, showed in Figure 3-26. This was the area the force was transferred from the glulam to the plywood due to the glued mid-element. For the unsymmetrical configurations, the load was modeled as a point load, as illustrated in Figure 3-27. The load applied to each configuration in the models was the mean maximum force F_{max}, turned into a line load for the symmetrical configurations.

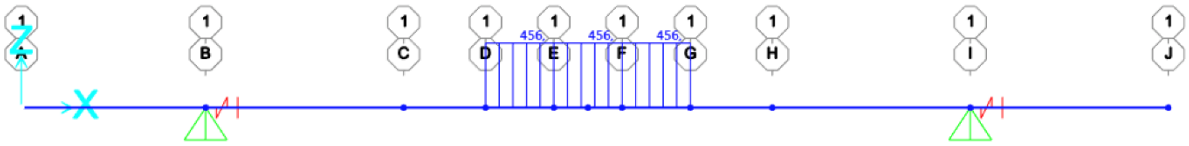

Figure 3-25 – The applied load on S-1-0D in SAP2000. The unit of the line load is N/mm. The line load was calculated with the mean F_{max}, and the screw group width.

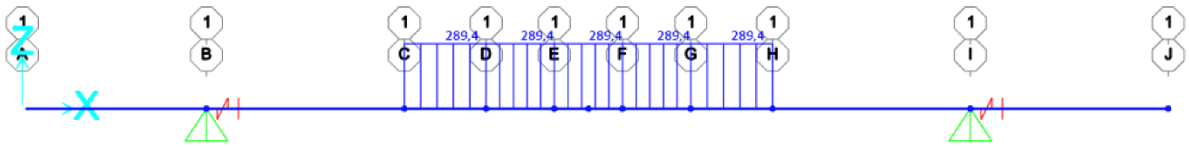

Figure 3-26 – The applied load on S-1-0D-G in SAP2000. The unit of the line load is N/mm. The line load was calculated with the mean F_{max}, and the glulam width of the column element.

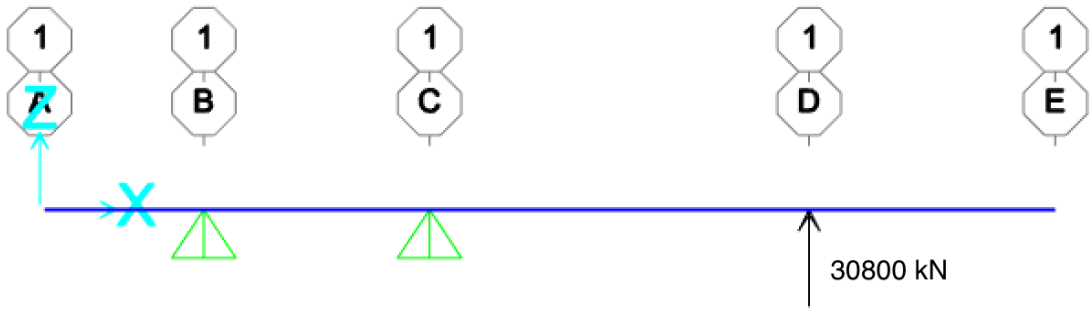

Figure 3-27 – The applied point load on U-1-0D. The point load is the mean F_{max} for the test group..

Figure 3-28 shows the exaggerated deflection mode of a loaded screwed plywood plate. For the glued connection, rotational constraints were modeled on the mid-element. The reason for this was that the strong glue did not allow the plywood to bend inside the mid-element. This

was found to be the most realistic implementation. Figure 3-29 shows the deflection mode of a loaded glued plywood plate, assuming the glue bond does not fail:

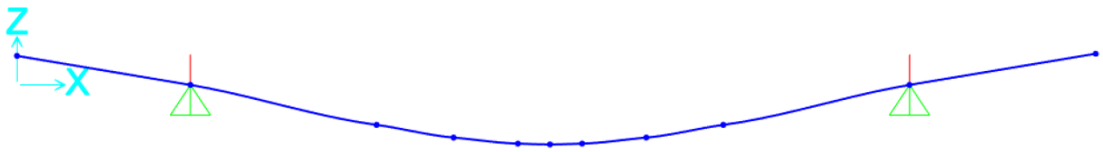

Figure 3-28 – The exaggerated deflection mode of the plywood with a screwed column connection. The model considers the plywood as a beam with two pinned supports with rotational springs to represent the lateral screw groups.

Figure 3-29 – The exaggerated deflection mode of the plywood in test groups S-1-0D-G and S-2-0D-G. The model considers the plywood as a beam with two rotational springs to represent the lateral screw groups. The glued part of the plywood is modeled with rotational constraints to avoid deflection of the plywood in this area.

Each test group model was analyzed with a load equal to its average F_{max} (presented in Chapter 4.1). The corresponding stresses were found and compared with the mean material capacities in tables in Chapter 4.2. The differences are then discussed in Chapter 5.3.1.

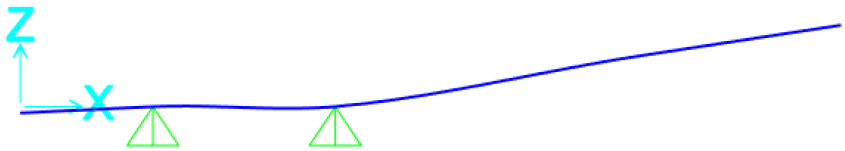

Figure 3-30 – The exaggerated deflection mode of the plywood in the unnsymmetrical tests. The model consider the plywood plate as a beam of two pinned supports.

4 Results

In 4.1 of this chapter, all results drawn from the experimental testing is presented. Initially, mean force-deformation graphs for all test groups are presented in unified plots. Each test group has its own force-deformation plot and a table with all relevant mechanical parameters. For each test, the mean values for displacement were calculated from the two vertical transducers. In 4.2, the estimated stresses from the SAP2000 models are presented in tables that also contain the mean capacities of the plywood.

a)

b)

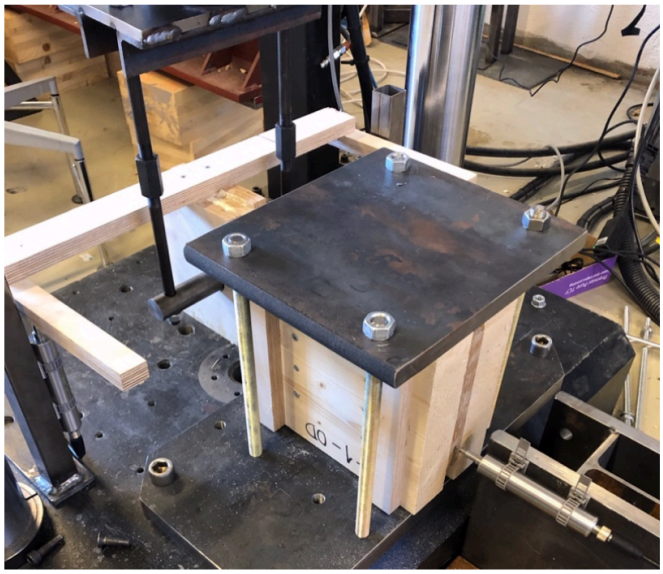

Figure 4-1 – Test setup for the symmetrical (a) and unsymmetrical (b) configurations.

4.1 Results from Experimental Investigation

In the following chapters, the mechanical characteristics for each test group are presented with plots and tables.

4.1.1 Mean force-deformation plot for each test group

Figure 4-2 and Figure 4-3 shows the mean force-deformation graph for each test group. The symmetrical and unsymmetrical test groups are labeled in two different figures due to the much higher deformation for the unsymmetrical test groups.

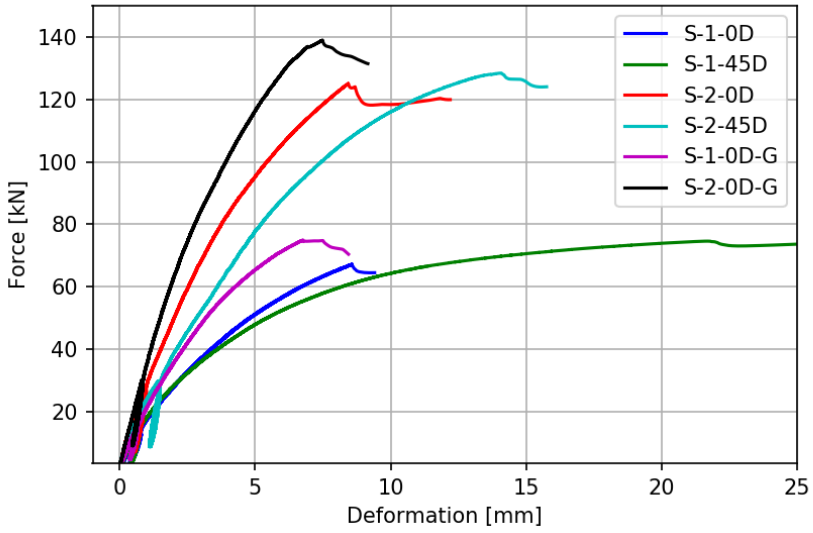

Figure 4-2 – Mean force-deformation curves for all six symmetrical test groups. Each curve represents the average force- and displacement-values for all specimens in each test group.

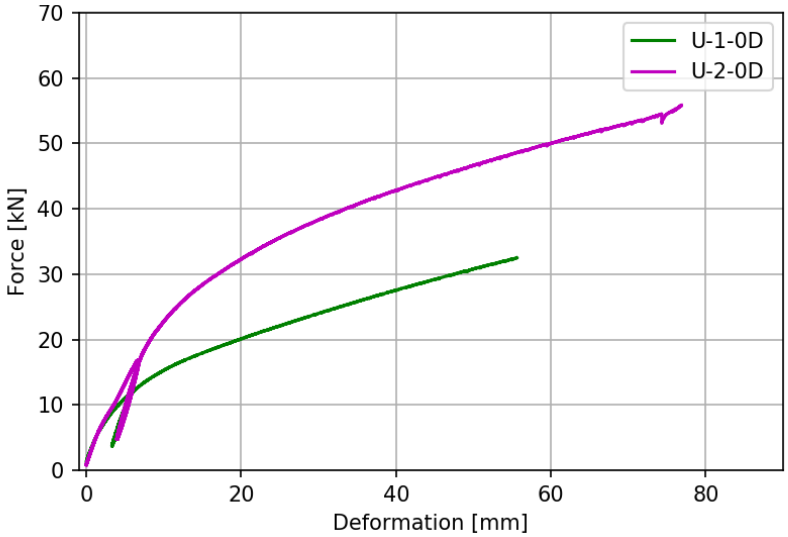

Figure 4-3 – Mean force-deformation curves for both unsymmetrical test groups. Each curve represents the average force- and displacement-values for all specimens in each test group.

4.1.2 S-1-0D

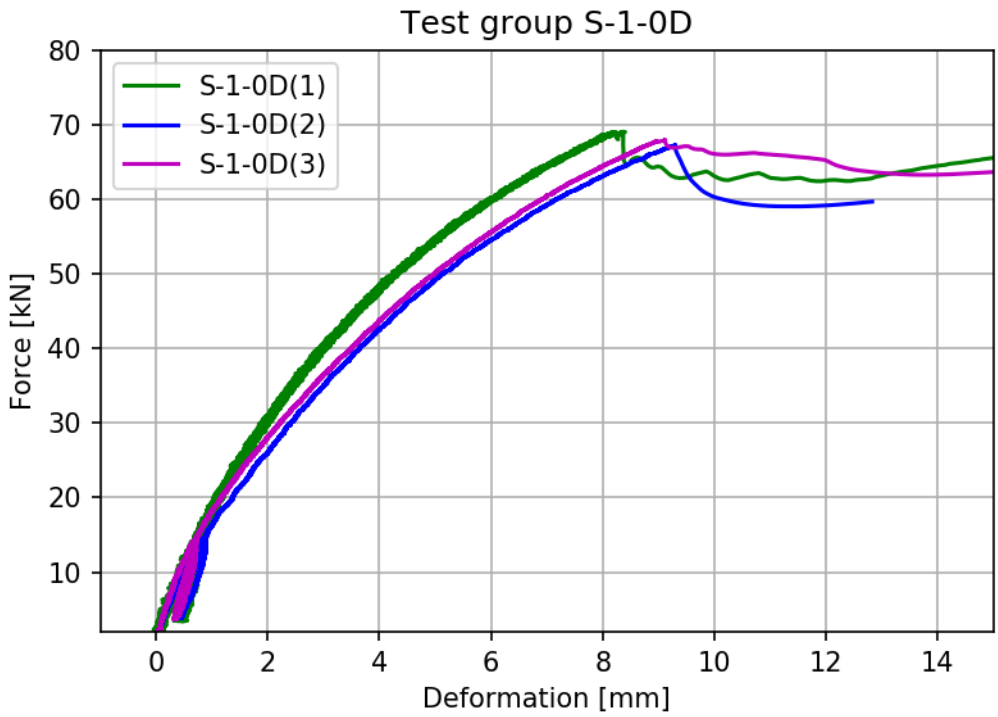

Figure 4-4 – Load-deformation diagrams of test group S-1-0D. Each curve is plotted with the mean values from the two displacement transducers.

Table 4-1 – Mechanical properties for each specimen in test group S-1-0D. F_{max} and F_y refer to the maximum and yield load. δ_{max} refers to the maximum deformation measured by the transducers. $K_{el,global}$ and $K_{pl,global}$ are the calculated global elastic and plastic stiffness of the connection.
D_u is the ductility ratio. Mean values and standard deviation (SD) is included.

S-1-0D					
	1	2	3	Mean	SD
F_{max} [kN]	69,06	67,30	68,85	68,40	0,96
F_y [kN]	34,53	33,65	34,45	34,21	0,49
δ_{max} [mm]	8,04	9,06	8,63	8,58	0,51
$K_{el,global}$ [kN/mm]	17,40	15,80	18,47	17,22	1,34
$K_{pl,global}$ [kN/mm]	7,40	6,45	6,38	6,74	0,57
D_u	3,41	3,24	3,18	3,28	0,12

4.1.3 S-1-45D

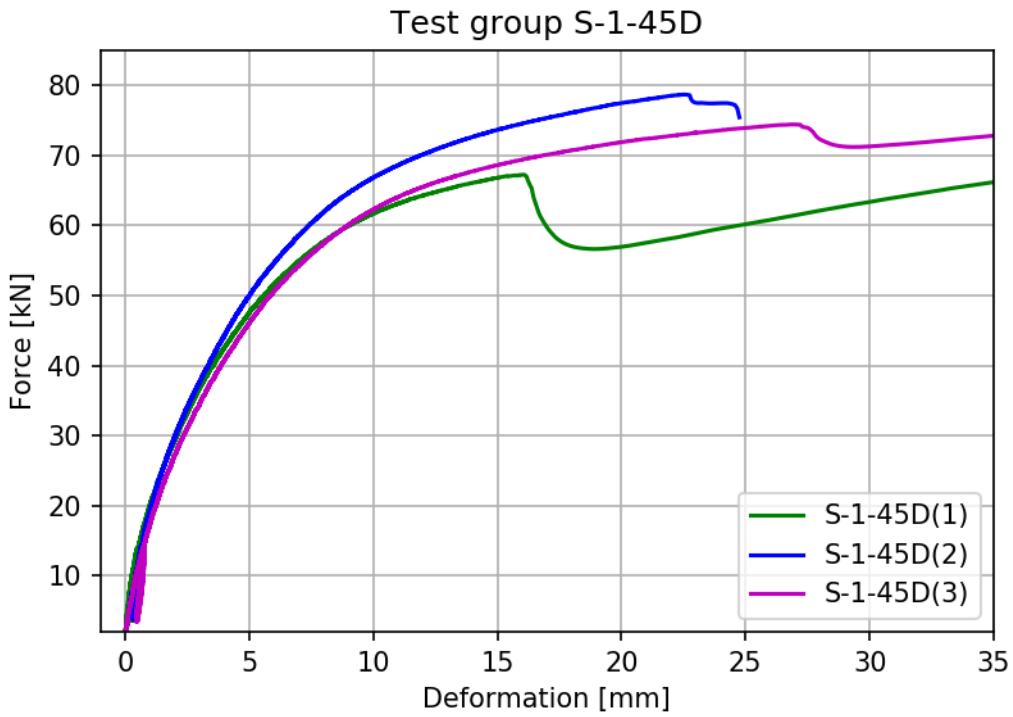

Figure 4-5 – Load-deformation diagrams of test group S-1-45D. Each curve is plotted with the mean values from the two displacement transducers.

Table 4-2 – Mechanical properties for each specimen in test group S-1-45D. F_{max} and F_y refer to the maximum and yield load. δ_{max} refers to the maximum deformation measured by the transducers. $K_{el,global}$ and $K_{pl,global}$ are the calculated global elastic and plastic stiffness of the connection.
D_u is the ductility ratio. Mean values and standard deviation (SD) is included.

S-1-45D					
	1	2	3	Mean	SD
F_{max} [kN]	67,44	78,69	73,77	73,30	5,64
F_y [kN]	33,73	39,35	36,85	36,64	2,82
δ_{max} [mm]	16,12	22,30	27,61	22,01	5,75
$K_{el,global}$ [kN/mm]	25,14	20,18	30,88	25,40	5,35
$K_{pl,global}$ [kN/mm]	4,40	3,83	3,81	4,01	0,34
D_u	6,37	7,01	5,69	6,36	0,66

4.1.4 S-2-0D

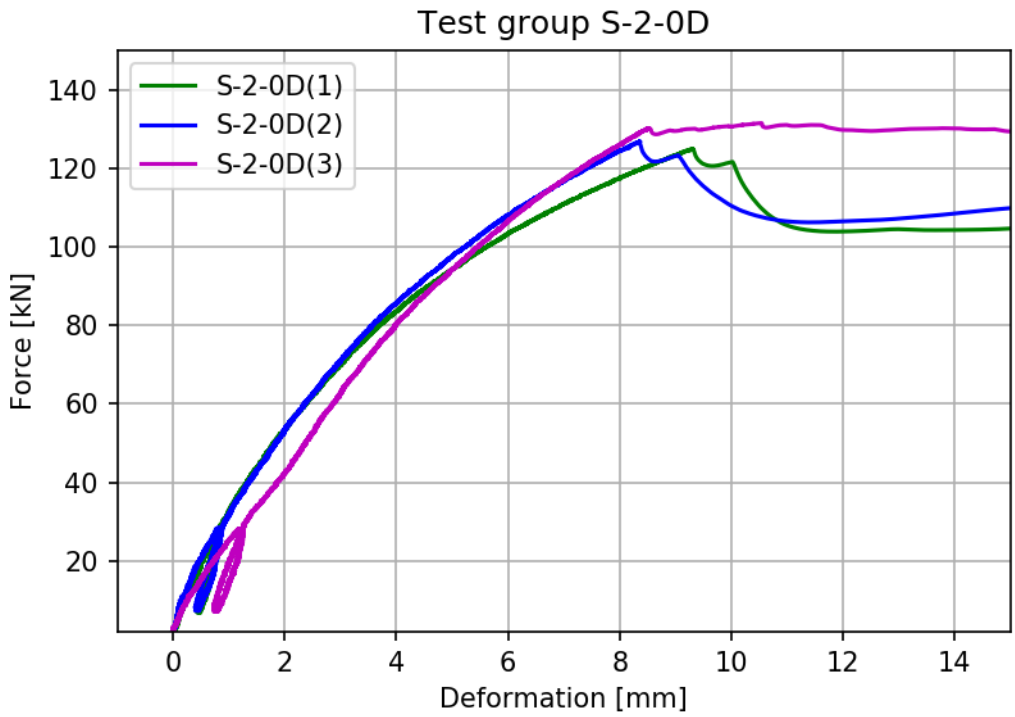

Figure 4-6 – Load-deformation diagrams of test group S-2-0D. Each curve is plotted with the mean values from the two displacement transducers.

Table 4-3 – Mechanical properties for each specimen in test group S-2-0D. F_{max} and F_y refer to the maximum and yield load. δ_{max} refers to the maximum deformation measured by the transducers. $K_{el,global}$ and $K_{pl,global}$ are the calculated global elastic and plastic stiffness of the connection.
D_u is the ductility ratio. Mean values and standard deviation (SD) is included.

S-2-0D					
	1	2	3	Mean	SD
F_{max} [kN]	125,91	126,78	133,60	128,76	4,21
F_y [kN]	62,95	63,4	67,95	64,77	2,77
δ_{max} [mm]	9,27	8,31	8,49	8,69	0,51
$K_{el,global}$ [kN/mm]	31,48	50,00	44,68	42,05	9,54
$K_{pl,global}$ [kN/mm]	11,56	13,89	14,26	13,24	1,46
D_u	3,73	3,26	2,56	3,18	0,59

4.1.5 S-2-45D

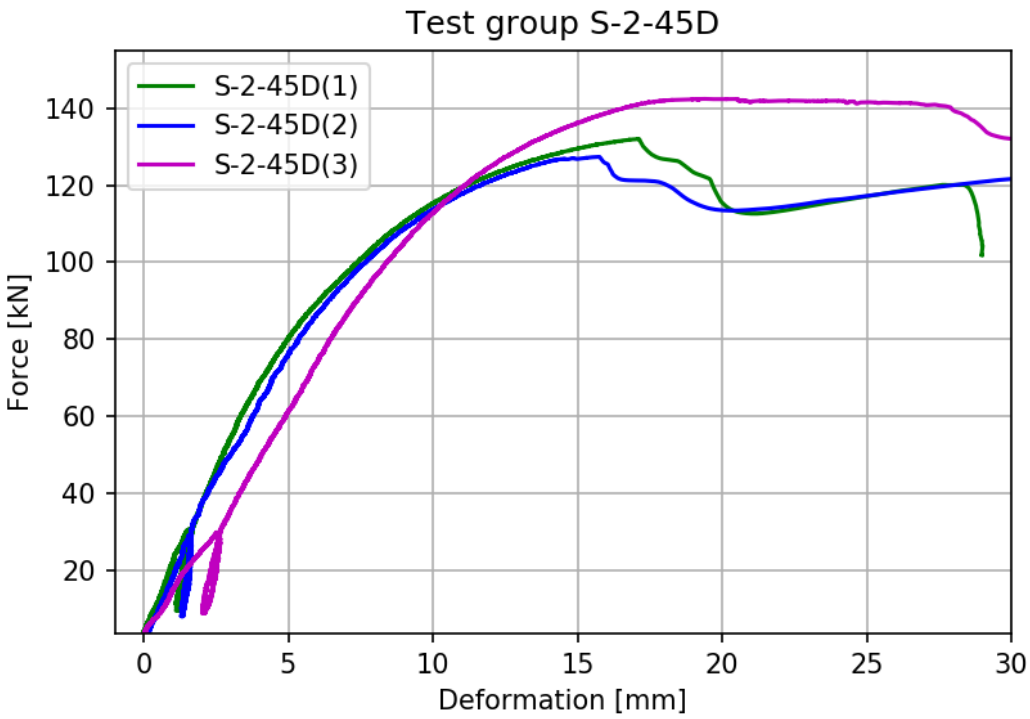

Figure 4-7 – Load-deformation diagrams of test group S-2-45D. Each curve is plotted with the mean values from the two displacement transducers.

Table 4-4 – Mechanical properties for each specimen in test group S-2-45D. F_{max} and F_y refer to the maximum and yield load. δ_{max} refers to the maximum deformation measured by the transducers. $K_{el,global}$ and $K_{pl,global}$ are the calculated global elastic and plastic stiffness of the connection.
D_u is the ductility ratio. Mean values and standard deviation (SD) is included.

S-2-45D					
	1	2	3	Mean	SD
F_{max} [kN]	132,03	127,41	141,99	133,81	7,45
F_y [kN]	66,02	63,71	71,00	66,91	3,73
δ_{max} [mm]	17,09	15,71	27,28	20,03	6,32
$K_{el,global}$ [kN/mm]	44,68	75,00	38,18	52,62	19,65
$K_{pl,global}$ [kN/mm]	8,76	9,51	9,40	9,22	0,41
D_u	4,18	3,51	2,93	3,54	0,63

4.1.6 S-1-0D-G

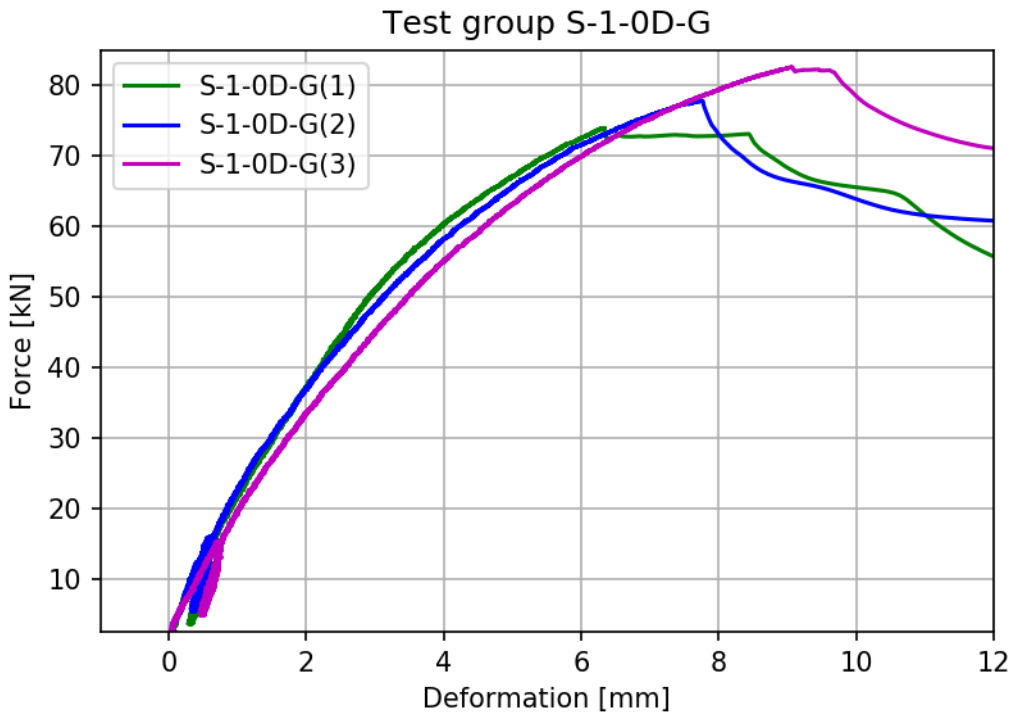

Figure 4-8 – Load-deformation diagrams of test group S-1-0D-G. Each curve is plotted with the mean values from the two displacement transducers.

Table 4-5 – Mechanical properties for each specimen in test group S-1-0D-G. F_{max} and F_y refer to the maximum and yield load. δ_{max} refers to the maximum deformation measured by the transducers. $K_{el,global}$ and $K_{pl,global}$ are the calculated global elastic and plastic stiffness of the connection. D_u is the ductility ratio. Mean values and standard deviation (SD) is included.

S-1-0D-G					
	1	2	3	Mean	SD
F_{max} [kN]	73,98	77,79	82,62	78,13	4,33
F_y [kN]	36,99	38,90	41,31	39,07	2,16
δ_{max} [mm]	6,59	7,70	9,02	7,77	1,22
$K_{el,global}$ [kN/mm]	30,18	23,40	18,73	24,10	5,76
$K_{pl,global}$ [kN/mm]	11,10	9,43	8,58	9,70	1,28
D_u	2,95	3,61	3,38	3,31	0,34

4.1.7 S-2-0D-G

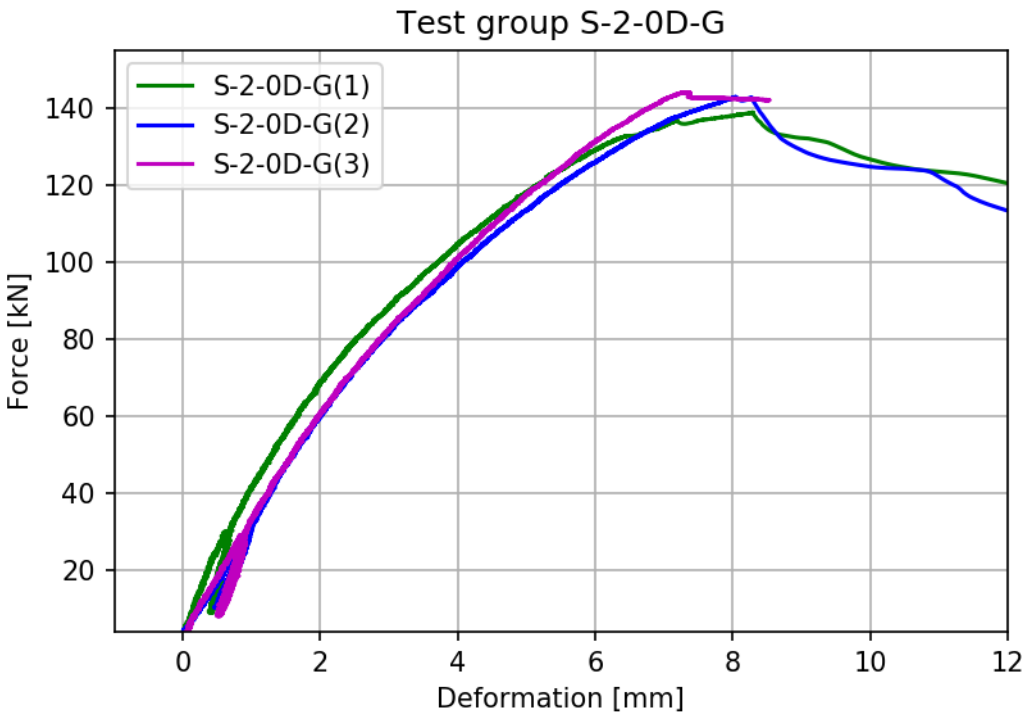

Figure 4-9 – Load-deformation diagrams of test group S-2-0D-G. Each curve is plotted with the mean values from the two displacement transducers.

Table 4-6 – Mechanical properties for each specimen in test group S-2-0D-G. F_{max} and F_y refer to the maximum and yield load. δ_{max} refers to the maximum deformation measured by the transducers. $K_{el,global}$ and $K_{pl,global}$ are the calculated global elastic and plastic stiffness of the connection. D_u is the ductility ratio. Mean values and standard deviation (SD) is included.

S-2-0D-G					
	1	2	3	Mean	SD
F_{max} [kN]	138,87	142,77	144,06	141,90	2,70
F_y [kN]	69,44	71,39	72,03	70,95	1,35
δ_{max} [mm]	8,26	8,00	7,52	7,93	0,38
$K_{el,global}$ [kN/mm]	43,30	28,31	52,50	41,37	12,21
$K_{pl,global}$ [kN/mm]	17,02	16,32	18,15	17,16	0,92
D_u	4,12	3,27	2,25	3,21	0,94

4.1.8 U-1-0D

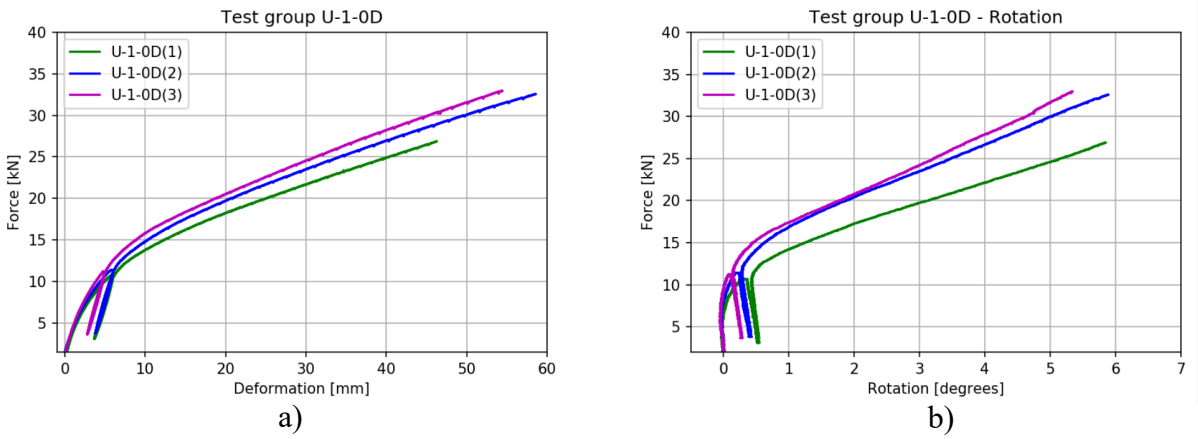

Figure 4-10 – Load-deformation (a) and load-rotation (b) diagrams of test group U-1-0D. Each curve in (a) is plotted with the mean values from the two displacement transducers.

Table 4-7 – Mechanical properties for each specimen in test group U-1-0D. F_{max} and F_y refer to the maximum and yield load. δ_{max} and φ_{max} refer to the maximum deformation and rotation measured by the transducers. $K_{el,global}$ and $K_{pl,global}$ are the calculated global elastic and plastic stiffness of the connection. D_u is the ductility ratio. Mean values and standard deviation (SD) is included.

U-1-0D					
	1	2	3	Mean	SD
F_{max} [kN]	26,88	32,57	32,94	30,80	3,40
F_y [kN]	13,44	16,29	16,47	15,40	1,70
δ_{max} [mm]	46,26	58,58	78,43	53,09	6,27
φ_{max} [°]	5,84	5,87	5,34	5,68	0,30
$K_{el,global}$ [kN/mm]	2,49	3,28	3,21	3,00	0,44
$K_{pl,global}$ [kN/mm]	0,44	0,42	0,45	0,44	0,02
D_u	4,96	4,71	4,92	4,86	0,13

4.1.9 U-2-0D

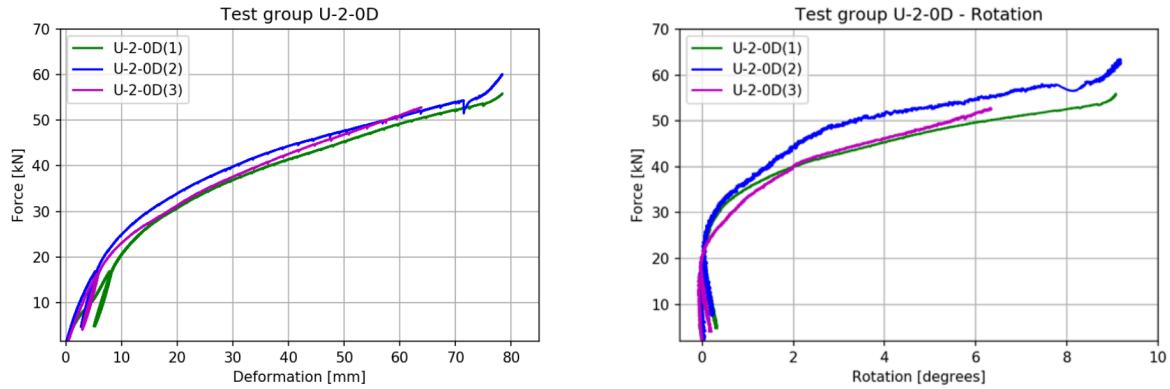

a) b)

Figure 4-11 – Load-deformation (a) and load-rotation (b) diagrams of test group U-2-0D. Each curve is plotted with the mean values from the two displacement transducers.

Table 4-8 – Mechanical properties for each specimen in test group U-2-0D. F_{max} and F_y refer to the maximum and yield load. δ_{max} and φ_{max} refer to the maximum deformation and rotation measured by the transducers. $K_{el,global}$ and $K_{pl,global}$ are the calculated global elastic and plastic stiffness of the connection. D_u is the ductility ratio. Mean values and standard deviation (SD) is included.

U-2-0D					
	1	2*	3	Mean	SD
F_{max} [kN]	55,84	60,07	52,80	54,32	2,15
F_y [kN]	27,92	30,04	26,40	27,16	1,07
δ_{max} [mm]	78,43	82,34	63,82	71,13	10,33
φ_{max} [°]	9,06	9,17	6,39	7,73	1,89
$K_{el,global}$ [kN/mm]	4,55	5,17	4,80	4,68	0,18
$K_{pl,global}$ [kN/mm]	0,56	0,51	0,64	0,60	0,06
D_u	4,89	5,35	4,74	4,82	0,11

*Values from test specimen U-2-0D (2) were neglected from the mean values due to not achieving failure of the plywood before maximum deformation was reached.

4.2 Results from SAP2000 Analysis

In this chapter, the stress values drawn from the SAP2000 analysis are matched up with the plywood capacities stated in the Declaration of Performance (Metsä Wood, 2019). Only one test group is presented visually in the figures, as the fractures were similar for both the one- and two-plate groups. Some aspects of the values in the tables should be taken into consideration; The theoretical characteristic capacities were increased by 10 % to imitate the mean values. The mean bending capacity of the plywood is calculated in Appendix C – Hand Calculations. The capacities for plywood with 45-degreed face grain was not officially known and was set to the same as for 0-degreed plywood. Stress values for each group were found by using the average F_{max}, given in Chapter 4.1

4.2.1 S-1-0D & S-2-0D

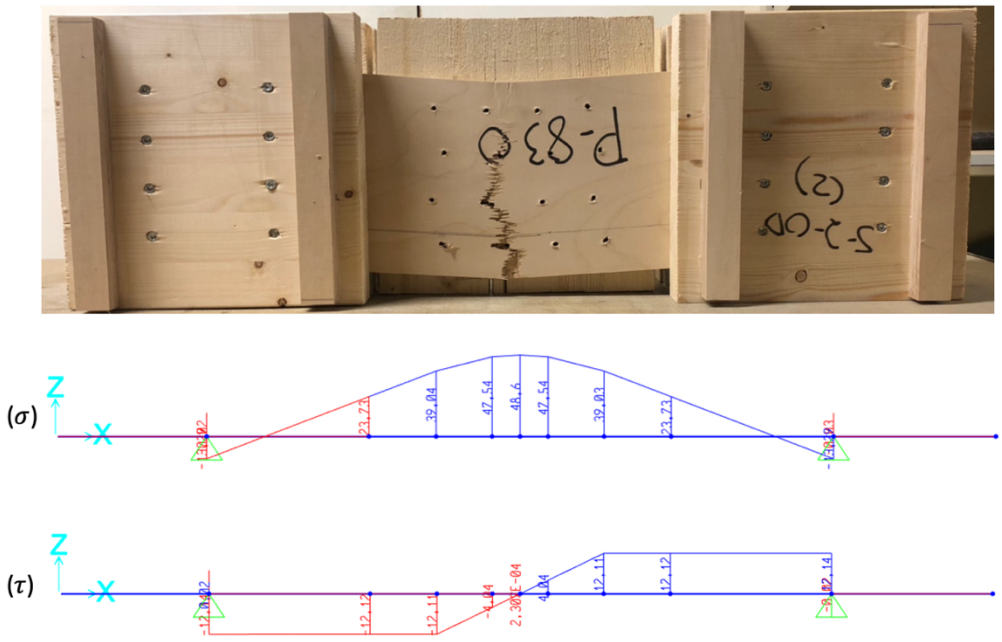

Figure 4-12 – Comparison of fracture location in S-2-0D, and tensile/compressive (σ) and shear (τ) stress distribution from SAP2000. The values displayed are measured in MPa.

Table 4-9 – Comparison of the theoretical capacities of the plywood and the achieved stresses in S-1-0D and S-2-0D, drawn from the SAP2000 models. σ_{max} and τ_{max} refer to the maximum tensile/compressive and shear stress. $f_{t,mean}$, $f_{c,mean}$, $f_{m,mean}$ and $f_{v,mean}$ refer to the mean tension, compression, bending and shear stress capacity of the plywood.

		S-1-0D	S-2-0D
Estimates from SAP2000 model	σ_{max} [MPa]	57,0	48,6
	τ_{max} [MPa]	12,9	12,1
Tensile stress capacity	$f_{t,mean}$ [MPa]	42,9	42,9
	Utilization [%]	132,9	113.3
Compressive stress capacity	$f_{c,mean}$ [MPa]	29,7	29,7
	Utilization [%]	191,9	163,6
Bending stress capacity	$f_{m,mean}$ [MPa]	53,7	53,7
	Utilization [%]	106,1	90,5
Shear stress capacity	$f_{v,mean}$ [MPa]	10,5	10,5
	Utilization [%]	122,9	115,2

4.2.2 S-1-45D & S-2-45D

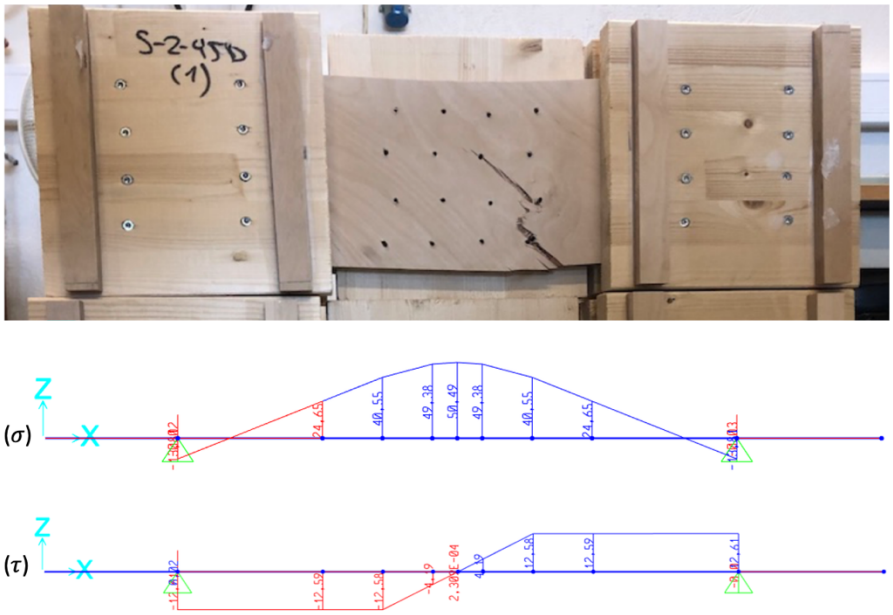

Figure 4-13 – Comparison of fracture location in S-2-45D and tensile/compressive (σ) and shear (τ) stress distribution from SAP2000. The values displayed are measured in MPa.

Table 4-10 – Comparison of the theoretical capacities of the plywood and the achieved stresses in S-1-45D and S-2-45D, drawn from the SAP2000 models. σ_{max} and τ_{max} refer to the maximum tensile/compressive and shear stress. $f_{t,mean}$, $f_{c,mean}$, $f_{m,mean}$ and $f_{v,mean}$ refer to the mean tension, compression, bending and shear stress capacity of the plywood.

		S-1-45D	S-2-45D
Estimates from SAP2000 model	σ_{max} [MPa]	61,1	50,5
	τ_{max} [MPa]	13,8	12,6
Tensile stress capacity	$f_{t,mean}$ [MPa]	42,9	42,9
	Utilization [%]	142,4	117,7
Compressive stress capacity	$f_{c,mean}$ [MPa]	29,7	29,7
	Utilization [%]	205,7	170
Bending stress capacity	$f_{m,mean}$ [MPa]	53,7	53,7
	Utilization [%]	113,8	94,0
Shear stress capacity	$f_{v,mean}$ [MPa]	10,5	10,5
	Utilization [%]	131,4	120,0

4.2.3 S-1-0D-G & S-2-0D-G

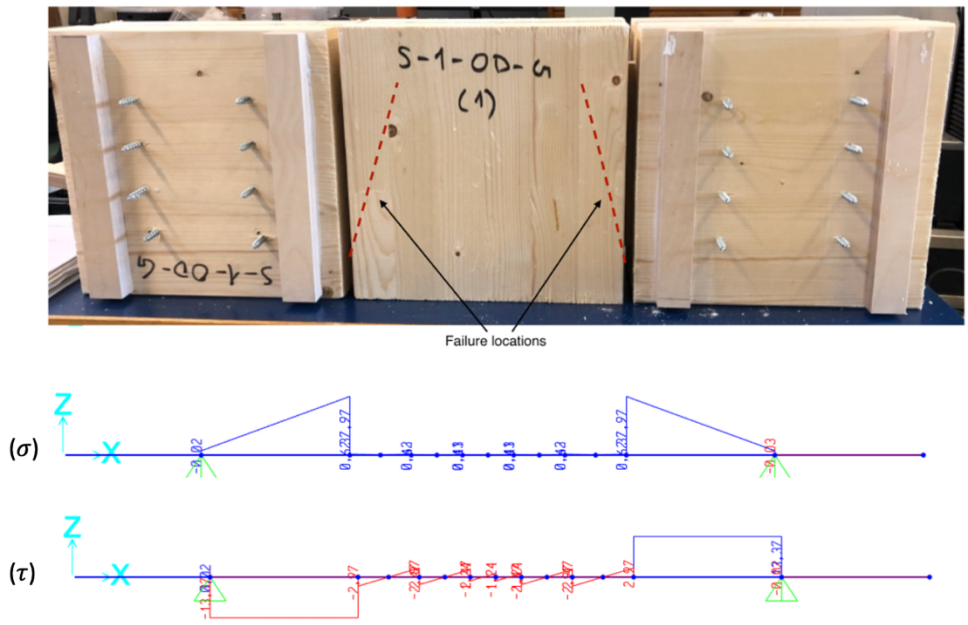

Figure 4-14 – Comparison of fracture location in S-1-0D-G and tensile/compressive (σ) and shear (τ) stress distribution from SAP2000. The values displayed are measured in MPa.

Table 4-11 – Comparison of the theoretical capacities of the plywood and the achieved stresses in S-1-0D-G and S-2-0D-G, drawn from the SAP2000 models. σ_{max} and τ_{max} refer to the maximum tensile/compressive and shear stress. $f_{t,mean}$, $f_{c,mean}$, $f_{m,mean}$ and $f_{v,mean}$ refer to the mean tension, compression, bending and shear stress capacity of the plywood.

		S-1-0D-G	S-2-0D-G
Estimates from SAP2000 model	σ_{max} [MPa]	41,8	35,8
	τ_{max} [MPa]	14,7	13,4
Tensile stress capacity	$f_{t,mean}$ [MPa]	42,9	42,9
	Utilization [%]	97,4	83,4
Compressive stress capacity	$f_{c,mean}$ [MPa]	29,7	29,7
	Utilization [%]	140,7	120,5
Bending stress capacity	$f_{m,mean}$ [MPa]	53,7	53,7
	Utilization [%]	77,8	66,7
Shear capacity	$f_{v,mean}$ [MPa]	10,5	10,5
	Utilization [%]	140,0	127,6

4.2.4 U-1-0D & U-2-0D

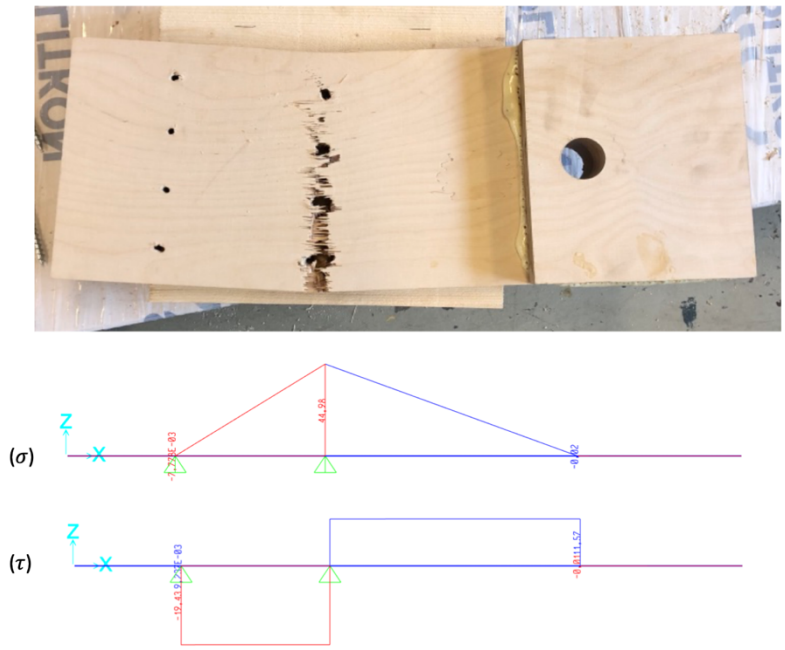

Figure 4-15 – Comparison of fracture location in U-1-0D and and tensile/compressive (σ) and shear (τ) stress distribution from SAP2000. The values displayed are measured in MPa.

Table 4-12 – Comparison of the theoretical capacities of the plywood and the achieved stresses in U-1-0D and U-2-0D, drawn from the SAP2000 models. σ_{max} and τ_{max} refer to the maximum tensile/compressive and shear stress. $f_{t,mean}$, $f_{c,mean}$, $f_{m,mean}$ and $f_{v,mean}$ refer to the mean tension, compression, bending and shear stress capacity of the plywood.

		U-1-0D	**U-2-0D**
Estimates from SAP2000 model	σ_{max} [MPa]	45,0	39,7
	τ_{max} [MPa]	19,4	17,1
Tensile stress capacity	$f_{t,mean}$ [MPa]	42,9	42,9
	Utilization [%]	104,9	92,5
Compressive stress capacity	$f_{c,mean}$ [MPa]	29,7	29,7
	Utilization [%]	151,5	133,7
Bending stress capacity	$f_{m,mean}$ [MPa]	53,7	53,7
	Utilization [%]	83,8	73,9
Shear stress capacity	$f_{v,mean}$ [MPa]	10,5	10,5
	Utilization [%]	184,7	162,8

5 Discussion

The various results, both experimental and numerical from SAP2000, will be discussed in the light of failure mode and its location, load capacity, and the stiffness. Initially, the mechanical properties of the different comparable test groups are presented in tables to better visualize the differences. Then, the differences are analyzed and reasoned for as well as possible. The results from the SAP2000 analysis are then evaluated. An assessment of the possibility of using plywood as a replacement for steel in beam-column connections is discussed in Chapter 5.4. Finally, an evaluation of the experimental process is presented along with implications and limitations of the work, before a proposal for necessary further research is suggested.

5.1 Comparison of Test Group Characteristics

In this chapter, the mechanical properties of each test group are compared against each other. Numbers presented in the following tables are gathered from tables in Chapter 4.1. When two test groups with a different number of plywood plates were compared, the global plastic stiffness per shear plane ($K_{pl,global,sp}$) and global elastic stiffness per shear plane ($K_{el,global,sp}$) were introduced. Thus, two shear planes for the specimens with one gusset plate and four shear planes for the specimens with two plates. Another new parameter was introduced; $F_{max,ply}$ describes the maximum force capacity per plywood plate to more easily represent the difference in capacity for two groups with a different number of plywood plates.

5.1.1 S-1-0D vs. S-2-0D

The test results showed a 6,24 % higher load capacity per plywood plate in S-1-0D. S-2-0D showed 22 % higher global elastic stiffness than S-1-0D, but the global plastic stiffness is approximately the same. Test group S-2-0D also had a slightly higher total deformation. See Table 5-1 for the values.

Table 5-1 – Comparison of test results for test groups S-1-0D and S-2-0D. $F_{max,ply}$ refers to the maximum load per plate. δ_{max} refers to the maximum deformation measured by the transducers. $K_{el,global,sp}$ and $K_{pl,global,sp}$ are the calculated global elastic and plastic stiffness of the connection per shear plane. D_u is the ductility ratio.

S-1-0D vs. S-2-0D					
Test group	$F_{max,ply}$ [kN]	δ_{max} [mm]	$K_{el,global,sp}$ [kN/mm]	$K_{pl,global,sp}$ [kN/mm]	D_u
S-1-0D	68,40	8,58	8,61	3,37	3,28
S-2-0D	64,38	8,69	10,51	3,31	3,18

5.1.2 S-1-45D vs. S-2-45D

The test results showed a 9,68 % higher load capacity per plywood plate in S-1-45D, while the global elastic stiffness per shear plane was 3,6 % lower than S-2-45D. Test group S-1-45D also had a 9,8 % higher total deformation. S-1-45D had a 79,7 % higher ductility ratio than S-2-45D, which makes sense as it also had a lower global plastic stiffness. The values are presented in Table 5-2.

Table 5-2 – Comparison of test results for test groups S-1-45D and S-2-45D. $F_{max,ply}$ refers to the maximum load per plate. δ_{max} refers to the maximum deformation measured by the transducers. $K_{el,global,sp}$ and $K_{pl,global,sp}$ are the calculated global elastic and plastic stiffness of the connection per shear plane. D_u is the ductility ratio.

S-1-45D vs. S-2-45D					
Test group	$F_{max,ply}$ [kN]	δ_{max} [mm]	$K_{el,global,sp}$ [kN/mm]	$K_{pl,global,sp}$ [kN/mm]	D_u
S-1-45D	73,30	22,01	12,70	2,01	6,36
S-2-45D	66,91	20,03	13,16	2,31	3,54

5.1.3 S-1-0D-G vs. S-2-0D-G

Both test groups had the same failure mode in the plywood. However, the maximum load per plywood plate was significantly higher (10,12 %) for S-1-0D-G. The global elastic stiffness per shear plane was 16,5 % higher for S-1-0D-G, while the global plastic stiffness per shear plane was 13,1 % higher for S-1-0D-G. The values are presented in Table 5-3.

Table 5-3 – Comparison of test results for test groups S-1-0D-G and S-2-0D-G. $F_{max,ply}$ refers to the maximum load per plate. δ_{max} refers to the maximum deformation measured by the transducers. $K_{el,global,sp}$ and $K_{pl,global,sp}$ are the calculated global elastic and plastic stiffness of the connection per shear plane. D_u is the ductility ratio.

S-1-0D-G vs. S-2-0D-G					
Test group	$F_{max,ply}$ [kN]	δ_{max} [mm]	$K_{el,global,sp}$ [kN/mm]	$K_{pl,global,sp}$ [kN/mm]	D_u
S-1-0D-G	78,13	7,77	12,05	4,85	3,31
S-2-0D-G	70,95	7,93	10,34	4,29	3,21

5.1.4 S-1-0D vs. S-1-45D vs. S-1-0D-G

It has to be stated that the failure modes of all these groups were not the same. S-1-0D-G suffered to be a shear failure while S-1-0D and S-1-45D had bending failures.

Of all the symmetrical test groups, S-1-0D-G had the highest maximum load capacity at 78,13 kN and was 14,23 % more than S-1-0D, which had the lowest load capacity. The glued test group also had the least amount of deformation. S-1-45D had the most deformation of all. S-1-0D-G and S-1-45D had a quite similar elastic stiffness, but S-1-45D had 47,50 % higher than S-1-0D. The global plastic stiffness was higher for S-1-0D compared to S-1-45D, which corresponded well with the fact that S-1-45D had a lower ductility ratio. The values are presented in Table 5-4.

Table 5-4 - Comparison of test results for test groups S-1-0D, S-1-45D, and S-1-0D-G. F_{max} refers to the maximum load for the test group. δ_{max} refers to the maximum deformation measured by the transducers. $K_{el,global}$ and $K_{pl,global}$ are the calculated global elastic and plastic stiffness of the connection. D_u is the ductility ratio.

S-1-0D vs. S-1-45D vs. S-1-0D-G					
Test group	F_{max} [kN]	δ_{max} [mm]	$K_{el,global}$ [kN/mm]	$K_{pl,global}$ [kN/mm]	D_u
S-1-0D	68,40	8,58	17,22	6,74	3,28
S-1-45D	73,30	22,01	25,40	4,01	6,36
S-1-0D-G	78,13	7,77	24,10	9,70	3,31

5.1.5 S-2-0D vs. S-2-45D vs. S-2-0D-G

The failure modes for these test groups were also different and followed the same pattern as in chapter 5.1.4.

The highest maximum load capacity occurred in S-2-0D-G, 9,5 % more than the S-2-0D, which had the lowest load-bearing capacity. S-2-45D had 6,7 % lower capacity than S-2-0D-G and 3,3 % higher capacity than S-2-0D. In addition, S-2-45D showed a much higher displacement before failure than the other two, 130 % more. The global elastic stiffness was 25 % higher for S-2-45D compared to S-2-0D. The glued test group had the lowest global elastic stiffness. The global plastic stiffness clearly illustrated how test group S-2-45D behaved in a ductile manner compared to the others. S-2-0D was 44 % stiffer in the plastic area than S-2-45D. This corresponded well with the ductility ratio of S-2-45D being 24,21 % higher than S-2-0D. S-2-0D-G had the highest global plastic stiffness of them all. The values are presented in Table 5-5.

Table 5-5 – Comparison of test results for test groups S-2-0D, S-2-45D, and S-2-0D-G. F_{max} refers to the maximum load for the test group. δ_{max} refers to the maximum deformation measured by the transducers. $K_{el,global}$ and $K_{pl,global}$ are the calculated global elastic and plastic stiffness of the connection. D_u is the ductility ratio.

S-2-0D vs. S-2-45D vs. S-2-0D-G					
Test group	F_{max} [kN]	δ_{max} [mm]	$K_{el,global}$ [kN/mm]	$K_{pl,global}$ [kN/mm]	D_u
S-2-0D	128,76	8,69	42,05	13,24	3,18
S-2-45D	133,81	20,03	52,62	9,22	3,54
S-2-0D-G	141,90	7,93	41,37	17,16	3,21

5.1.6 U-1-0D vs. U-2-0D

Both U-1-0D and U-2-0D showed excessive deformation and rotation from the start. As opposed to the symmetrical test groups, U-2-0D with two plywood plates appeared to have less global elastic stiffness than its opposing group with one plate (U-1-0D). U-2-0D had a 13,40 % smaller maximum failure load per plate compared to U-1-0D, as well as substantially more deformation (33,98 %) and rotation (36,09%). However, the global plastic stiffness per shear plane was higher (29,54 %). There did not seem to be a significant difference in ductility. The values are presented in Table 5-6.

Table 5-6 – Comparison of test results for test groups U-1-0D and S-2-0D. Values from test specimen U-2-0D (2) are neglected from the mean values. $F_{max,ply}$ refers to the maximum load per plate. δ_{max} and φ_{max} refer to the maximum deformation and rotation measured by the transducers. $K_{el,global,sp}$ and $K_{pl,global,sp}$ are the calculated global elastic and plastic stiffness of the connection per shear plane. D_u is the ductility ratio.

U-1-0D vs. U-2-0D						
Test group	$F_{max,ply}$ [kN]	δ_{max} [mm]	φ_{max} [°]	$K_{el,global,sp}$ [kN/mm]	$K_{pl,global,sp}$ [kN/mm]	D_u
U-1-0D	30,80	53,09	5,68	1,50	0,22	4,86
U-2-0D	27,16	71,13	7,73	1,17	0,15	4,82

5.2 Evaluation of Experimental Results

To discuss the reason for the difference in experimental parameter values between test groups, an evaluation was made.

5.2.1 Failure mode and location of the fracture

Difference in failure due to different column fasteners

The testing brought out three different failure modes in the plywood; tension-, compression- and shear failure. The configurations with a screwed column connection had compressive failure on top (see Figure 5-1) and tension failure at the bottom of the plywood plate. These stresses developed as a result of bending of the plate. The configurations with the glued column connection had shear failure in the plywood plate, which occurred directly on the edge of the glued area. The column connection was entirely stiff due to the glue, so bending in the column part of the plywood was therefore not possible. This gave a concentrated shear stress on the outside of the glued area, which led to the shear failure in that location.

Figure 5-1 – Compressive failure of the plywood as a result of bending of the plate.

It should be noted that all test groups had some bending of the screws, even though they suffered plywood failure. Not all screws did yield; Only the screws in certain positions had noticeable bending. The deformed screws were placed in the critical positions shown in Figure 5-2, where the resultant force due the eccentricity moment from the load, was most significant. The failures can be regarded as balanced; The yielding of some of the screws contributed to the plasticity of the failures, while the plywood failed in a brittle manner.

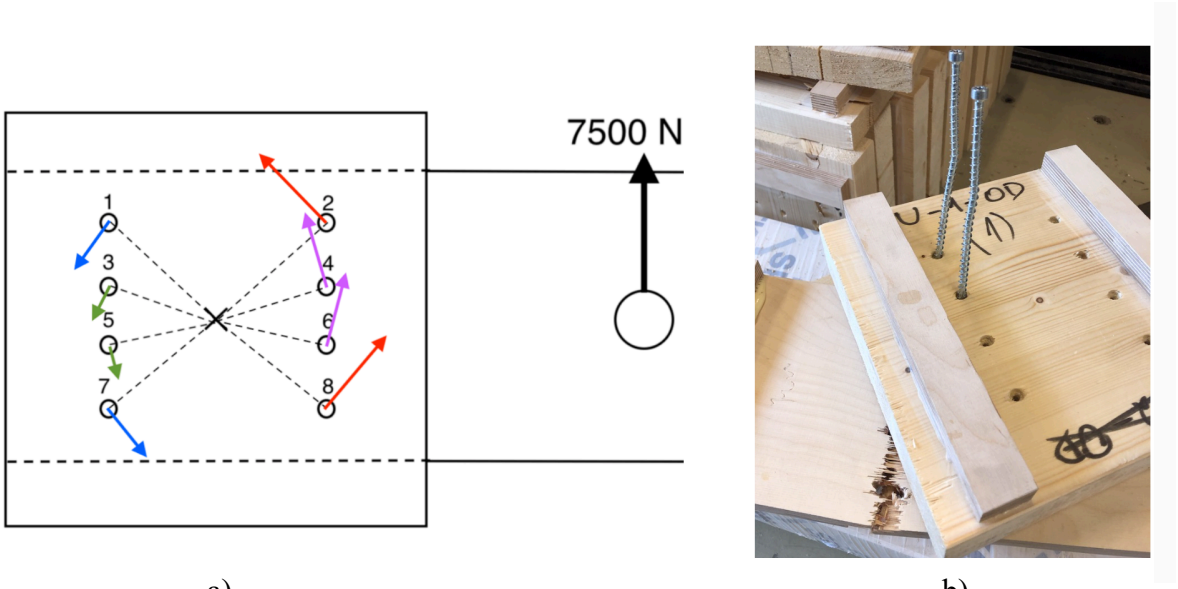

a) b)

Figure 5-2 – Magnitude of the force resultant on each screw in a screw group, illustrated with arrows (a). The red and purple arrows represent the biggestforce resultants. Hand calculation of these resultants are presented in Appendix C – Hand Calculations. Screws in their respective positions, illustrating the difference in bending (b).

Difference in failure mode due to plywood grain angle

The compression failure in the plywood looked similar and happened in approximately the same location for both grain angles. The tension fracture, however, was affected by the face grain angle of the plywood. The fractures are shown in Figure 5-3.

a) b)

Figure 5-3 – Difference of tensile failure due to the face grain angle in the screwed connection. 0-degree oriented plywood is pictured in (a) and 45-degree oriented plywood in (b).

The fracture of the 45-degreed plywood had a zig-zag pattern, while the 0-degreed plywood had a more or less vertical fracture. For the 0-degreed plywood plate, all layers orientated

parallel to the tension forces tore in bundles on different points of the layers. This is referred to as bundle rupture. The layers orientated perpendicular to the face grain separated between the fibers. For the 45-degreed plywood plate, the situation was different. This failure was a combination of bundle rupture and failure along the fibers, which led to the zig-zag shape.

The location of the failure differed due to the face grain direction, as illustrated in Figure 5-3. The failure in both cases showed clear signs of going through the screw holes, which weakens the cross-section. The failure of the 0-degreed plywood, Figure 5-3a was almost where the stress had its maximum value, but it was skewed because the fracture went through the screw rows, see Figure 4-12. S-1-0D (3) was an exception (photo of fracture is found in Appendix D – Fracture Photography of each Test Specimen). In this sample, the fracture originated in the outer screw row but moved inwards into the inner row. The assumed reason for this was imperfections in the plywood. On the other hand, the failure of the 45-degreed plywood started under the outer screw row (Figure 5-3b). This was far from the location of maximum tension, see Figure 4-13. The reason for why the failure originated here is not concluded in this work. Further research may be needed in this area.

Shear failure occurred in all the glued configurations, as illustrated in Figure 5-4. It was no surprise that the failure occurred where it did, as the glue acted like a fixed support and the maximum shear stress is often directly outside of the supports.

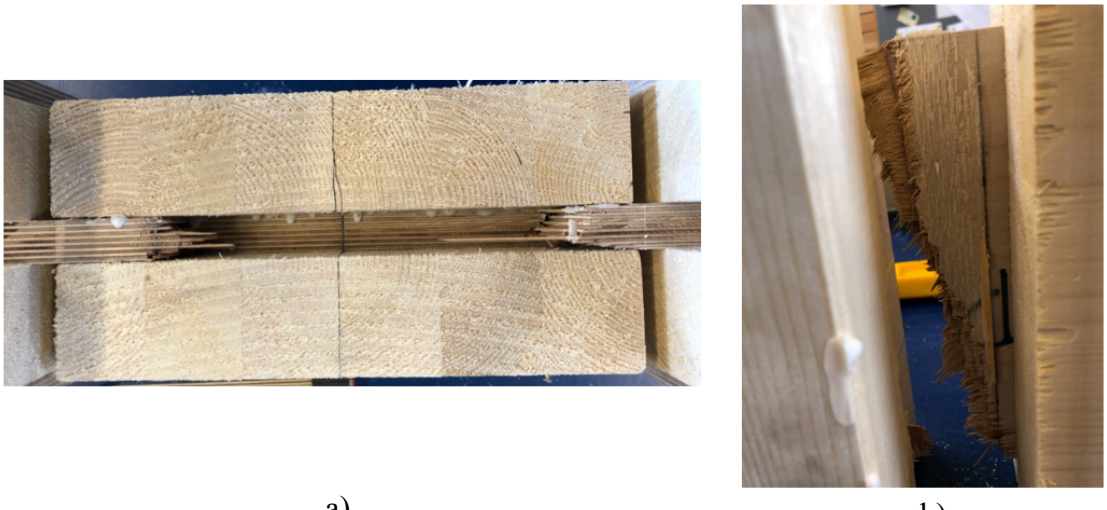

a) b)

Figure 5-4 – Shear failure of the plywood plates in glued configurations. Both fractures pictured are from test group S-1-0D-G, (a) from above and (b) from the side.

Failure of the unsymmetrical configurations

All the unsymmetrical specimens failed by tension failure originating in the bottom of the plywood plate. Figure 5-5 shows clear signs of tensile failure, but the compressed area is barely visible. This makes the failure of the unsymmetrical tests less bending characterized than the symmetrical tests. The reason for this can be the rotation and lifting of glulam while tested. The failures occurred in the screw row closest to the applied force. The failure followed the same pattern as the screwed symmetrical tests, which is not surprising.

Figure 5-5 – Fracture appearance of the plywood plate in test group U-1-0D.

Test specimen U-2-0D (2) did not achieve failure of the plywood at all before the test was aborted, due to excessive deformation and collision with the steel plate on top of the specimen.

5.2.2 Load capacity

Difference in capacity due to the number of plywood plates

It was no surprise that all test groups with two plywood plates endured a larger load than the corresponding ones with one plate. All groups suffered fracture failure in the plywood, so it would be natural to expect a doubling of the load capacity for the groups with two plates. As presented in chapter 5.1 and Table 5-7, this was not the case. The groups with two plywood plates consistently had a lower $F_{max,ply}$ than the ones with one plate. There are two possible reasons for this; the bending mode of the screws and thickness of the glulam.

The screws in the test groups with two plywood plates had a different bending mode than the one-plate ones; The extra plywood plate led to the forming of five plastic hinges in the screws instead of three, as illustrated in Figure 5-6.

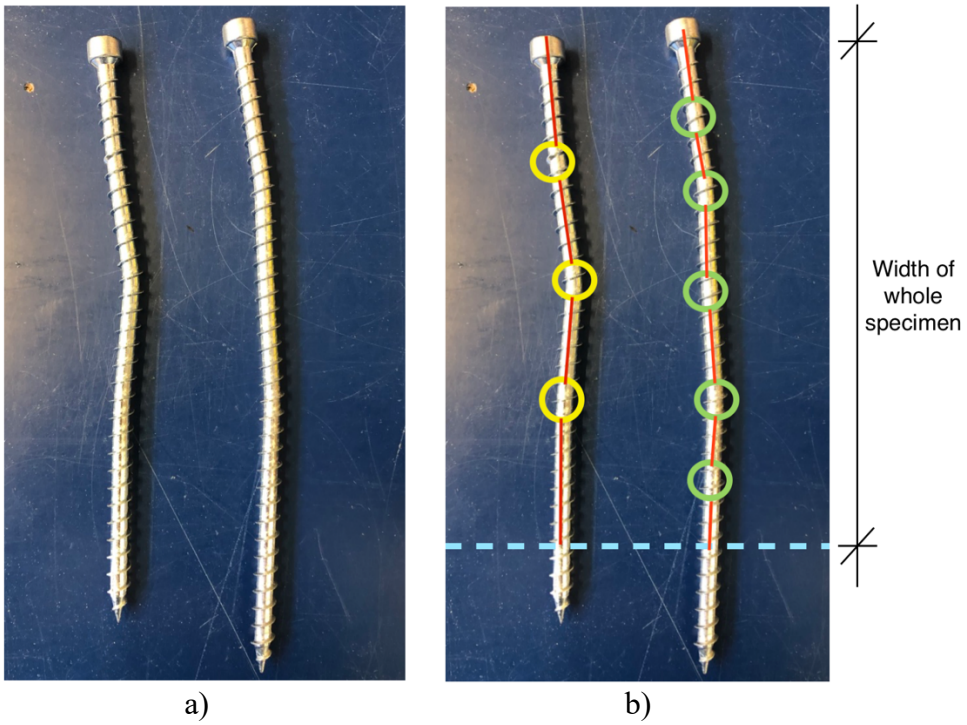

Figure 5-6 – Screws from 1-plate and 2-plate specimens (a). Plastic hinges in screws from 1-plate and 2-plate specimens (b).

When the load was transmitted from the hydraulic press machine to the screws, they led the load onto the plywood until they reached their yield moment, then the screws started to yield. While bending, the screws absorbed some of the energy, while embedment failure of the glulam occurred. When the embedded glulam was compressed and gained enough embedding capacity to slow down the bending process of the screws, a more significant portion of the load could be transmitted to the plywood, and the failure eventually happened. Since the bending mode of the screws in the 2-plate specimens required a more significant bending moment to create the plastic hinges, it can be assumed that this higher portion of load would be transmitted to the plywood earlier, leading to an earlier fracture. This difference in bending mode could also explain why all the screwed 2-plate test groups had a higher global elastic stiffness than their corresponding 1-plate test groups.

The other possible reason for the difference in $F_{max,ply}$ is the thickness of the glulam elements. Since the total thickness of the glulam was constant, the glulam pieces were thinner in the two-plate groups since the original glulam beam was split in three widths instead of

two. The difference in thickness of test group S-1-0D and S-2-0D is used as examples shown in Figure 5-7.

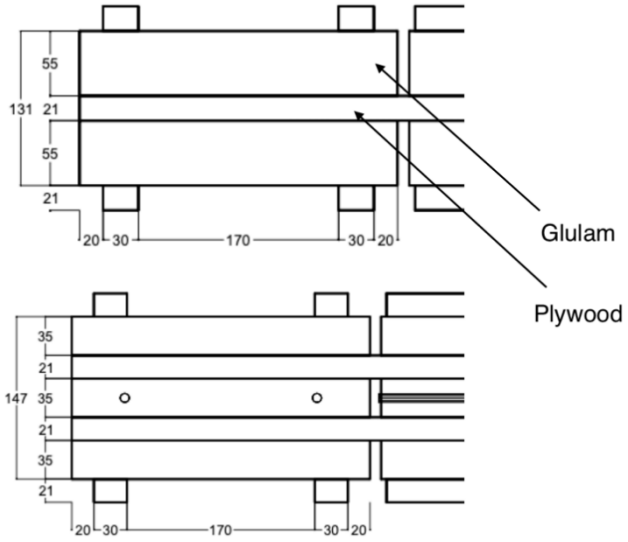

Figure 5-7 – Overhead view of test groups S-1-0D and S-2-0D to illustrate the difference in glulam thickness.

This difference in thickness led to an increased risk of splitting of the glulam in the two-plate test groups. The sandwiched glulam between the two plywood plates was the critical element as this did not have glued reinforcement to prevent splitting; it had reinforcement screws inserted on both sides instead. Since the screws used for the reinforcement (2 x 120 mm VGZ) did not cover the whole width of the element (270 mm), there was a 30 mm area in the middle of the glulam without splitting reinforcement. Inspection of the specimens after testing unveiled that every single S-2-0D specimen had this splitting on the underside of the sandwiched glulam, as pictured in Figure 5-8.

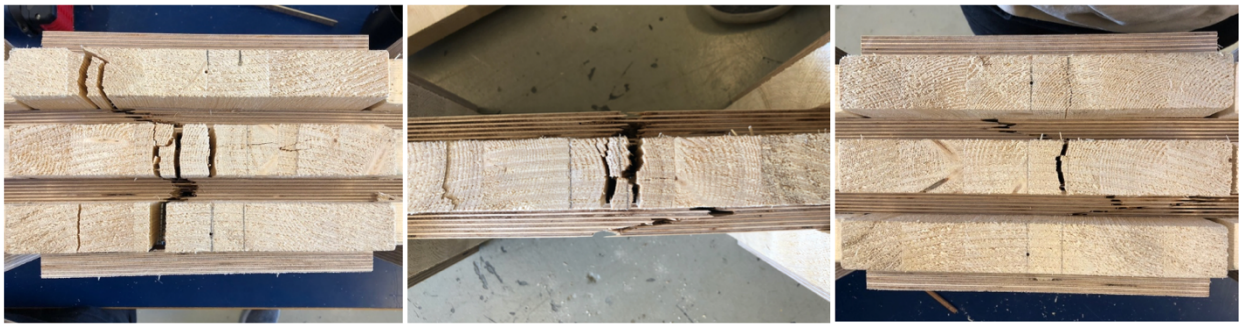

a) b) c)

Figure 5-8 – Splitting on the underside of sandwiched glulam elements in test specimens S-2-0D (1) (a), S-2-0D (2) (b) and S-2-0D (3) (c), as a consequence of no reinforcement screw in the middle.

It is conceivable that when this splitting occurred in the glulam, the total stiffness of the tensile area of the cross-section was reduced, causing the plywood to receive a sudden increase of tensile stress and go to failure. On the load-deformation curves of test group S-2-0D, a sudden drop of capacity can be observed, see Figure 5-9. An explanation for these drops could be the glulam cracking.

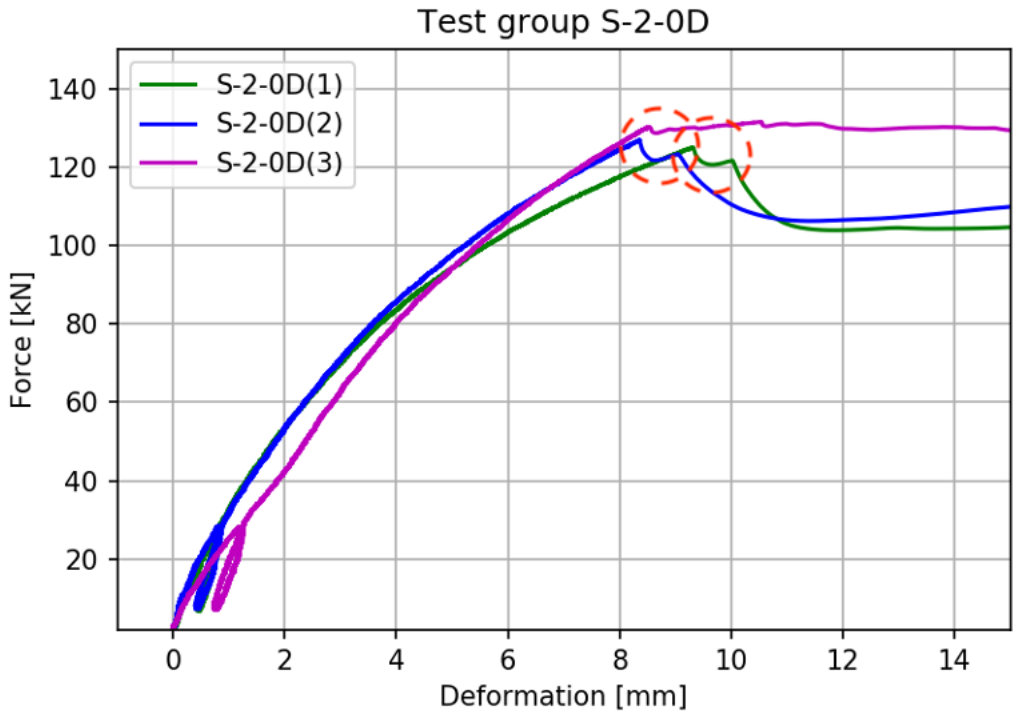

Figure 5-9 – Sudden drops of capacity observed for test group S-2-0D as a consequence of splitting in the sandwiched glulam element.

The glued test groups also had a significant difference in load capacity per plywood plate. The mean $F_{max,ply}$ were 78,13 kN for S-1-0D-G and 70,95 kN for S-2-0D-G. It was noticed that in test group S-1-0D-G, almost no cracking in the glulam occurred, and the shear failure happened on both sides of the column element. However, in test group S-2-0D-G, there were severe cracking of the glulam and the shear failure happened on only one side of the column element, see Figure 5-10. This detail could explain why $F_{max,ply}$ was lower for the two plate specimens, but the reasoning for the difference in fracture occurrence is challenging to determine. Especially since video replays show that the glulam cracking occurs after the shear failure of the plywood. It could be related to eventual small imperfections, such as the difference of the exact placement of the plywood, or uneven glue-lines.

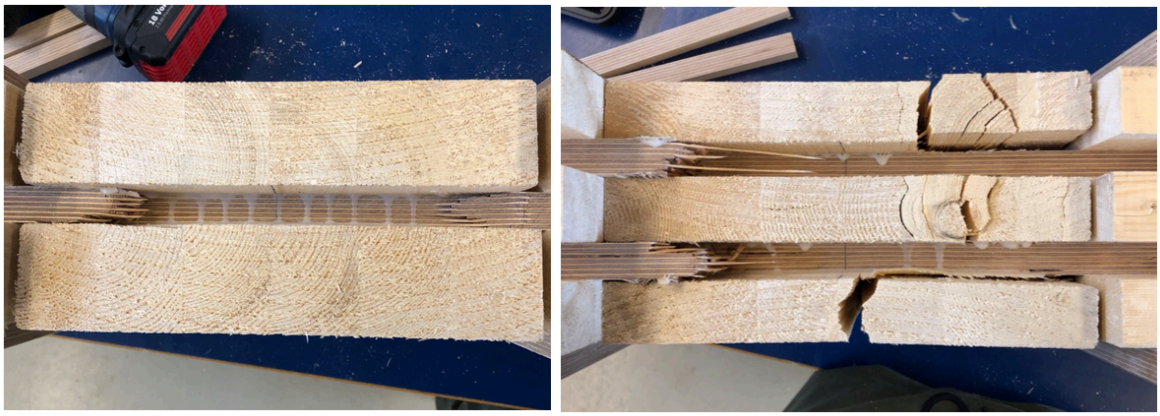

a) b)

Figure 5-10 – Overhead view of the shear failures of test groups S-1-0D-G (a) and S-2-0D-G (b). The other specimens in these test groups failed in the same manner.

For the unsymmetrical test groups, U-2-0D had a lower $F_{max,ply}$ compared with U-1-0D, in the same manner as the previously mentioned test groups. This configuration had some weaknesses. The steel setup was not optimal for the eccentric load applied. There were some bending of the steel rods, causing the whole specimen to lift itself from the floor closest to the load, see Figure 5-11. The sandwiched glulam element was lifted even more than the outer ones. This can be explained by the width of the glulam not being wide enough to allow a plastic hinge to form between the plywood plates. Therefore, the sandwiched glulam was pulled upwards along with the plywood plates and became compressed against the steel plate on top of the specimen. This could also explain the fact that U-2-0D had more rotation of the plywood plates than U-1-0D. The extra load on the steel setup in the second test group caused more bending in the rods, causing a more significant lift of the glulam and therefore increased rotation.

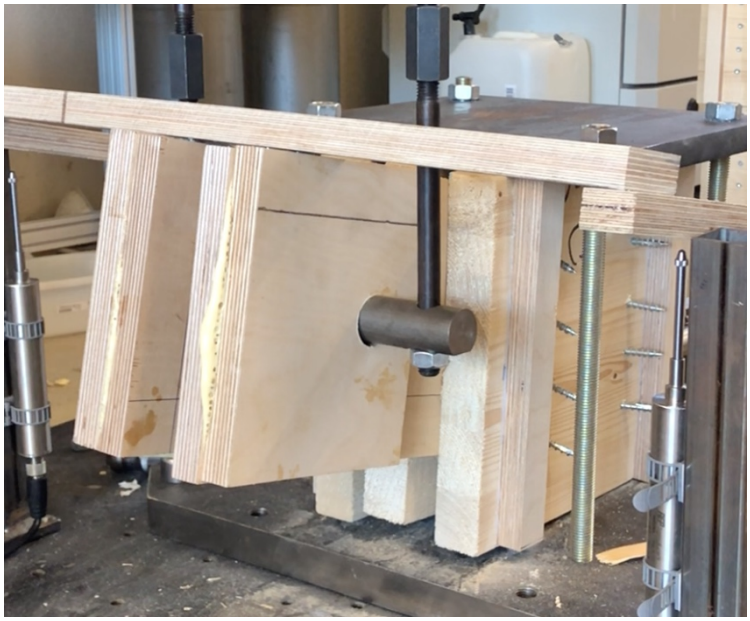

Figure 5-11 – Specimen from test group U-2-0D lifted from the floor due to the bending of steel rods.

On two of the tests, the rotation was extreme enough to allow the plywood plates to come in contact with the steel plate on top of the specimen. This contact can be observed by the sudden increase of capacity before failure in U-2-0D(1) and (2), see Figure 5-12. This could have induced the failure to happen earlier than it would have without the contact with the steel plates. Test specimen U-2-0D (2) did not have failure in the plywood. The test was stopped when the plywood hit the steel plate.

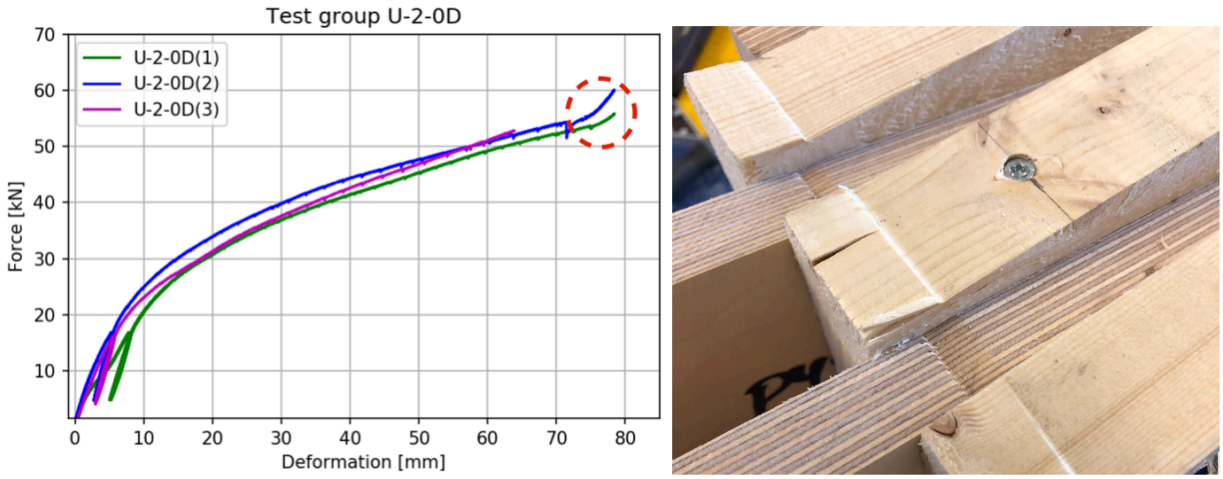

a) b)

Figure 5-12 – Increase of capacity before failure due to plywood plates crushing against steel as a consequence of the excessive rotation (a). Indenting showing that the plywood plates were embedded by the top steel plate (b).

A comparison of the maximum load for one and two plates has been done for each test group. For each test group, the increase of load capacity is calculated by using the mean values for each group in Table 5-7. This increase is similar to the findings of (Debije, 2017). It would be beneficial to confirm this value by testing a larger amount of test specimens.

Table 5-7 – Effect on the maximum load capacity from having two slotted-in plates instead of one. The capacity increase is denominated with percentage.

Test groups	Capacity increase effect [%]
S-1-0D/S-2-0D	88,24
S-1-45D/S-2-45D	82,33
S-21-0D-G/S-2-0D-G	81,62
U-1-0D/U-2-0D	82,60
Mean	**83,70**

Difference in capacity due to angle of the face grain of the plywood

It was apparent that the test specimens with a 45-degree face grain angle of the plywood consistently showed a higher load capacity than the specimens with 0-degree plywood. Test group S-1-45D had a mean F_{max} 7,31 % higher than S-1-0D, and S-2-45D had a mean F_{max} 3,30 % higher than S-2-0D. However, the cracking phenomenon in the two plate groups may have affected the F_{max} of test group S-2-0D. It is conceivable that S-2-0D could have reached the same capacity as the S-2-45D had the cracking not happened, but this cannot be concluded.

It would be natural to imagine that the capacity of the plates at 45-degrees is substantially lower than 0-degrees because the tensile capacity of fibers is much lower at 45-degrees. This turned out to be the opposite, and the reason for this is not obvious. Something that can contribute to this is that all layers of fibers were active and able to resist tension simultaneously, as opposed to at 0-degrees when only half of the layers would contribute at the same time.

5.2.3 Stiffness

Difference in global stiffness due to the number of plates

For test groups S-1-0D and S-2-0D, the latter showed higher global stiffness values both for $K_{el,global,sp}$ (global elastic stiffness per shear plane). A hypothesis for this difference in capacity per shear plane was presented in chapter 5.2.2. Parallels can be drawn to explain the stiffness. The global elastic stiffness is dependent on the yield moment of the screws, which requires a higher load for the two-plate groups due to the bending mode.

The glued samples turned out to behave differently. Here, S-2-0D-G showed a lower plastic and elastic global stiffness than S-1-0D-G, which was the opposite of the previously mentioned test groups. For the glued groups, it can be assumed that the column element had an indefinitely high stiffness for both S-1-0D-G and S-2-0D-G since the glue line is stronger than the wood. Therefore, the reason for the difference in global stiffness must lie in the beam (lateral) parts of the connection. One hypothesis could be that the screws in the beam elements of the specimen will receive a more significant portion of the load in the glued test groups than in the other ones because there were no screws in the column element to absorb some of the energy by yielding. There was a shorter eccentricity from the load to the center of the screws, which means that a more significant portion of the force would go down vertically. This direction was unfavorable in the beam elements because it went 90-degrees on the fiber. Since the sandwiched glulam element in S-2-0D-G is not wide enough for the forming of a plastic hinge between the plates, this glulam would more easily have embedding failure leading to lower stiffness.

It is not possible to conclude on any significant difference in global stiffness of the unsymmetrical test groups U-1-0D and U-2-0D. Test results were affected by the fact that global displacements had to be used, as well as the deformation of the steel setup during loading, which meant that the specimens were not fixed firmly to the bottom of the machine. Both groups showed an excessive amount of rotation and ductility, reasoned in chapter 5.2.2. The values for $K_{el,global}$ and $K_{pl,global}$ were remarkably low for both groups. The global stiffness of these groups is highly dependent on the yielding of the screws, enhanced by the long eccentricity. Hand calculations on the force resultant on each screw are presented in Appendix C – Hand Calculations.

Difference in global stiffness due to the face grain direction of the plywood

The fiber orientation of the plates appears to affect the global stiffness of the joint. Both S-1-45D and S-2-45D had a significantly higher $K_{el,global}$ than S-1-0D and S-2-0D, and it was the opposite for $K_{pl,global}$. Since the only difference in these groups was the fiber orientation in the plates, the difference in stiffness is related to this.

The reason for this difference in $K_{el,global}$ was not entirely clear. It may be related to the fact that only half of the layers were active in the 0-degree plates, and the transverse layers did not contribute to any stiffness. In the 45-degree plywood, all layers of the plates were contributing to the tensile capacity at once. It is also conceivable that the stiffness values were affected by the embedding strength of the plywood. The force from the machine onto the screws went 90-degrees to the longitudinal direction of face grain in the plates at 0-degrees. It can therefore be assumed that the screws would lead to some embedding failure in the plywood of the 0-degree test groups, and presumably a little less in the plates with 45-degree fiber orientation.

The high global elastic stiffness in the 45-degree specimens could also be explained by the shear stress distribution at a microscopic level, see Figure 5-13. When the plywood is oriented at 45-degrees, half of the layers will receive tensile stress as a result of the shear forces (V) acting on the infinitely small area pictured. When the tensile forces resulting from shear act along with the fiber, the shear capacity of the cross-section increases. This may be related to the increased stiffness.

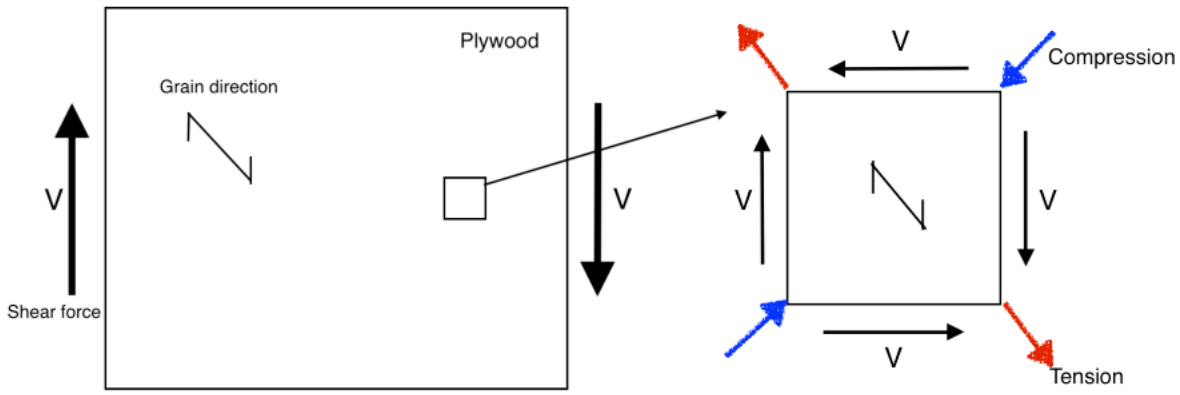

Figure 5-13 – How the shear stress affects an arbitrary infinite small area of plywood in the case of shear forces.

The global plastic stiffness $K_{pl,global}$ was significantly lower for the 45-degree test groups. This was also seen in the force-deformation diagrams and in the values for deformation and ductility. Test group S-1-45D had a doubled ductility ratio and a significant lower $K_{pl,global}$ than S-1-0D. There was a difference for the two-plate groups as well, only less prominent.

Difference in global stiffness due to the column fastener

The glue used in the column element in test groups S-1-0D-G and S-2-0D-G substantially increased the global stiffness of the connection. Since the glue entirely fixed the plywood in the column element, no slip occurred in the column element and bending was prevented. This played a big role when it came to the high global stiffness of the glued test groups. The glue fixed the plywood in place, which meant that the eccentricity from the lateral screw groups to the load was shorter than in the groups without glue. This resulted in a lower force resultant from eccentricity moment on each screw in the beam elements and less deformation.

5.3 Evaluation of SAP2000 Analysis

It has to be pointed out that the models made in SAP2000 were simplifications. The simplified models did however give an impression of how the moments and shear forces varied over the length of the plywood, which was illustrative when comparing them to the experimental results. The plywood plate was modeled as a beam for all test groups. The simplification of modeling the screw groups as pinned supports with rotational springs turned out to give the most realistic stress values for the symmetrical test groups. For the unsymmetrical test groups, each screw column was modeled as a regular pinned support.

5.3.1 Test groups

S-1-0D & S-2-0D

The tensile failure location in S-1-0D and S-2-0D matched well with the stress distribution found in SAP2000, presented in Figure 4-12. The fracture went through one of the middle rows of screws, as it was the weakest cross-section. The maximum tensile stresses in the plates according to the SAP2000 model were 57,0 MPa for S-1-0D and 48,6 MPa for S-2-0D, as illustrated in Table 4-9. Both these values were significantly exceeding the mean capacities for both tension and compression, while they were quite close to the calculated mean bending capacity (106,1 % and 90,5 % utilization for S-1-0D and S-2-0D respectively). This matched well with the fact that the test groups suffered both compressive and tensile

failures, which is typical for bending failure. The fact that the compressive capacity was so severely exceeded (191,9 % and 163,6 %) proves that the compressive failure occurs first like illustrated in Figure 2-4. It is also evident from Table 4-9 that the mean shear capacity was more than fully utilized (122,9 % and 115,2 % for S-1-0D and S-2-0D respectively) without having shear failure.

S-1-45D & S-2-45D

As was discussed in Chapter 5.2.1, the exact reason for the location of the fracture for the 45-degree specimens is unclear. As seen in Figure 4-13, the fracture location differed quite a bit from the location of the maximum tensile stress. The estimated capacities and utilization ratios are presented in Table 4-10. The maximum tensile stress, according to the SAP2000 model, was 61,1 MPa for S-1-45D and 50,5 MPa for S-2-45D. Both these values were significantly exceeding the mean capacities for both tension and compression, while they were quite close to the calculated mean bending capacity (113,8 % and 94,0 % utilization for S-1-45D and S-2-45D respectively). This matches well with the fact that the test groups suffered both compressive and tensile failure, which is typical for bending failure. It is also for these groups, evident from Table 4-10 that the mean shear capacity was more than fully utilized (131,4 % and 120,0 %) without having shear failure.

S-1-0D-G & S-2-0D-G

The glued test groups differed from the rest by having shear failure instead of bending or tensile failure. Figure 4-14 shows that the failure occurred in the areas where the shear stresses were at their maximum. Table 4-11 states that neither the mean tensile nor bending capacities of the plywood were reached, which matched the experimental results. However, the compressive capacities were exceeded according to the analysis (140,7 % and 120,5 % for S-1-0D-G and S-2-0D-G, respectively), although compressive failure was not observed due to the shear failure. The shear failures in these two glued test groups occurred at 140,0 % and 127,6 % shear stress utilization for S-1-0D-G and S-2-0D-G, respectively, according to the analysis.

The fact that the shear stresses exceeded the mean shear capacities by such degree may indicate that the mean capacities, in reality, are higher than 1,10 times the characteristic values, which was assumed in this work.

U-1-0D & U-2-0D

The unsymmetrical test groups had bending failure, which corresponded well with SAP2000. The failure location along the nearest screw row from the load was the location with the highest bending stress, as shown in Figure 4-15. From Table 4-12, the shear capacities was significantly exceeded (184,7 % and 162,8 % utilized for U-1-0D and U-2-0D, respectively). This did not coincide at all with the experimental result and was therefore considered as a consequence of the simplicity of the model. The tensile stress estimations seemed to be the most accurate, with 104,9 % and 92,5 % utilization for U-1-0D and U-2-0D, respectively. The bending capacities were not reached according to the analysis.

5.3.2 Limitations of model

The SAP2000 model had several weaknesses. Since the plywood plate was modeled as a beam instead of a plate, it was not possible to see the stress distribution throughout the cross-section. The load in this model was applied on top of the beam as a distributed line load. In reality, it was applied to the plate as point loads from each screw in the column element. Each screw in the lateral elements should have been modeled as springs with a specific stiffness for a more accurate representation. The load chosen for each model was based on the average F_{max} for each test group, which gave average stress, instead of specific stress for each specimen.

5.4 Assessment of the possibility of replacing Steel Plates with Birch Plywood

A comparison of steel vs. birch plywood in gusset plate connections was made to discuss the usability in real design. A beam of width 165 mm was considered for the calculations, with a span of 8,0 m and 3,6 m center-to-center distance. It was focused on the column part of the connection in this investigation. The resulting loads are presented in Chapter 2.6 and Appendix A – Connection Example. A continuous gusset plate connection, like in the experimental work of this research, was used as a basis for the calculation. The column in focus was regarded as a central column when calculating load widths and lengths. The beams were the critical connection part for embedding failure due to the grain direction, so the perpendicular embedding capacity was used in the calculation. The steel plate connection capacities were calculated with the same method used in (Swedish Wood, 2016). The plywood connection capacities for the screws were calculated with the method used in

Appendix C – Hand Calculations. Table 5-8 presents the calculated values. An estimated slip modulus K_{ser} was also calculated and is presented in Table 5-9 for both the plywood and steel connections. K_{ser} was calculated according to EC5 (NS-EN 1995-1-1:2004, 2004).

The steel connection considered, consists of 8 mm steel plates in slots of 10 mm. 12 mm STA dowels from Rothoblaas of S355 quality were considered as fasteners. Eight dowels were regarded in these calculations, see Figure 5-15 a). Only one and two slotted-in steel plates were considered.

The plywood connection considered consists of 21 mm birch plywood plates. The slots for the plates were also assumed to be 21 mm. Sixteen Rothoblaas 7 mm VGZ screws were used as fasteners, see Figure 5-15b. This was the same amount and dimension used in the experimental part of this research. In addition to one and two slotted-in plywood plates, the capacity of three and four plates was considered. In a real situation, extra plywood plates can be added by mounting them to the outside of the connection.

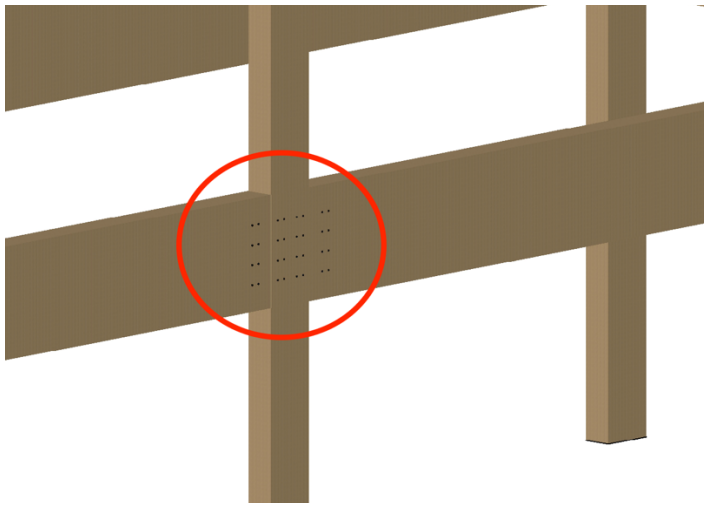

Figure 5-14 – Zoomed in 3D overview picture of the connection considered in the example of this chapter.

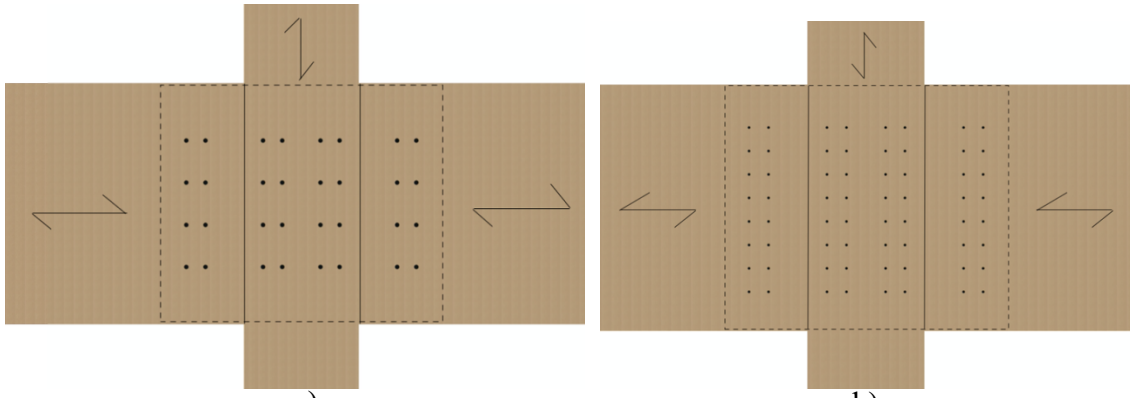

Figure 5-15 – Two connections compared in the example. The dowelled connection with 8 mm steel plates and 12 mm dowels is pictured in (a), and the screwed connection 7 mm screws and 21 mm plywood in (b). Fastener distances in this illustration are longer than the minimum distances.

Table 5-8 – Comparison of column connection capacities with gusset plates of steel and birch plywood. Eight 12 mm dowels were considered with the steel plates and sixteen 7 mm screws with the plywood. The beam width was 165 mm. The height of both the beam and the plywood was 630 mm. For the plywood connection, the maximum load which led to the failure of the screws, bending failure, and shear failure, are included. These load values were found through the SAP2000 analysis.

Load capacity [kN]				
Plate type	**Steel (8mm)**	**Plywood (21mm)**		
	Dowels	**Screws**	**Bending**	**Shear**
1 plate	281,9	280,6	588,6	167,7
2 plates	510,5	488,5	1177,2	335,5
3 plates	-	569,8	1765,8	503,1
4 plates	-	653,3	2354,4	670,8

It was not surprising that the slotted-in steel plate connection was estimated to be the stronger one (per fastener). The dowels had a significantly higher $M_{y,k}$ (yielding moment), which allowed a more significant load on each fastener before plastic hinges started to form. Another factor affecting the capacity was the bigger width of the plywood plate compared to the steel plate. Since the connections were limited to the width of the beam, the thickness of the glulam parts were smaller for the plywood connections. This smaller thickness led to less embedment capacity.

From Table 5-8, it became evident that it was the shear capacity of the plywood which was the critical capacity for design in this case, when one and two plates were considered. The shear capacity with one plywood plate was not sufficient for the design load (which was 254,4 kN) from the example in Chapter 2.6. However, by increasing from one to two plates, the shear capacity would be doubled, and the connection would be secure for design. The bending capacity of the plywood was more than sufficient for all cases.

An estimated slip modulus K_{ser} was also calculated and is presented in Table 5-9 for both the plywood and steel connections. K_{ser} was calculated according to EC5 (NS-EN 1995-1-1:2004, 2004).

Table 5-9 – Comparison of estimated slip modulus K_{ser} for connections with gusset plates of steel and birch plywood. Eight 12 mm dowels were used with the steel plates, and sixteen 7 mm screws were used with the plywood. The beam width was 165 mm. In the case of 3 and 4 plates, the plywood was mounted to the outside of the connection.

Estimated slip modulus K_{ser} [kN/mm]		
Plate type	**Steel (8mm)**	**Plywood (21mm)**
1 plate	148,9	122,2
2 plates	297,7	244,4
3 plates	-	244,4
4 plates	-	366,6

Plywood connections with the same load-bearing capacity were estimated to be slightly less stiff than the equivalent ones with steel plates and dowels. However, the differences were not huge and could easily be equalized by adding some screws or extra plywood plates to the outside of the connection. Furthermore, due to the minimum distances to the edge of the beam being slightly shorter for 7 mm screws compared with 12 mm dowels, the eccentricity from the load to the column would be slightly shorter with screws. This could positively affect the stiffness of the screwed plywood connection due to smaller force resultants on the screws from eccentricity moments.

To link the values in Table 5-8 with reality, one could consider the ULS design load of 254,4 kN from the example in Chapter 2.6. The one-plate plywood connection was not approved for the design load due to the shear capacity. However, one plate could be feasible for smaller

span constructions. The two-plate plywood connection had sufficient capacity, which would increase further with an increased number of screws. However, the number of screws should be reduced in this case to make ductile yielding of the screws the critical capacity, instead of brittle shear failure of the plywood.

Another advantage of using plywood may be the possibility of adding plates to the outside of the connection. By adding outer plywood plates, one would get two extra shear planes, which would increase the capacity and stiffness of the connection without increasing the number of screws and the size of the screw group. External plates are not feasible with 12 mm dowels and steel plates. Partially because the distance between the plates would be too narrow for the dowels to form plastic hinges, but the weight of the plates and accuracy needed for the holes would make it impractical to do on-site. A disadvantage of using external plywood plates is the increase of connection width. However, a solution could be external plates with a smaller thickness than the gusset plates. Extra capacity and stiffness from the added shear planes could then be benefitted from, without adding too much width to the connection.

The use of birch plywood as gusset plates in beam-column connections, based on the findings in this research, may be considered a possibility.

5.5 Implications and Limitations of the Research

In the design of connections, one would strive to have a ductile failure in the screws, rather than brittle failure in the glulam or plywood. So, the capacities of the test specimens in this study did not reflect how much capacity plywood connections could have in real constructions.

When designing the test specimens, it was challenging to make them fully represent a real connection. For instance, it was not possible to have solid glulam elements with grooves for the plywood. This was not possible to do for Moelven at this time due to a lack of grooving equipment for the plywood plate thickness. Instead, a glulam beam was split along the grain direction, cut in pieces, and then screwed together with plywood plates in between, to resemble a column or beam with plates slotted in.

In a real continuous column with a beam attached like simulated in this research, splitting of wood along the grain direction between the screws would be less likely, due to a bigger area to distribute the screws. In this test configuration, the splitting of timber was a real possibility and a problem, because of the relatively short distance from the screws to the grain-end of the

glulam and between each other. Some splitting did occur and has affected the capacity of some test groups.

The specimens were manually assembled by hand, which might have led to tiny differences between the different samples.

5.5.1 Review of experimental execution

The overall impression of the experimental investigation is that it was successful. Relatively concise results were found for most of the test groups, and many of the differences in results between groups could be explained. The measures after the preliminary testing to improve the setup worked significantly well, see Chapter 3.5.1 The preliminary splitting problems that affected capacity disappeared almost completely. Every single sample failed in the plywood, which was the intention behind over-designing the screw connections. However, it was surprising that all test groups except the glued ones suffered a tensile failure on the underside of the plywood plate from bending, instead of shear failure.

There were several uncertainties in the tests that could have been improved and may have affected the results, as mentioned in the former chapter; the specimens were manually assembled by hand. This might have led to tiny differences between each sample. Since the screws were inserted with a regular drill without extra equipment, they may not have been inserted precisely 90-degrees to the wood surface. It was not possible to acquire wood drills longer than 55 mm, so pre-drilling was only done in the glulam and not the plywood as it was considered too time-consuming. Some screws did not hit the hole in the glulam on the other side of the plywood as a result, see Figure 5-16. The angle of these screws may have been affected, and possibly the embedding strength of the glulam due to the extra hole. However, it did not seem to have a noticeable effect on the results.

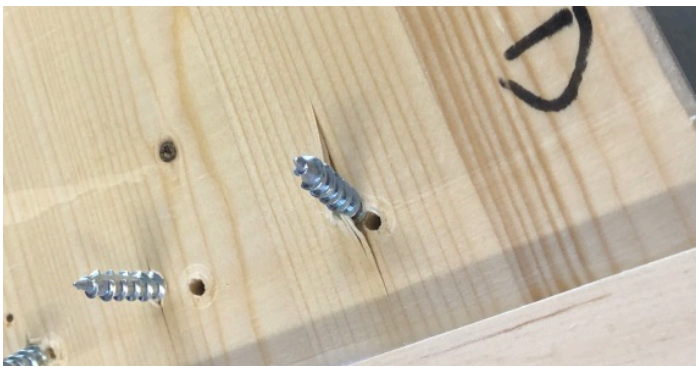

Figure 5-16 – Screws missing the hole on the other side of the specimen during insertion, as a result of not pre-drilling through the plywood plate.

It was disadvantageous that the global displacement data had to be used for the unsymmetrical samples. The amount of displacement was too significant for the 50 mm displacement transducers used in this research. They should ideally have been replaced by transducers with a greater measurement span than 50 mm. The global displacements measured by the hydraulic press were used instead, meaning that these data were not precisely accurate. The global deformations were affected by the fact that the steel bars of the steel setup started to bend. This bending was not expected and may have been a consequence of the quite large eccentricity from the load.

In some two-plate specimens, splitting occurred in the sandwiched glulam element as a consequence of the reinforcement screws not being long enough to cover the whole width. These screws were not available at the appropriate length. It was evident in retrospect that they should have been longer than necessary instead of too short.

5.6 Further Research

Based on the results and discussion from this work, the following further research is of interest:

- The effects of using different plywood thicknesses could be studied.
- A glued configuration with 45-degree plywood was not included in this work. The shear failure mode and shear capacity of plywood could be researched with such a configuration.
- A precise numerical FE model of a plywood beam-column connection should be assessed and compared to experimental values.
- An assessment of a plywood beam-column connection in the Serviceability Limit State (SLS) should be made and compared with equivalent steel plate connection values, to further strengthen the validity of plywood as a connection material.
- Experimental work on the behavior of a connection with external gusset plates of birch plywood should be investigated.
- Experimental work on the behavior of a plywood connection with self-tapping dowels could be investigated.
- Experiments with realistic dimensions in the plates, beams, and column could be performed, with a number of fasteners designed for ductile failure.

6 Conclusion

Based on the experimental and numerical work of this thesis, the following conclusions can be drawn for beam-column connections with gusset plates of birch plywood:

- The bending failure of the plywood at 45-degree fiber orientation indicates a ductile behavior compared to the plywood at 0-degree fiber orientation.
- Birch plywood at 45-degree fiber orientation appears to have higher bending capacity than 0-degree plywood in equivalent configurations.
- The use of two plates instead of one increases the mean load carrying capacity by approximately 83,70 %.
- Screwed test groups with two plywood plates reveals a higher $K_{el,global}$ compared to corresponding test groups with one plywood plate.
- Test groups with plywood at 45-degrees indicate a higher $K_{el,global}$ than the equivalent connections with 0-degree plywood.
- Test groups with plywood at 0-degrees indicate a higher $K_{pl,global}$ than the equivalent connections with 45-degree plywood.
- The use of glue in the column may increase the global stiffness of the connection significantly.
- Continuous plates throughout the column may increase the overall global stiffness significantly compared to single lateral plates.
- Eccentricity from the load to the stiffness center may have a great negative impact on the stiffness of the connection due to the increased force resultant on each screw.

Regarding the use of birch plywood as a replacement for steel plates in beam-column connections, the following can be concluded based on this investigation:

- Beam-column connections with gusset plates of birch plywood and screws could reach sufficient capacities for realistic design in the Ultimate Limit State (ULS).
- Beam-column connections with both slotted-in and external gusset plates of birch plywood, and screws, could reach the same capacities and stiffness as slotted-in steel plate connections with dowels.
- To further reduce the amount of steel in beam-column connections, prefabricated columns with glued-in plywood could be a feasible possibility.

7 References

AEP Transducers. (2020). *Data Sheet: LDT.700.R7*. Italy.

Bell, K. (2017). *Dimensjonering av trekonstruksjoner*: Fagbokforlaget.

Bier, H. (1984). Strength properties of Pinus Radiata plywood at angles to face grain. *New Zealand Journal of Forestry Science*: 349-367.

Blaß, H. J. & Sandhaas, C. (2017). *Timber Engineering*. Principles for Design. Germany: KIT Scientific Publishing.

Bodig, J. & Jayne, B. (1993). *Mechanics of wood and wood composites*, vol. 2. New York: Krieger Publishing Company.

Bouchair, A., Racher, P. & Bocquet, J. (2007). Analysis of dowelled timber to timber moment-resisting joints. *Materials and Structures*: 1127-1141.

Debije, J. J. B. (2017). *Dowel type connections in laminated bamboo with multiple slotted-in steel plates*. Netherlands: Delft University of Technology.

Dynea. (2019). *Prefere 4546 - liquid melamine urea adhesive for the wood industry*. Technical data sheet.

ESSVE Norway. (2019). *Trelim PU* (accessed: 16.03.2020).

Fragiacomo, M., Dujic, B. & Sustersic, I. (2011). Elastic and ductile design of multi-storey crosslam massive wooden buildings under seismic actions. *Engineering Structures*, 33 (11): 3043-3053.

Karacabeyli, E. & Ceccotti, A. (1996). Quasi-static reversed cyclic testing of nailed joints. *Proceedings of International Council for Building and Research Studies and Documentation Working Commission W18 – Timber Structures.*

Kollmann, F. & Côté, W. (1968). *Principles of Wood Science and Technology*, vol. 1 – Solid Wood. Berlin, Germany: Springer-Verlag.

Koskisen Group. (2002). *Handbook of Finnish Plywood*. Järvelä, Finland: Finnish Forest Industries Federation.

Lappalainen, K. & Backman, M. (2019). *Connections in timber trusses with gusset plates of timber material*. Stockholm: KTH.

Massé, M. & Salinas, J. (1988). Analysis of timber trusses using semi-rigid joints. *Can. Agric. Eng. 30*: 111-124.

Metsä Wood. (2019). *Declaration of Performance – Birch Plywood*: Metsä Wood.

Muñoz, W., Salenikovich, A., Mohammad, M. & Quenneville, P. (2008). Determination of Yield Point and Ductility of Timber Assemblies: In Search for a Harmonised Approach. 1-8.

Norske Limtreprodusenters Forening. (2015). *Limtreboka*, vol. 1: Norske Limtreprodusenters Forening.

NS-EN 1991-1-1:2002. (1991). *Eurocode 1: Actions on structures*: Standard Norge.

NS-EN 1993-1-1:2005. (1993). *Eurocode 3: Design of steel structures*: Standard Norge.

NS-EN 1995-1-1:2004. (2004). *Eurocode 5: Design of timber structures*: Standard Norge.

NS-EN 12512:2002. (2002). *Timber Structures – Test Methods – Cyclic testing of joints with mechanical fasteners.* : Standard Norge.

NS-EN 26891:1991. (1991). *Timber Structures – Joints made with mechanical fasteners – General principles or the determination of strength and deformation characteristics*: Standard Norge.

Rothoblaas. (2019). *VGZ*. Data sheet. Home page: Rothoblaas.

Swedish Wood. (2013). *Design of Timber Structures – Structural aspects of timber construction*. 2:2016 ed., vol. 1. Stockholm, Sweden: Swedish Forest Industries Federation.

Swedish Wood. (2016). *Limträhandbok – Dimensionering av limträkonstruktioner – Del 3*. Stockholm, Sweden: Swedish Forest Industries Federation.

United States Forest Service. (1999). *Wood Handbook: Wood as an Engineering Material*. Rev. ed. Madison, Wisconsin: USDA.

Yasumura, M. & Kawai, N. (1998). Estimating Seismic Performance of Wood – Framed Structures. . *Proceedings of.*

Åström, P. W. (2019). *Experimental study on innovative connections for large span structural timber trusses*: KTH Royal Institute of Technology.

Appendix A – Connection Example

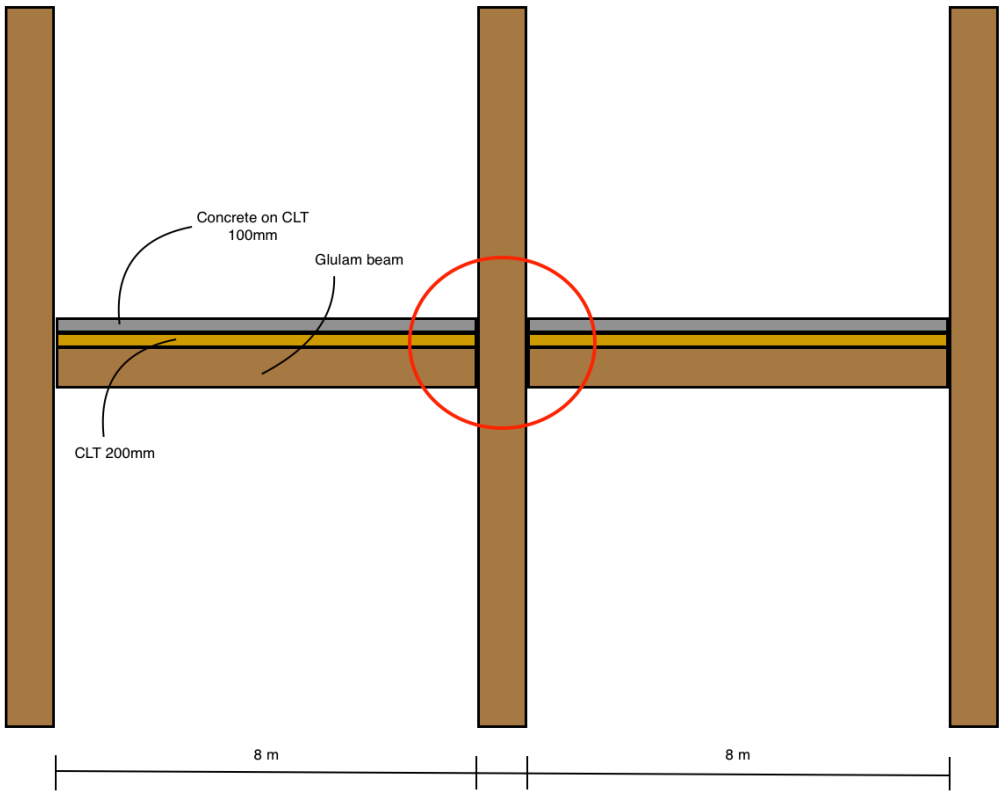

Beams center-to-center distance = 3,6 m

Load calculation:

CLT:

Density [kg/m^3]: $\rho = 500$

Width [m]: $w = 3.60$

Thickness [m]: $t = 0.20$

Length [m]: $l = 8.0$

Weight: $m_{CLT} = \rho * w * t * l = 2880$ kg

Concrete on CLT:

Density [kg/m^3]: $\rho = 2400$

Width [m]: $w = 3.60$

Thickness [m]: $t = 0.10$

Length [m]: $l = 8.0$

Weight: $m_c = \rho * w * t * l = 6912$ kg

GL30c beam:

Density [kg/m^3]: $\rho = 390$

Width [m]: $w = 0.165$

Height [m]: $h = 0.630$

Length [m]: $l = 8$

Weight: $m_b = \rho * w * t * l = 324$ kg

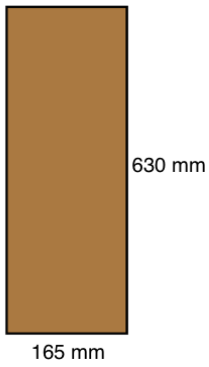

Permanent load:

$$q_p = \frac{(m_c + m_b + m_{CLT}) * 9.81 \frac{N}{kg}}{8{,}0\ m} = 12.4\ kN/m$$

Variable load:

$3\ kN/m^2$	(Office cat. B)	EC1-1

Line load: $q_n = 3{,}0 \frac{kN}{m^2} * 3.6\ m = 10.8\ kN/m$

Total line load:

$$q_{tot} = 1.2 * q_p + 1.5 * q_n = 31.8\ kN/m$$

Column connection load:

$$Q_{tot} = q_{tot} * (8{,}0\ m) = 254.4\ kN$$

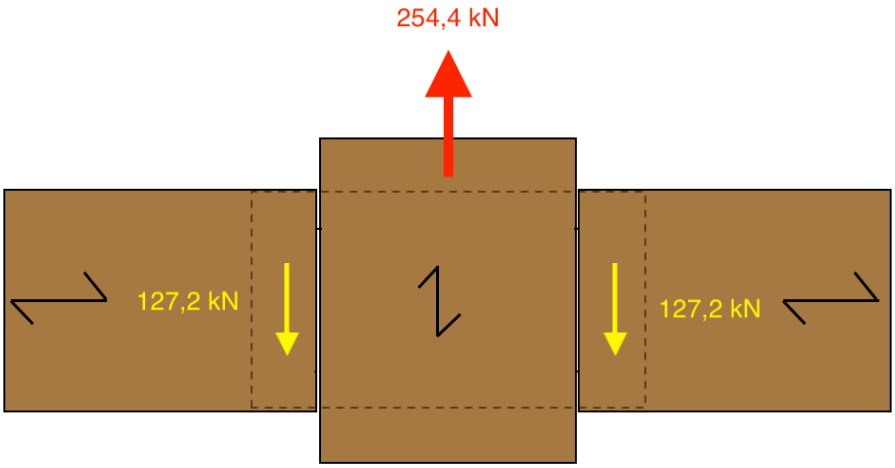
254,4 kN
127,2 kN
127,2 kN

Appendix B – Density and Moisture Values

Test cube	Width [mm]	Length [mm]	Height [mm]	Volume [m^3]	Weight before [kg]	Weight dried [kg]	**Density [kg/m^3]**	**Moisture content [%]**
1	49,86	50,1	56,3	0,0001406958	0,06989	0,06276	496,7	11,36
2	49,91	50,0	54,7	0,0001365335	0,05987	0,05401	438,5	10,85
3	50,08	50,3	56,7	0,0001429138	0,06171	0,05573	431,8	10,73
4	50,03	50,2	37,1	0,0000931930	0,04225	0,03801	453,4	11,15
5	50,02	50,3	37,8	0,0000950861	0,04656	0,04188	489,7	11,17
6	49,94	50,4	37,5	0,0000943304	0,05051	0,04552	535,5	10,96
						Mean value:	**474,3**	**11,04**

Appendix C – Hand Calculations

All calculations are done according to Eurocode 5.

Connection calculation

S-1-0D/S-1-45D/S-1-0D-G

Note: Mean values are used instead of characteristic values. The glulam density is the value measured in the lab, presented in Appendix B – Density and Moisture Values.

The beam part of the specimen was the critical part since the screws were pushed perpendicular to the grain. Therefore, the embedding strength perpendicular to the grain was used in the calculations, which is the weakest direction. The glue bond in the glued test groups was stronger than the screwed connection, so the beam connection is the critical part in these groups as well.

The reinforcement of the glulam is not taken into account.

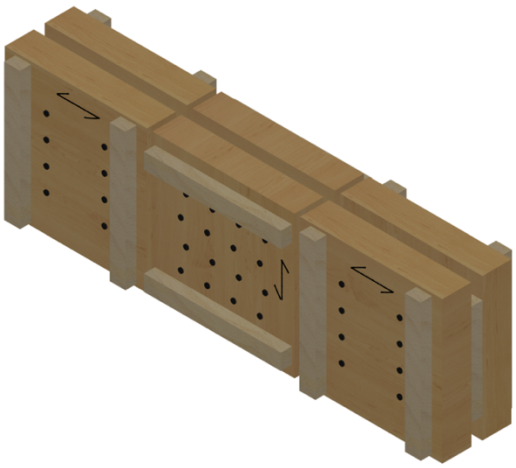

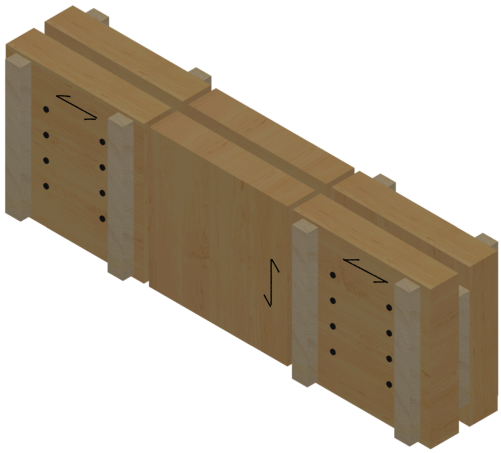

Glulam properties

Mean density [kg/m^3]:	$\rho_{mean,glulam} = 474$
Thickness [mm]:	$t_{glulam} = 55$
Screw diameter [mm]:	$d = 7$
	$k_{90,glulam} = 1.35 + 0.015d = 1.46$
Embedding strength 0° [MPa]:	$f_{h,0,k} = 0.082 * (1 - 0.01d) * \rho_{mean,glulam} = 36.15$
Angle:	$\alpha = 90°$
Embedding strength 90° [MPa]:	$f_{h,90,k} = \frac{f_{h,0,k}}{k_{90} * sin^2\alpha + cos^2\alpha} = 24.76$

Plywood properties

Mean density [kg/m^3]:	$\rho_{mean,plywood} = 680$
Thickness [mm]:	$t_{plywood} = 21$
Embedding strength [MPa]:	$f_{h,k} = 0.11 * (1 - 0.01d) * \rho_{mean,plywood} = 69.56$

Screw properties

Diameter [mm]:	$d = 7$
Yield moment [Nmm]:	$M_{y,Rk} = 14174$
Withdrawal capacity [MPa]:	$f_{ax,k} = 11.7$

Embedding strength [MPa] and thickness [mm]

Glulam:	$f_{h,1} = 24.76$	$t_1 = 55$
Plywood:	$f_{h,2} = 69.56$	$t_2 = 21$
Embedding strength ratio:	$\beta = \frac{f_{h,1}}{f_{h,2}} = 0.356$	

Rope effect [N]

Thread length into wood [mm]: $l_{ef} = 121$

$k_d = \min\left(\frac{d}{8}, 1\right) = 0.875$

Screw-to-grain angle: $\alpha = 90°$

Rope effect [N]: $F_{ax,Rk} = \frac{1 * f_{ax,k} * d * k_d * l_{ef}}{1.2 * cos^2\alpha + sin^2\alpha} = 8671$

Possible failure cases [N]

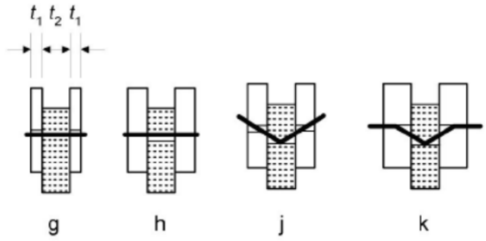

$F_{v,Rk,g} = f_{h,1} t_1 d = 9533$

$F_{v,Rk,h} = 0{,}5 f_{h,2} t_2 d = 5113$

$$F_{v,Rk,j} = 1{,}05 \frac{f_{h,1} t_1 d}{2+\beta}\left[\sqrt{2\beta(1+\beta) + \frac{4\beta(2+\beta)M_{y,Rk}}{f_{h,1} d {t_1}^2}} - \beta\right] + \frac{F_{ax,Rk}}{4} = 5722$$

$$F_{v,Rk,k} = 1{,}15\sqrt{\frac{2\beta}{1+\beta}}\sqrt{2M_{y,Rk} f_{h,1} d} + \frac{F_{ax,Rk}}{4} = 4015$$

Total capacity per fastener per shear plane

$$F_{v,Rk} = \frac{\min\left(F_{v,Rk,i},\ F_{v,Rk,i},\ F_{v,Rk,i},\ F_{v,Rk,i}\right)}{1000} = 4.01\ kN$$

Total capacity of the connection

Number of shear planes: $s = 2$

Number of fasteners: $n_{ef} = 8$

Number of connections: $u = 2$

Capacity [kN]: $F_{est} = F_{v,Rk} * s * n_{ef} * u = 128.3$

S-2-0D/S-2-45D/S-2-0D-G

Note: Mean values are used instead of characteristic values. The glulam density is the value measured in the lab, presented in Appendix B – Density and Moisture Values.

The beam part of the specimen was the critical part since the screws were pushed perpendicular to the grain. Therefore, the embedding strength perpendicular to the grain was used in the calculations, which is the weakest direction. The glue bond in the glued test groups was stronger than the screwed connection, so the beam connection is the critical part in these groups as well.

The reinforcement of the glulam is not taken into account.

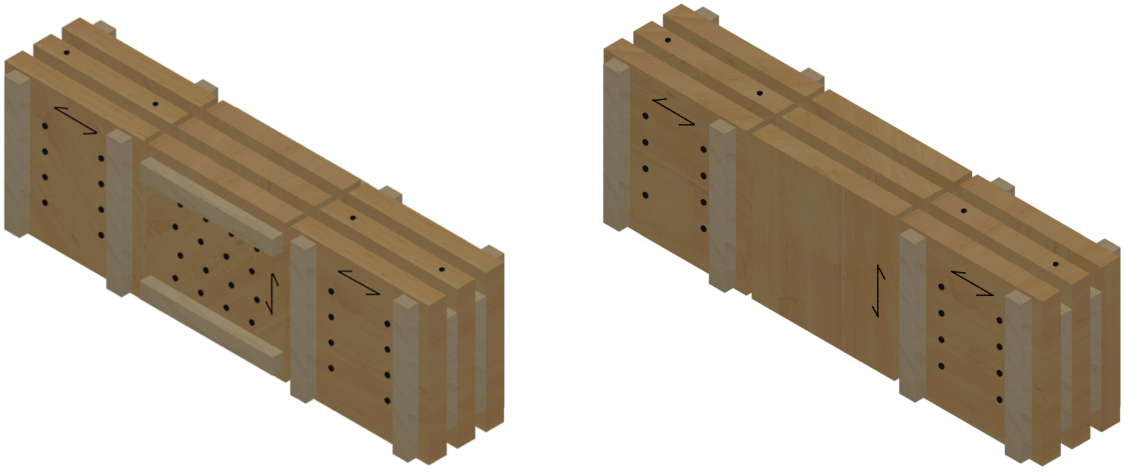

Glulam properties

Mean density [kg/m^3]:	$\rho_{mean,glulam} = 474$
Thickness [mm]:	$t_{glulam} = 35$
Screw diameter [mm]:	$d = 7$
	$k_{90,glulam} = 1.35 + 0.015d = 1.46$
Embedding strength 0° [MPa]:	$f_{h,0,k} = 0.082 * (1 - 0.01d) * \rho_{mean,glulam} = 36.15$
Angle:	$\alpha = 90°$
Embedding strength 90° [MPa]:	$f_{h,90,k} = \frac{f_{h,0,k}}{k_{90} * sin^2\alpha + cos^2\alpha} = 24.76$

Plywood properties

Mean density [kg/m^3]:	$\rho_{mean,plywood} = 680$
Thickness [mm]:	$t_{plywood} = 21$
Embedding strength [MPa]:	$f_{h,k} = 0.11 * (1 - 0.01d) * \rho_{mean,plywood} = 69.56$

Screw properties

Diameter [mm]:	$d = 7$
Yield moment (10% added) [Nmm]:	$M_{y,Rk} = 14174$
Withdrawal capacity [MPa]:	$f_{ax,k} = 11.7$

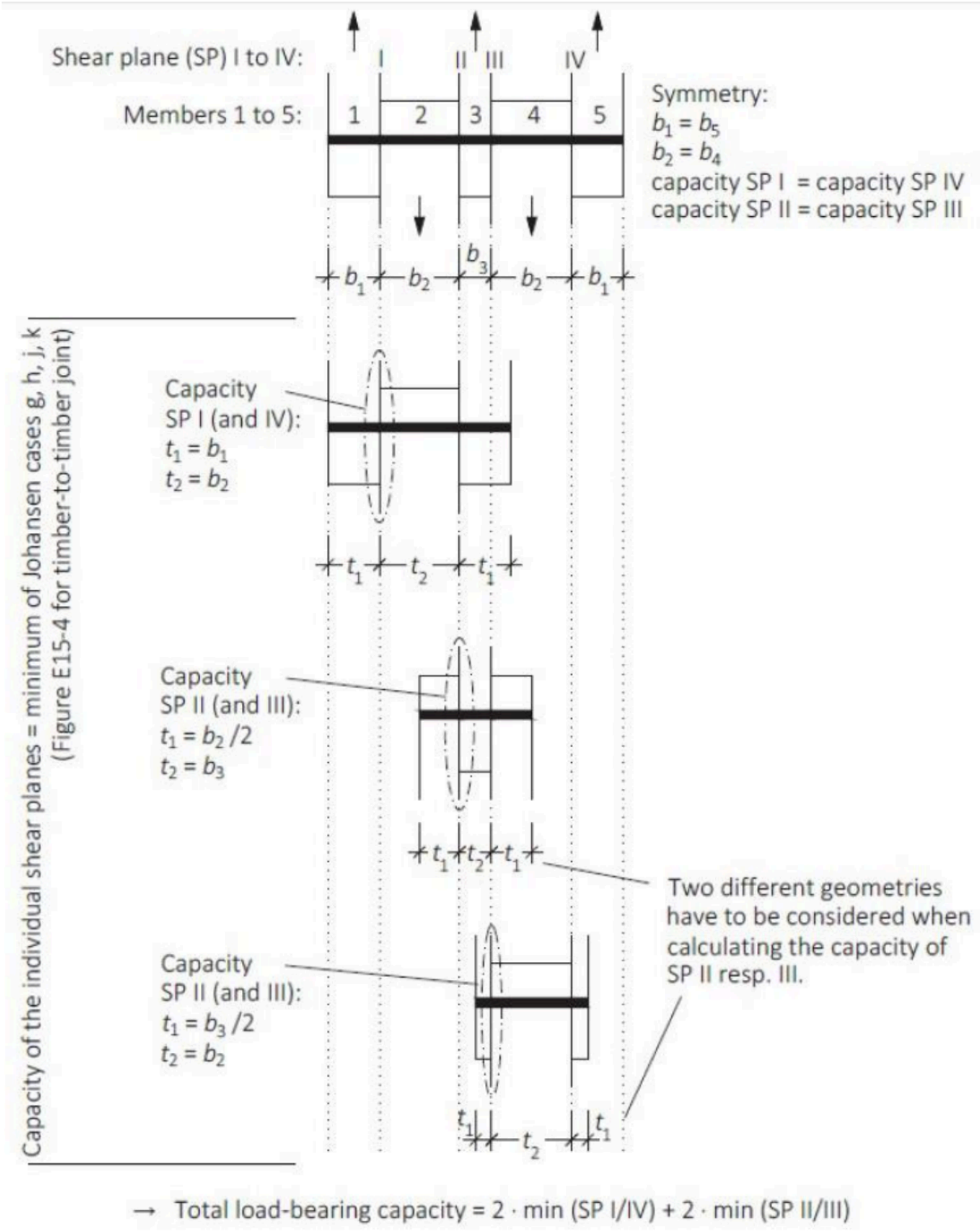
Shear plane (SP) I to IV:
I
II
III
IV
Members 1 to 5:
1
2
3
4
5
Symmetry:
$b_1 = b_5$
$b_2 = b_4$
capacity SP I = capacity SP IV
capacity SP II = capacity SP III
b_1 b_2 b_3 b_2 b_1
Capacity of the individual shear planes = minimum of Johansen cases g, h, j, k
(Figure E15-4 for timber-to-timber joint)
Capacity
SP I (and IV):
$t_1 = b_1$
$t_2 = b_2$
t_1 t_2 t_1
Capacity
SP II (and III):
$t_1 = b_2 /2$
$t_2 = b_3$
t_1 t_2 t_1
Two different geometries have to be considered when calculating the capacity of SP II resp. III.
Capacity
SP II (and III):
$t_1 = b_3 /2$
$t_2 = b_2$
t_1 t_2 t_1
→ Total load-bearing capacity = 2 · min (SP I/IV) + 2 · min (SP II/III)

Shear plane 1 and 4

Calculated with the same method as used in S-1-0D/S-1-45D calculations.

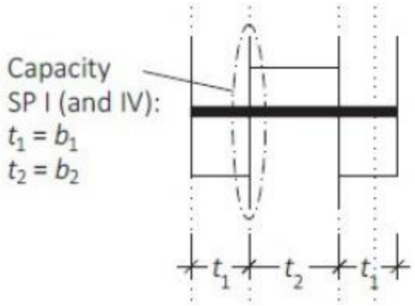

Embedding strength [MPa] and thickness [mm]

Glulam:	$f_{h,1} = 24.76$	$t_1 = 35$
Plywood:	$f_{h,2} = 69.56$	$t_2 = 21$
Embedding strength ratio:	$\beta = \frac{f_{h,1}}{f_{h,2}} = 0.356$	

Rope effect

Thread length into wood [mm]: $l_{ef} = 2 * t_1 + t_2 = 81$

$k_d = \min\left(\frac{d}{8}, 1\right) = 0.875$

Screw- to- grain angle: $\alpha = 90°$

Rope effect [N]: $F_{ax,Rk} = \frac{1 * f_{ax,k} * d * k_d * l_{ef}}{1.2 * cos^2\alpha + sin^2\alpha} = 5805$

Possible failure cases [N]

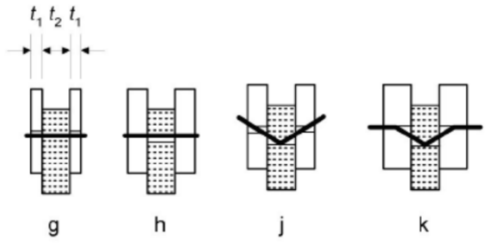

$F_{v,Rk,g} = f_{h,1} t_1 d = 6066$

$F_{v,Rk,h} = 0{,}5 f_{h,2} t_2 d = 5113$

$$F_{v,Rk,j} = 1{,}05 \frac{f_{h,1} t_1 d}{2+\beta}\left[\sqrt{2\beta(1+\beta) + \frac{4\beta(2+\beta)M_{y,Rk}}{f_{h,1} d {t_1}^2}} - \beta\right] + \frac{F_{ax,Rk}}{4} = 3919$$

$$F_{v,Rk,k} = 1{,}15\sqrt{\frac{2\beta}{1+\beta}}\sqrt{2M_{y,Rk}f_{h,1}d} + \frac{F_{ax,Rk}}{4} = 3298$$

Load bearing capacity [kN]: $F_{v,R,1.4} = \frac{\min(F_{v,Rk,g},\ F_{v,Rk,h},\ F_{v,Rk,h},\ F_{v,Rk,k})}{1000} = 3.30$

Shear plane 2 and 3 (Geometry 1)

Two different geometries must be considered for shear plane 2 and 3. Geometry 1 divides the plywood thickness in two and uses the original glulam thickness. This leads to new values for the rope effect and thicknesses. $f_{h,1}$ and $f_{h,2}$ and changes because the glulam element is now in the middle.

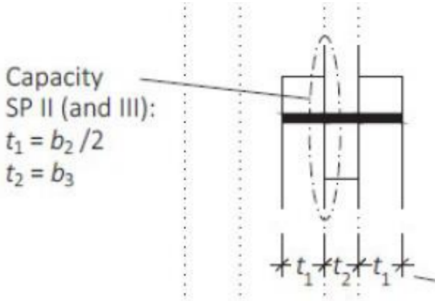

Embedding strength [MPa] and thickness [mm]

Plywood:	$f_{h,1} = 69.56$	$t_1 = \frac{t_{plywood}}{2} = 10.5$
Glulam:	$f_{h,2} = 24.76$	$t_2 = 35$
Embedding strength ratio:	$\beta = \frac{f_{h,1}}{f_{h,2}} = 2.83$	

Rope effect

Thread length into wood [mm]: $l_{ef} = 2 * t_1 + t_2 = 56$

$$k_d = \min\left(\frac{d}{8}, 1\right) = 0.875$$

Screw- to- grain angle: $\alpha = 90°$

Rope effect: $F_{ax,Rk} = \frac{1 * f_{ax,k} * d * k_d * l_{ef}}{1.2 * cos^2\alpha + sin^2\alpha} = 4013$

Possible failure cases [N]

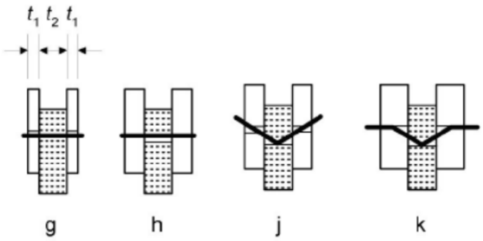

$F_{v,Rk,g} = f_{h,1} t_1 d = 5113$

$F_{v,Rk,h} = 0{,}5 f_{h,2} t_2 d = 3009$

$$F_{v,Rk,j} = 1{,}05 \frac{f_{h,1} t_1 d}{2+\beta}\left[\sqrt{2\beta(1+\beta) + \frac{4\beta(2+\beta)M_{y,Rk}}{f_{h,1} d {t_1}^2}} - \beta\right] + \frac{F_{a,Rk}}{4} = 7417$$

$$F_{v,Rk,k} = 1{,}15\sqrt{\frac{2\beta}{1+\beta}}\sqrt{2M_{y,Rk} f_{h,1} d} + \frac{F_{a,Rk}}{4} = 6198$$

Load bearing capacity [kN]: $F_{v,R,2.3.1} = \frac{\min(F_{v,Rk,g},\ F_{v,Rk,h},\ F_{v,Rk,h},\ F_{v,Rk,k})}{1000} = 3.01$

Shear plane 2 and 3 (Geometry 2)

This geometry is the same as shear plane 1 and 4, but the thickness of the glulam element is divided by two.

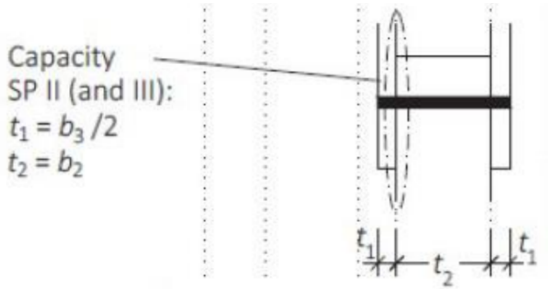

Embedding strength [MPa] and thickness [mm]

Glulam:	$f_{h,1} = 24.76$	$t_1 = \frac{t_{glulam}}{2} = 17.5$
Plywood:	$f_{h,2} = 69.56$	$t_2 = 21$
Embedding strength ratio:	$\beta = \frac{f_{h,1}}{f_{h,2}} = 0.356$	

Rope effect [N]

Thread length into wood [mm]: $l_{ef} = 2 * t_1 + t_2 = 56$

$k_d = \min\left(\frac{d}{8}, 1\right) = 0.875$

Screw- to- grain angle: $\alpha = 90°$

Rope effect [N]: $F_{ax,Rk} = \frac{1 * f_{ax,k} * d * k_d * l_{ef}}{1.2 * cos^2\alpha + sin^2\alpha} = 4013$

Possible failure cases [N]

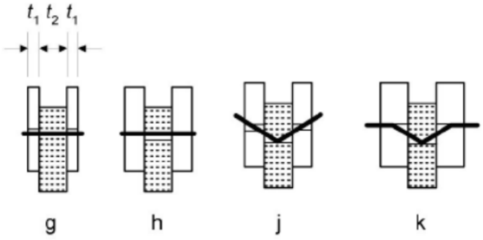

$F_{v,Rk,g} = f_{h,1} t_1 d = 3033$

$F_{v,Rk,h} = 0{,}5 f_{h,2} t_2 d = 5113$

$F_{v,Rk,j} = 1{,}05 \frac{f_{h,1} t_1 d}{2+\beta}\left[\sqrt{2\beta(1+\beta) + \frac{4\beta(2+\beta)M_{y,Rk}}{f_{h,1} d {t_1}^2}} - \beta\right] + \frac{F_{a,Rk}}{4} = 2662$

$F_{v,Rk,k} = 1{,}15\sqrt{\frac{2\beta}{1+\beta}}\sqrt{2M_{y,Rk} f_{h,90,k} d} + \frac{F_{a,Rk}}{4} = 2850$

Load bearing capacity [kN]: $F_{v,R,2.3.2} = \frac{\min\left(F_{v,Rk,g},\ F_{v,Rk,h},\ F_{v,Rk,h},\ F_{v,Rk,k}\right)}{1000} = 2.66$

Total capacity per fastener [kN]

$F_{v,Rk} = 2 * F_{v,R,1.4} + 2 * \min\left(F_{v,R,2.3.1}, F_{v,R,2.3.2}\right) = 11.92$

Total capacity connection [kN]

Number of fasteners:	$n_{ef} = 8$
Number of connections:	$u = 2$
Capacity [kN]:	$F_{est} = F_{v,Rk} * n_{ef} * u = 190.1$

U-1-0D

Note: Mean values are used instead of characteristic values. The glulam density is the value measured in the lab, presented in Appendix B – Density and Moisture Values.

The calculation for this specimen is the same as the symmetrical ones with one plate. The only difference is the numbers of supports which leads to half the capacity of the symmetrical ones.

The reinforcement of the glulam is not taken into account.

Total capacity per fastener [kN]

$$F_{v,Rk} = \frac{2 * \min\left(F_{v,Rk,g}, F_{v,Rk,h}, F_{v,Rk,j}, F_{v,Rk,k}\right)}{1000} = 8.03$$

Total capacity of connection [kN]

Number of fasteners:	$n_{ef} = 8$
Number of supports:	$u = 1$
Capacity:	$F_{est} = F_{v,Rk} * n_{ef} * u = 64.2$

U-2-0D

Note: Mean values are used instead of characteristic values. The glulam density is the value measured in the lab, presented in Appendix B – Density and Moisture Values.

The calculation for this specimen is the same as the symmetrical ones with one plate. The only difference is the numbers of supports which leads to half the capacity of the symmetrical ones.

The reinforcement of the glulam is not taken into account.

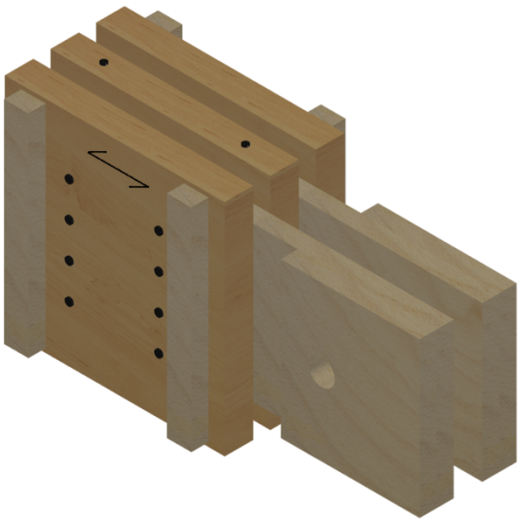

Total capacity per fastener [kN]

$F_{v,Rk} = 2 * F_{v,R,1.4} + 2 * \min\left(F_{v,R,2.3.1}, F_{v,R,2.3.2}\right) = 11.92$

Total capacity of connection [kN]

Number of fasteners:	$n_{ef} = 8$
Number of supports:	$u = 1$
Capacity:	$F_{est} = F_{v,Rk} * n_{ef} * u = 95.4$

Screw load distribution

Test group U-1-0D

This calculation presents the different resultant forces acting on each screw in the unsymmetrical test group U-1-0D. The resulting force for each screw is determined by both the vertical load generated by the pressing machine, and the force generated by the moment created from an eccentricity from the load to the screw group. The method used is from (Swedish Wood, 2013)

The force F is chosen from visual inspection of force-deformation diagrams in Chapter 4.1. The calculated F_y fits poorly for these test groups, so F = 7,5 kN is chosen from the visual check (where the curve enters the plastic region).

Only screws 1, 2, 3 and 4 are checked due to symmetry.

Drawings:

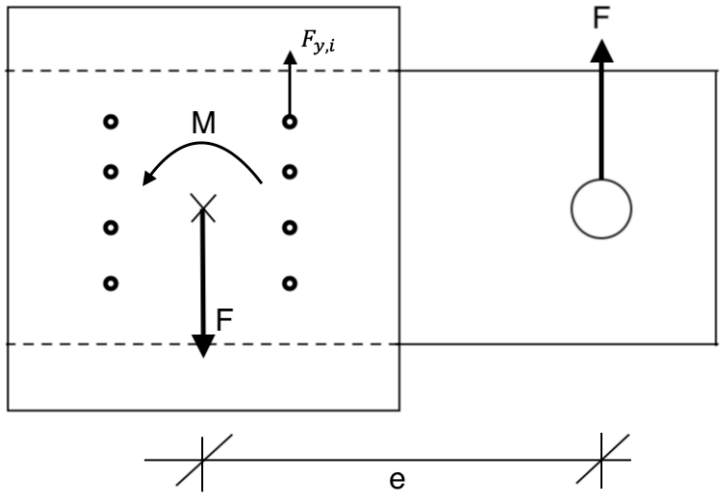

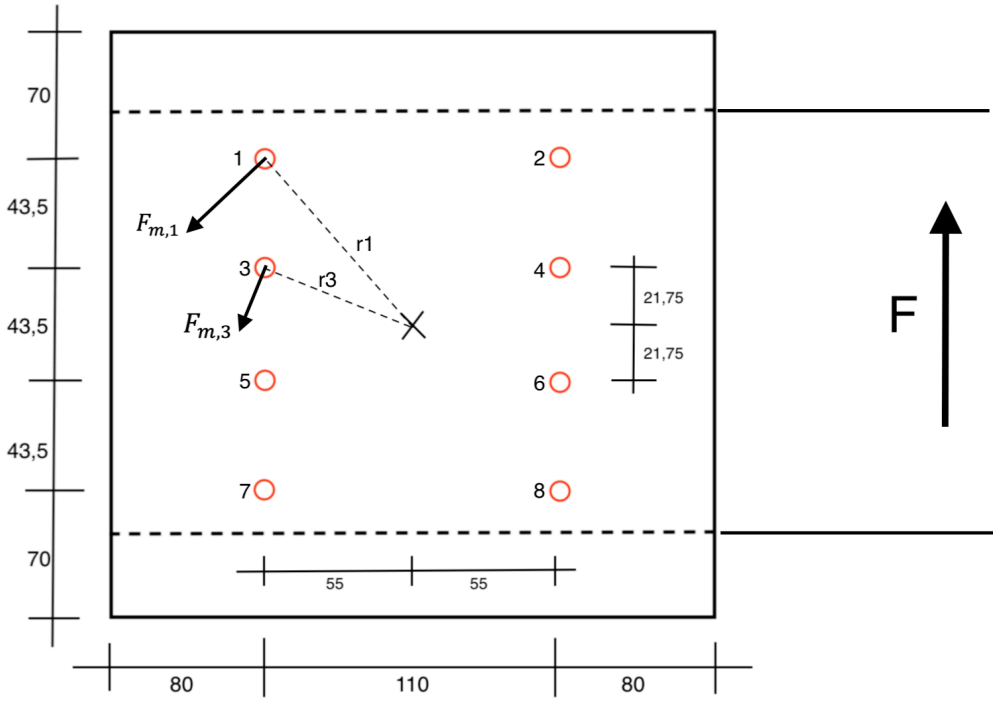

Given data

Eccentricity from load [mm]:	$e = 240$
Distance screw center to screw row 1 [mm]:	$y_1 = 21{,}75 + 43{,}5 = 65{,}25$
Distance screw center to screw row 2 [mm]:	$y_2 = 21{,}75$
Distance screw center to screw columns [mm]:	$x_1 = 55$
Force applied [N]:	$F = 7500$
Number of screws:	$n = 8$

General calculations

Moment [Nmm]:	$M = F * e = 1{,}80 * 10^6$
Vertical force component acting on screws [N]:	$F_{y,1} = F_{y,2} = F_{y,3} = F_{y,4} = \frac{F}{n} = 937{,}50$
Polar moment of inertia [mm^2]:	$I_p = \sum r_i^2 = \sum(x_i^2 + y_i^2) = 4 * (x_1^2 + y_1^2) + 4 * (x_3^2 + y_3^2) = 4{,}31 * 10^4$

Force on screws from moment [N]: $F_{m,i} = \frac{M*r_i}{I_p}$

$F_{mx,i} = -\frac{M*y_i}{I_p}$

$F_{my,i} = \frac{M*x_i}{I_p}$

Total resultant force [N]: $F_i = \sqrt{F_{mx,i}^2 + (F_{y,i} + F_{my,i})^2}$

Screw 1

Forces on screw from moment [N]: $F_{mx,1} = -\frac{M*y_1}{I_p} = -2725$

$F_{my,1} = \frac{M*x_1}{I_p} = -2297$

Total resultant force [N]: $F_1 = F_7 = \sqrt{F_{mx,1}^2 + (F_{y,1} + F_{my,1})^2} = \mathbf{3045}$

Screw 2

Forces on screw from moment [N]: $F_{mx,2} = -\frac{M*y_2}{I_p} = -2725$

$F_{my,2} = \frac{M*x_2}{I_p} = 2297$

Total resultant force [N]: $F_2 = F_8 = \sqrt{F_{mx,2}^2 + (F_{y,2} + F_{my,2})^2} = \mathbf{4229}$

Screw 3

Forces on screw from moment [N]: $F_{mx,3} = -\frac{M*y_3}{I_p} = -908$

$F_{my,3} = \frac{M*x_3}{I_p} = -2297$

Total resultant force [N]: $F_3 = F_5 = \sqrt{F_{mx,3}^2 + (F_{y,3} + F_{my,3})^2} = \mathbf{1635}$

Screw 4

Forces on screw from moment [N]: $F_{mx,4} = -\frac{M*y_4}{I_p} = -908$

$F_{my,4} = \frac{M*x_4}{I_p} = 2297$

Total resultant force [N]: $F_4 = F_6 = \sqrt{F_{mx,4}^2 + (F_{y,4} + F_{my,4})^2} = \mathbf{3359}$

Resultant force diagram

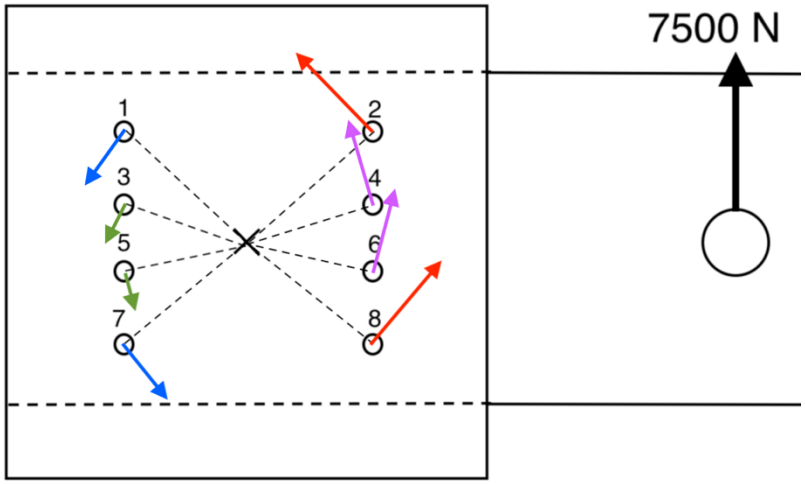

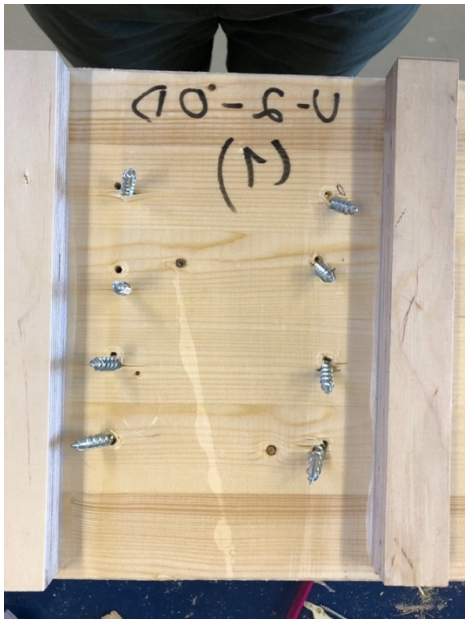

Bending capacity of plywood plate

Mean values of the capacities are considered.

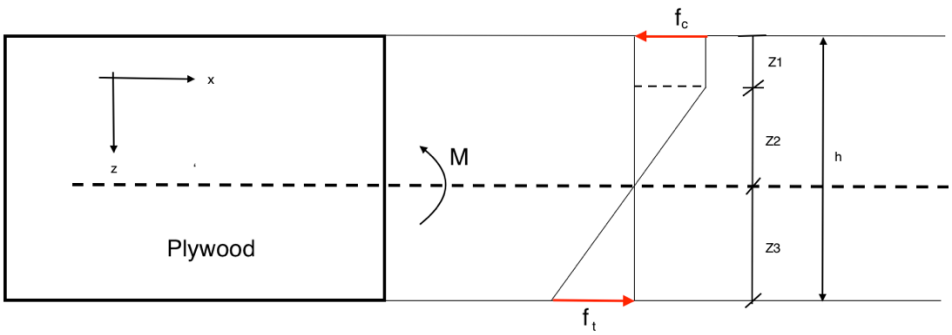

$$\sum F_x = 0 \rightarrow f_c * z_1 * t + f_c * z_2 * \frac{t}{2} = f_t * z_3 * \frac{t}{2} \qquad (1)$$

a) $\frac{f_c}{z_2} = \frac{f_t}{z_3} \rightarrow z_2 = z_3 * \frac{f_c}{f_t}$

b) $z_1 = h - z_3 - z_2 = h - z_3 - z_3 * \frac{f_c}{f_t} = h - z_3 * (1 + \frac{f_c}{f_t})$

Puts a) and b) into (1):

$$f_c * \left[h - z_3 * \left(1 + \frac{f_c}{f_t}\right)\right] + f_c * \frac{z_3}{2} * \frac{f_c}{f_t} - f_t * \frac{z_3}{2} = 0$$

Plywood properties

Thickness [mm]:	$t = 21$
Compression capacity [MPa]:	$f_{c,mean} = 29{,}7$
Tension capacity [MPa]:	$f_{t,mean} = 42{,}9$
Height [mm]:	$h = 190$

Moment calculation

$z_1 = 34{,}5\ mm$

$z_2 = 63{,}64\ mm$

$z_3 = 91{,}86\ mm$

$$M_{Rd} = f_{c,mean} * z_1 * t * \left(\frac{z_1}{2} + z_2\right) + f_{c,mean} * z_2 * t * \frac{z_2}{2} + f_{t,mean} * z_3 * t * \frac{z_3}{2}$$

$M_{Rd} = 6{,}79\ kNm \rightarrow f_{m,mean} = \frac{M*y}{I} = 53{,}74\ MPa$

Appendix D – Fracture Photography of each Test Specimen

Test group S-1-0D

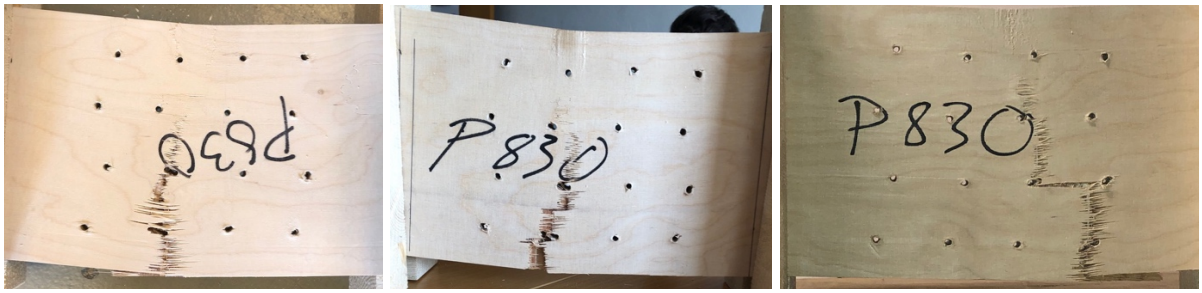

Test group S-1-45D

Test group S-2-0D

Test group S-2-45D

Test group S-1-0D-G

Test group S-2-0D-G

Test group U-1-0D

Test group U-2-0D

Due to excessive deformation, the screws could not be removed. Fractures are therefore pictured from the bottom of the specimen. Specimen U-2-0D (2) had no plywood failure and is not pictured.

Appendix E – Python Scripts

```
2.  ##########################################################################################
    ######################
3.  # PROCESS TESTING DATA TO PLOT FORCE-DEFORMATION DIAGRAMS #
4.  ##########################################################################################
    ######################
5.
6.  import matplotlib.pyplot as plt
7.
8.  #%%
9.  # Import the .txt data file from file trajectory on computer
10.
11. Datafil = '/Users/eysteinfuruheim/Documents/MASTER/Datafiler fra tester/Hovedtestin
    g/Laptop/S-1-0D(1).txt'
12.
13.
14. #%%-----------------------------------------------------------------------------------
    ------------------------------------------------
15. # Change the commas in the .txt file to dots to let python process the data
16.
17. data = ""
18. with open(Datafil, 'r') as file:
19.     data = file.read().replace(',', '.')
20.
21. with open(Datafil, "w") as out_file:
22.     out_file.write(data)
23.
24. #%%-----------------------------------------------------------------------------------
    ------------------------------------------------
25. # Make empty lists where the force and displacement data from the .txt file will be
     added
26.
27. force = []
28. disp1 = []
29. disp2 = []
30.
31. # Make python understand which column in the .txt file is the force and displacemen
    t data
32.
33. with open(Datafil, 'r') as file:
34.     lines = file.readlines()
35.     force = [line.split()[0] for line in lines]
36.     disp1 = [line.split()[1] for line in lines]
37.     disp2 = [line.split()[2] for line in lines]
38.
39. # Convert the data in each list from strings(text) to floats(numbers)
40.
41. force = list(map(float, force))
42. disp1 = list(map(float, disp1))
43. disp2 = list(map(float, disp2))
44.
45. # Each measurement data in the lists needs to be multiplied by a factor to be
46. converted into kN and mm
47. # This factor is determined by the voltage signal produced by the load cell and
48. transducers
49.
50. force = [i * -30 for i in force]
51. disp1 = [(i - disp1[200]) * 2000 for i in disp1] # The displacement data lists are
    modified to make the plot start at 0 mm
52.
53. disp2 = [(i - disp2[200]) * -2000 for i in disp2]
54.
```

```
55.
56.
57. #%%
58. # Create a new list which will be the average deformation from the two transducers
59.
60. disp_mean = []
61.
62. n = 0
63.
64. for i in disp1:
65.     disp_mean.append((disp1[n]+disp2[n])/2)
66.     n = n + 1
67.
68. #Creating the plot
69.
70. plt.plot(disp_mean, force, 'm-')
71. plt.grid(True)
72. plt.ylim(2, 150)                              # Set the range of the y axis
73. plt.xlim(-1, 30)                             # Set the range of the x axis
74. plt.xlabel('Deformation [mm]')
75. plt.ylabel('Force [kN]')
76. plt.title('Test specimen S-1-0D(1)')
77. plt.legend()
78. fig = plt.gcf()
79. fig.set_size_inches(6, 4)
80. fig.savefig('S-1-0D(1)', dpi=150) # Save the plot as a picture on the computer
81.
82. plt.show()
```

```
1.  ########################################################################
2.  # CALCULATING THE PLASTIC STIFFNESS AND DUCTILITY OF THE CONNECTION #
3.  ########################################################################
4.
5.  # The goal of this script is to pull out displacement values for different values
6.  of F and use these to calculate the stiffness and ductility
7.
8.  #%% Count the number of rows in the force list
9.
10. a = 0
11. for i in force:
12.     a = a+1
13.
14. #%% Input values for each test. F_max is the maximum force in kN and Disp is which
    displacement transducer data to be used
15.
16. F_max = 144.06
17. Disp = disp1
18.
19. # Gather displacement value at 0,4*F_max
20.
21. n = 0
22. for i in force:
23.     n = n+1
24.     if F_max * 0.399 < i < F_max * 0.401:
25.         break
26.
27. disp04_Fmax = Disp[n]
28.
29. # Gather displacement value at 0,9*F_max
30.
31. n = 0
```

```
for i in force:
    n = n+1
    if F_max * 0.899 < i < F_max * 0.901:
        break

disp09_Fmax = Disp[n]

# The plastic stiffness can be calculated (Yasumura & Kawai method)

K_pl = (0.9*F_max - 0.4*F_max)/(disp09_Fmax - disp04_Fmax)

#%% Calculating the ductility ratio

# The yield force is calculated (K&C method)

F_y = 0.5 * F_max

# Gather displacement value at the yield point

n = 0
for i in force:
    n = n+1
    if F_y * 0.99 < i < F_y * 1.01:
        break

disp_y = Disp[n]

# Gather maximum displacement value

n = 0
for i in force:
    n = n+1
    if F_max * 0.99 < i < F_max * 1.01:
        break

disp_u = Disp[n]

# The ductility ratio can be calculated

D_u = disp_u/disp_y
```

Norges miljø- og biovitenskapelige universitet
Noregs miljø- og biovitskapelege universitet
Norwegian University of Life Sciences

Postboks 5003
NO-1432 Ås
Norway